COTUTELLE DE THÈSE ENTRE

Université de Liège and Université de Gand

METHODS AND MODELS FOR BRAIN CONNECTIVITY ASSESSMENT ACROSS LEVELS OF CONSCIOUSNESS

Enrico Amico

Promotor Ulg:
Prof. Dr. Steven Laureys

Promotor UGent:
Prof. Dr. Daniele Marinazzo

Committee:

Prof. Dr. Christophe Phillips	University of Liège
Prof. Dr. Pierre Geurts	University of Liège
Prof. Dr. Rodolphe Sepulchre	University of Cambridge
Prof. Dr. Tom Loeys	University of Ghent
Dr. Ruth Seurinck	University of Ghent

Thèse présentée en vue de l'obtention du titre de *Docteur en Sciences biomédicales et pharmaceutiques* à l'Université de Liège et de *Docteur en Statistical data analysis* à l'Université de Gand

Liège, Année académique 2015–2016

Université de Liège

UNIVERSITEIT GENT

The work presented in this thesis was performed at the Coma Science Group, GIGA consciousness and Cyclotron Research Center, University of Liège, and at the Department of Data analysis, University of Ghent. Part of the work was done in collaboration with Prof. Joaquín Goñi, Purdue Institute for Integrative Neuroscience, School of Industrial Engineering and Weldon School of Biomedical Engineering, Purdue University, West-Lafayette, IN, USA.

The studies in this thesis were funded by This research was supported by the Wallonia-Brussels Federation of Concerted Research Action (ARC), European Commission (DECODER), Belgian Science Policy (CEREBNET), McDonnell Foundation, European Space Agency (ESA).

CONTENTS

LIST OF ABBREVIATIONS

fMRI	Functional magnetic resonance imaging
TMS	Transcranial magnetic stimulation
dMRI	Diffusion magnetic resonance imaging
DWI	Diffusion weighted imaging
DTI	Diffusion tensor imaging
dHb	Deoxyhemoglobin
MR	Magnetic resonance
MRI	Magnetic resonance imaging
FA	Fractional anisotropy
FOD(s)	Fiber orientation distribution(s)
FC	Functional connectivity
SC	Structural connectivity
ROI	Region of interest
PCA	Principal component analysis
ICA	Independent component analysis
DMN	Default mode network
DOC	Disorders of consciousness
UWS	Unresponsive wakefulness syndrome
MCS	Minimally conscious state

EMCS	Emerging from minimally conscious state
LIS	Locked-in syndrome
TBI	Traumatic brain injury
PCI	Perturbational complexity index
RSN(s)	Resting state network(s)
CAP(s)	Co-activation pattern(s)
PCC	Posterior cingulate cortex
AAL	Automated anatomical labeling template
swADTF	Spectrum-weighted adaptive directed transfer function
CRS-R	Coma Recovery Scale-Revised

ABSTRACT

The human brain is one of the most complex and fascinating systems in nature. In the last decades, two events have boosted the investigation of its functional and structural properties. Firstly, the emergence of novel non-invasive neuroimaging modalities, which helped improving the spatial and temporal resolution of the data collected from in vivo human brains. Secondly, the development of advanced mathematical tools in network science and graph theory, which has recently translated into modeling the human brain as a network, giving rise to the area of research so called Brain Connectivity or Connectomics.

In brain network models, nodes correspond to gray-matter regions (based on functional or structural, atlas-based parcellations that constitute a partition), while links or edges correspond either to structural connections as modeled based on white matter fiber-tracts or to the functional coupling between brain regions by computing statistical dependencies between measured brain activity from different nodes.

Indeed, the network approach for studying the brain has several advantages: 1) it eases the study of collective behaviors and interactions between regions; 2) allows to map and study quantitative properties of its anatomical pathways; 3) gives measures to quantify integration and segregation of information processes in the brain, and the flow (i.e. the interacting dynamics) between different cortical and sub-cortical regions.

The main contribution of my PhD work was indeed to develop and implement new models and methods for brain connectivity assessment in the human brain, having as primary application the analysis of neuroimaging data coming from subjects at different levels of consciousness. I have here applied these methods to investigate changes in levels of consciousness, from normal wakefulness (healthy human brains) or drug-induced unconsciousness (i.e. anesthesia) to pathological (i.e. patients with disorders of consciousness).

This thesis is structured as follows. Chapter 1 gives a general overview of the neuroimaging techniques employed for my studies. Chapter 2 provides a review of the field of brain connectivity. Chapter 3 covers the state of the art of brain connectivity methods and models for the investigation of different levels of consciousness.

The following three Chapters include the broad description of the three studies performed during my PhD and a brief discussion of the employed models and main findings. Particularly, the first study (Chapter 4) tests a new method to detect functional fluctuations in brain networks during propofol-induced modulation of consciousness. The second study (Chapter 5) aims to investigate changes of information flow in the brain after transcranial magnetic stimulation, both from a functional and structural perspective. The third study (Chapter 6) describes a novel data-driven methodology for the extraction of robust independent connectivity patterns from clinical populations, without imposing any a priori data stratification into groups.

For the interested reader, the full detailed manuscripts of these studies are attached in Appendices A, B and C, where detailed descriptions of the methods, results, and implications of these studies take place.

Finally, the thesis closes with concluding remarks summarizing the work performed and proposing future directions of research.

RÉSUMÉ

Le cerveau humain est l'un des systèmes les plus complexes et fascinants que l'on puisse trouver dans la nature. Au cours de ces dernières décennies, deux événements ont révolutionné l'étude de ses propriétés structurelles et fonctionnelles. Tout d'abord l'émergence de nouvelles modalités de neuroimagerie non invasive, permettant d'augmenter la résolution spatiale et temporelle des données acquises in vivo. Ensuite, le développement récent de nouveaux outils mathématiques avancés, en science des réseaux ainsi que sur la théorie des graphs, a permis la modélisation du cerveau humain en tant que réseau. Cet ensemble a donné naissance à de nouveaux champs d'investigation appelés Brain Connectivity ou Connectomics.

Dans les modèles de réseaux cérébraux, les noeuds correspondent à des régions de matière grise. En revanche, les liens ou les bordures représentent soit une connexion structurelle, comme pour les modèles basés sur les fibres de matières blanches, soit un couplage fonctionnel entre régions cérébrales. Ce dernier est obtenu par calcul des dépendances statistiques entre l'activité cerebrale mesuré dans différents noeuds.

En effet, cette approche par réseau possède plusieurs avantages: 1) elle facilite l'étude des comportements collectifs et des interactions entre régions; 2) elle permet la cartographie des voies anatomiques et d'étudier leurs propriétés quantitatives; 3) elle procure des mesures sur l'intégration du traitement de l'information par le cerveau, ainsi que sur le flux (i.e. la dynamique interactive) entre différentes régions corticales et sous-corticales.

L'apport majeur de mes travaux de thèse fut le développement de nouveaux modèles et de nouvelles méthodes pour l'évaluation de la connectivité cérébrale du cerveau humain. L'application principale de ces travaux a concerné les données de neuroimagerie de patients à différents niveaux de conscience.

Ainsi, j'ai appliqué ces méthodes à l'étude des changements de niveaux

de conscience, allant de l'éveil normal (cerveau humain sain) ou de l'inconscience pharmaco-induite (i.e. anesthésie) aux états pathologiques (i.e. patients atteints de troubles de la conscience).

Cette thèse est structuré selon le schéma suivant: le chapitre 1 est consacré à une revue générale des techniques de neuroimagerie utilisée lors de mon travail. Le chapitre 2 se focalise lui sur la connectivité cérébrale. Le troisième chapitre couvre l'état de l'art des méthodes utilisées pour la connectivité cérébrale, ainsi que les modèles utilisé pour l'étude des niveaux de conscience.

Les trois chapitres suivants sont consacrés à une description approfondie des trois études réalisées pendant mon travail de thèse, une brève discussion des modèles utilisés et les principaux résultats. Plus précisément, la première étude (chapitre 4) a testé une nouvelle méthode de détection des fluctuations fonctionnelles des réseaux cérébraux dans le cadre d'une conscience altérée induite par le propofol. La seconde étude (chapitre 5) fut consacrée à l'investigation des changements du flux d'information cérébrales après une stimulation magnétique transcranienne, et ce d'un point de vue structurel et fonctionnel. La troisième étude (chapitre 6) a décrit une nouvelle méthode pour l'extraction de schémas de connectivité indépendants robustes issus d'une population de patients, sans imposer de stratification a priori des données aux seins des groupes.

Pour le lecteur intéressé, les manuscrits complets de ces études sont en annexe A, B et C, dans lesquelles ont été détaillées les méthodes, les résultats ainsi que leur discussion.

Pour finir, cette thèse se termine sur les conclusions tirées des travaux effectués et ouvre des perspectives pour de futures investigations.

1 NEUROIMAGING METHODS: AN OVERVIEW

Neuroimaging refers to techniques that produce images of the brain without requiring surgery, incision of the skin, or any direct contact with the inside of the body. Because these technologies enable noninvasive visualization of the structure and functionality of the brain, neuroimaging has become a powerful tool for both research and medical diagnosis. Although still relatively young, the field of neuroimaging has rapidly advanced over the years due to breakthroughs in technology and computational methods. This chapter will cover the three neuroimaging techniques employed and analyzed in this thesis: functional magnetic resonance imaging (fMRI), diffusion magnetic resonance imaging (dMRI) and transcranial magnetic stimulation (TMS) combined with simultaneous electroencephalography (EEG) recordings.
***Keywords**: Neuroimaging, fMRI, DWI, TMS, EEG.*

1.1 Functional magnetic resonance imaging

Functional magnetic resonance imaging (fMRI) has improved our ability to investigate brain activity in humans. Thanks to the diffuse availability of magnetic resonance (MR) scanners, fMRI data have become the most employed and analyzed neuroimaging modality in neuroscience. Since its introduction, fMRI has evolved to become the most important method for investigating human brain function [1].

1.1.1 The MR Signal

MR scanners use strong magnetic fields, radio waves, and field gradients to form images of the body. In the specific case of brain measurements, the MR signal measures differences in the energy transitions of the hydrogen nuclei after the application of a magnetic field, and how it depends on the properties of the nearby tissue or the physiological state of the brain. The hydrogen

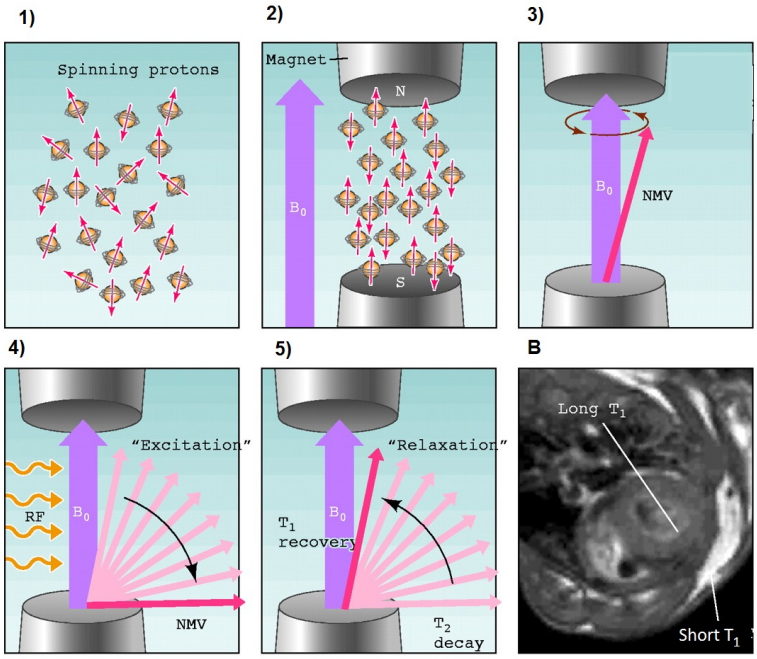

Figure 1.1: *Basic description of magnetic resonance imaging (MRI). 1) Hydrogen protons spin in random directions in absence of a magnetic field. 2) When an external magnetic field $B0$ is applied protons tend to align with it. 3) The net magnetization vector (NMV,i.e. the summation of all the magnetic moments of the individual hydrogen protons) starts precessing around $B0$. 4) When a radio frequency pulse is applied the NMV moves from the longitudinal to the transvers plane (excitation phase). 5) When the pulse is turned off the transverse component (T2) decays and the longitudinal component (T1) recovers. B) Contrast arises because different tissues have different recovery times. Adapted from [2].*

nuclei achieve a relatively organized, low-energy state when the subject enters the static (B0) field of the MR scanner. The strength of this magnetic field is specified in units of Tesla, and common field strengths range from 1.5 to 4.7 Tesla. In the presence of a strong magnetic field, there is a tendency for the magnetic moment of these nuclei to align parallel or antiparallel to the main field in much the same way as the dipole moment of a small bar magnet aligns itself with the local magnetic field (Fig. 1.1).

The magnetic resonance measurement begins when a radio frequency (rf) pulse into the tissue is introduced. This pulse elicits nuclei into a higher energy state. The rf excitation pulses and the magnetic field gradients superimposed on the static B0 field can be applied according to a variety of different timing and amplitude parameters. The tuning of these allows to obtain im-

ages that show different properties of the brain, including structure (anatomical imaging), flow (perfusion imaging), or neural activity (functional imaging).

Information about the nearby tissue is derived from the rate at which the hydrogen nuclei return to the low-energy state following the excitation. Two exponential processes with time constants (T1 and T2) describe the return to the low-energy state. The T1 constant measures the relaxation in the direction of the B0 magnetic field. The T2 constant measures the transverse relaxation of the dipole in the plane perpendicular to the B0 field. These changes in the local magnetic field are measured by sensors (coils) placed inside the scanner (Fig. 1.1).

1.1.2 *The BOLD signal*

The transverse relaxation is of special significance for fMRI. In an ideal homogeneous magnetic field, the transverse relaxation follows an exponential signal decay; the time constant of the decay is called T2. However, in physiological tissue the transverse relaxation is more rapid because of local field inhomogeneities: this rate is denoted T2*.

The mechanisms connecting neural activity to the measured T2* value are generally called the Blood Oxygen Level Dependent (BOLD) contrast mechanism. The BOLD contrast mechanism mainly measures changes in the relative concentration of oxygenated and deoxygenated blood. Deoxyhemoglobin (dHb) is paramagnetic and influences the MR signal [2]. The effects of dHb on T2* were first noticed by Ogawa et al. in their studies on the rat brain, where they observed that blood vessel contrast varied with changes in the blood oxygen demand [3] (Fig. 1.2).

The first simultaneous fMRI and electrophysiological recordings [5] clearly confirmed that the BOLD reflects aspects of the neural responses elicited by a stimulus. The way a neuronal activation translates into a change of the corresponding BOLD signal is characterized by the so-called hemodynamic response function [6]. Typically, a neuronal activation results in a change of the BOLD signal after $1-2$ seconds, with a peak in the BOLD signal after $4-6$ seconds, and these values can be significantly different for different regions of the brain [7]. It has been shown that the hemodynamic response primarily reflects the neuronal input to the relevant area of the brain and its processing

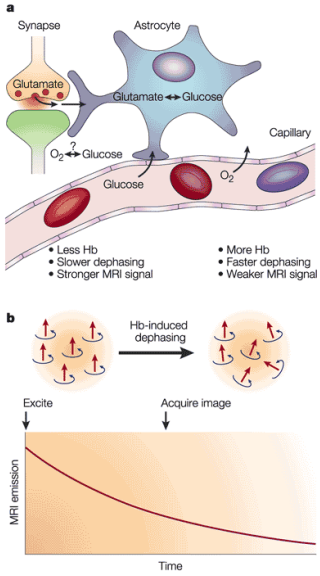

Figure 1.2: *Figure shows the relationship between synaptic activity, neurotransmitter recycling and metabolic demand (part a), and the effect of deoxyhemoglobin on the MRI signal (part b), depicting the three phases of the BOLD fMRI response to increases in neuronal activity: 1) an initial, small decrease in image intensity below baseline (during the initial period of oxygen consumption), 2) followed by a large increase above baseline (an oversupply of oxygenated blood, which is only partially compensated for by an increase in deoxygenated venous blood volume), and then 3) by a decrease back to below baseline again. Adapted from [4].*

there rather than the long-range signals transmitted by action potentials to other regions of the brain ([5], Fig. 1.3).

1.1.3 *The rise of resting-state fMRI*

Interestingly, around 15 years after the invention of fMRI, studies started to examine the possibility of measuring the level of co-activation of spontaneous functional MRI time-series, recorded during rest [8, 9]. Biswal and colleagues were the first to demonstrate that during rest the left and right hemispheric regions of the primary motor network are not silent, but show a high correlation between their fMRI BOLD time-series [10]. Studies showed that during rest the brain network is not idle, but rather shows a vast amount of spontaneous activity that is highly correlated between multiple brain regions [11] (Fig. 1.4).

Of special interest are the low frequency oscillations ($0.01 - 0.1$ Hz) of

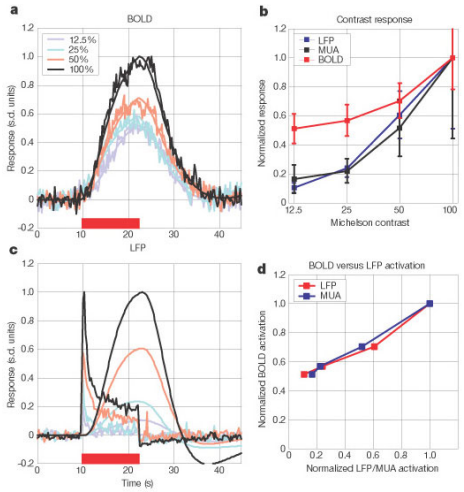

Figure 1.3: *Relationship between the BOLD fMRI signal, intra-cortical local field potentials (LFPs) and multi-unit spiking activity (MUA) in anaesthetized monkeys. Figure shows fMRI responses to pulse stimuli at four different contrasts (12.5, 25, 50 and 100%). a) Mean fMRI response superimposed with a model estimated with nonlinear curve fit. The scale parameter of the model was taken as the response amplitude. b) Normalized response amplitude of LFP and MUA against contrast. Data from five sessions with a pulse duration of 12.5 s. c) LFP responses for four different contrasts. Smooth lines are the result of convolution of the neural responses with the impulse response estimated by correlation analysis. d) Normalized BOLD response as a function of LFP and MUA. Responses were normalized by dividing each response by the maximum response. Adapted from [5].*

resting-state fMRI time-series [13]. The true neuronal basis of these low frequency resting-state fMRI oscillations is not yet fully understood and in the past years there has been an ongoing debate on whether these resting-state BOLD signals result from physiological processes, like respiratory and fMRI correlations and electrophysiological recordings of neuronal firing [14].

In general, a fast growing body of neuroimaging studies support the notion that resting-state BOLD fluctuations are generated from spontaneous neuronal activity [9, 11]. This makes spontaneous resting-state fMRI oscillations a robust measure to examine functional connections between brain regions (i.e. functional connectivity) on a whole-brain scale. The state of the art of functional connectivity will be extensively reviewed in the next chapters.

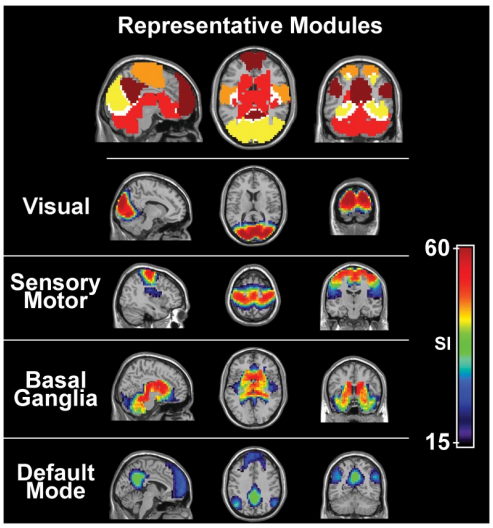

Figure 1.4: *Study showing four functional resting state networks that were found to be highly consistent across subjects. These modules include the visual (yellow), sensory/motor (orange) and basal ganglia (red) cortices as well as the default mode network (precuneus-posterior cingulate, inferior parietal lobes, and medial frontal gyrus; maroon). Overlap among these modules was present but minimal (white). Adapted from [12].*

1.2 *Diffusion weighted imaging*

Diffusion weighted imaging is a MRI method that measures the local mobility profile of water molecules. It is unique in its ability to measure diffusion non-invasively, making it the method of choice for in vivo diffusion measurements. By measuring the average diffusion of water molecules in the brain, diffusion MRI allows to model the geometry of the underlying tissue microstructure.

1.2.1 *Diffusion processes*

At the microscopic scale, individual water molecules are constantly in motion as a result of their thermal energy. This phenomenon is referred to as "Brownian motion". Diffusion, or the process in which particles move from a region of higher to one of lower concentration, can be considered the macroscopically observable effect of the microscopic Brownian motion of particles. The physical law describing this process is called Fick's first law [15]:

$$J = D\nabla C \tag{1.1}$$

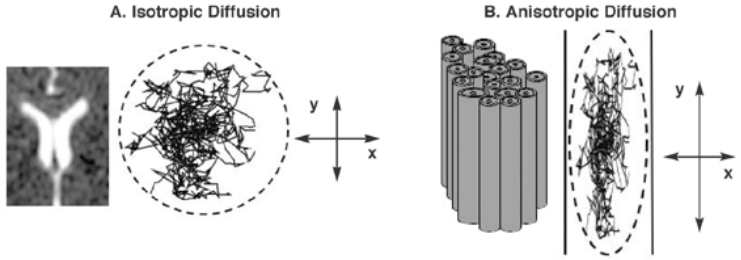

Figure 1.5: *Isotropic and anisotropic diffusion. (A) Water molecules in the brain are constantly moving (i.e., in Brownian motion). When motion is unconstrained, as in the large fluidfilled spaces deep in the brain (i.e., the ventricles, as illustrated in the MR image on the left), diffusion is isotropic, which means that motion occurs equally and randomly in all directions. (B) When motion is constrained, as in whitematter tracts (illustrated on the right), diffusion is anisotropic, meaning that motion is oriented more in one direction than another (e.g., along the y axis rather than along the x axis). Adapted from [17].*

Fick's first law embodies the notion that particles move from regions of high concentration to regions of low concentration. The rate of this flux is proportional to the concentration gradient C and to the diffusion coefficient D. While the random nature of Brownian motion prevents us from predicting the behavior of a single water molecule, it is possible to predict the behavior for a large collection of water molecules. In 1905, Einstein introduced the "diffusion probability density function", $p(r)$, which quantifies the fraction of particles that will have been displaced by r within a certain "diffusion time" t. Using this framework, Einstein showed that, provided that the number of particles is sufficiently large and provided that they are free to diffuse, $p(r)$ takes the form of a Gaussian distribution [16](Fig. 1.5).

The width of this Gaussian distribution is determined by the diffusion coefficient D and the diffusion time t. In an environment without any hindrances, e.g. a glass of water, the diffusion of water molecules is the same regardless of the direction in which it is measured. However, in fibrous tissue, such as the brain white matter, water molecules tend to diffuse more along the fibers, making the diffusion profile anisotropic. Therefore, the diffusion coefficient that we measure in a biological sample, is usually referred to as the apparent diffusion coefficient (ADC) [18]. This property of diffusion is key to diffusion MRI and it allows to acquire information about the microstructural features of biological tissue.

1.2.2 *Measuring diffusion in the brain*

In a typical MRI $T1$-weighted image, water molecules in a sample are excited with the imposition of a strong magnetic field. This causes many of the protons in water molecules to precess simultaneously, producing signals in MRI. To sensitize MRI images to diffusion, instead of a homogeneous magnetic field, the homogeneity is varied linearly by a pulsed field gradient. Since precession is proportional to the magnet strength, the protons begin to precess at different rates, resulting in dispersion of the phase and signal loss. Another gradient pulse is applied in the same magnitude but with opposite direction to refocus or rephase the spins. The refocusing will not be perfect for protons that have moved during the time interval between the pulses, and the signal measured by the MRI machine is reduced. This "field gradient pulse" method was initially devised by Stejskal and Tanner [19] who derived the reduction in signal due to the application of the pulse gradient related to the amount of diffusion that is occurring through the following equation:

$$S(b) = S_0 e^{-bADC} \tag{1.2}$$

where S_0 is the signal intensity without the diffusion weighting, and S is the signal after the pulse gradient is applied. The coefficient b bundles together all the diffusion MRI acquisition parameters, such as gyromagnetic ratio, applied pulse strength, time between pulses and pulse duration. The variable ADC in Equation 1.2 is the apparent diffusion coefficient, because diffusion in biological tissue is influenced by various factors (e.g. cellular structure). Diffusion imaging acquisitions typically apply the pulsed gradient sequence described above along many unique gradient directions [18]. In this manner the acquired signal reflects the rate of diffusion of water molecules within each voxel along the direction of the applied magnetic field. By mapping the diffusion profile in each direction one can infer properties about the macro and microscopic structure of the tissue being studied [20]. The analysis of diffusion-weighted images generally requires the selection of a model to represent the diffusion profile in each voxel. The typical choice is a tensor, and tensors can be fit to the diffusion signal in each voxel using a variety of different methods [21]. Briefly, the goal is to solve Equation 1.3 for $\mathbf{D}$.

$$S(g,b) = S_0 e^{-bg^T \mathbf{D} g} \tag{1.3}$$

Where $g = [g_x, g_y, g_z]$ is the gradient direction defined as a vector, and $\mathbf{D}$ is a tensor defined by:

$$\mathbf{D} = \begin{pmatrix} D_{xx} & D_{xy} & D_{xz} \\ D_{yx} & D_{yy} & D_{yz} \\ D_{zx} & D_{zy} & D_{zz} \end{pmatrix} \tag{1.4}$$

In neuroimaging studies, tensors are usually analyzed with metrics calculated from the eigenvalues of D. The most common measures are fractional anisotropy (FA) and mean diffusivity (MD). Mean diffusivity is calculated using Equation 1.5:

$$MD = \frac{\lambda_1 + \lambda_2 + \lambda_3}{3} \tag{1.5}$$

Where λ_1, λ_2, and λ_3 represent the eigenvalues of the tensor. Fractional anisotropy, which describes how directional a tensor is, can be calculated using:

$$FA = \sqrt{\frac{1}{2} \frac{(\lambda_1 - \lambda_2)^2 + (\lambda_1 - \lambda_3)^2 + (\lambda_2 - \lambda_3)^2}{{\lambda_1}^2 + {\lambda_2}^2 + {\lambda_3}^2}} \tag{1.6}$$

In order to convey anatomical qualities in tensor data, studies often colour each voxel using a convention based on the principal direction of its tensor. For example, in a voxel with the principal direction oriented left-to-right, the voxel may be given a red-green-blue (RGB) value for red. The standard convention is that left-to-right is red, anterior-to-posterior is green, and inferior-to-superior is blue. These colour maps can also be modulated by the FA values in each voxel, leading to what is known as an RGB-FA image [22] (Fig. 1.6).

In the human brain tensors cannot fully portray the real-world properties of the voxels they represent, as most white matter voxels contain more than one unique fiber population [24]. Their primary fault is their unidirectionality, and higher-order diffusion models aim to address this issue. This might be overcome by estimating fiber orientation distribution functions (FODs). Fiber orientation distributions represent the distribution of fiber tracts inside

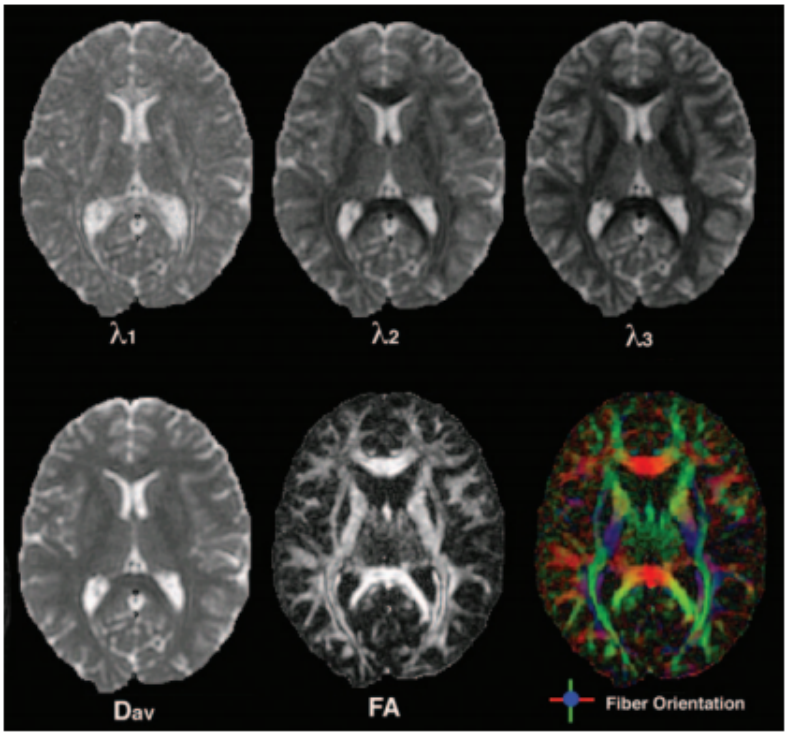

Figure 1.6: *Top row: The first, second, and third eigenvalues of the diffusion tensor are shown with the same intensity scaling. Note that the eigenvalues are always ordered in descending order of intensity with the first eigenvalue being the greatest. Bottom left: The directionally averaged diffusivity (i.e. mean diffusivity) is the mean of the 3 eigenvalues. Bottom middle: The FA indicates the coherence of white matter bundles. Bottom right: The FA map can be colorized to show the orientation of the primary eigenvector with left-to-right oriented axonal fibers green, anterior-to-posterior fibers red, and inferior-to-superior fibers blue. Colors are additively mixed to represent fiber populations oriented between these 3 cardinal axes. [23]*

a voxel. As such, their derivation is based on the idea that the diffusion profile in any single voxel is the sum of the diffusion profile of all the fibers passing through the voxel. FODs are commonly fit using spherical deconvolution [25], which attempts to model the diffusion profile as a combination of spherical harmonic basis functions. It has been estimated that as much as 90% of the white matter contains multiple intersecting fiber populations [24]. FOD estimation approaches offer multi-direction intra-voxel fiber modelling which is imperative for accurate tractography.

1.2.3 *Fiber tractography*

Streamline tractography algorithms can be used to create wiring models of the brain. Generally, the idea of tractography is that an algorithm individually estimates multiple streamline pathways from one part of the brain to another based on the diffusion or fiber orientation model calculated at each voxel. Fiber tracks are seeded in white matter regions and progressive tracking steps are taken until the streamline is terminated. There are multiple approaches for choosing a direction to step in, as well as for evaluating the probability that two voxels are connected by a track. For an extensive review and quantitative comparison of tracking algorithms see [26]. When referring to the results of fiber tractography, one can use the terms "fibers", "tracks", and "streamlines" interchangeably, and these should not be confused with actual biological tracts [27] (Fig. 1.7).

Tractography has recently evolved from deterministic to probabilistic. In deterministic tracking a single path is estimated by choosing the best available direction at each progressive step. Probabilistic tracking, on the other hand, tests numerous paths for each fiber track before choosing the most likely. Anatomically defined masks (e.g. of grey matter and cerebrospinal fluid) can be used to terminate or otherwise prevent "false positive" streamlines from being considered in the final tractogram [28]. Once tractography is complete the subsequent analysis steps depend on the goal of the study. Many types of analysis involves the extraction of a structural connectivity matrix (i.e. connectome) from the tractogram. Connectome construction methods will be extensively reviewed in Chapter 2.

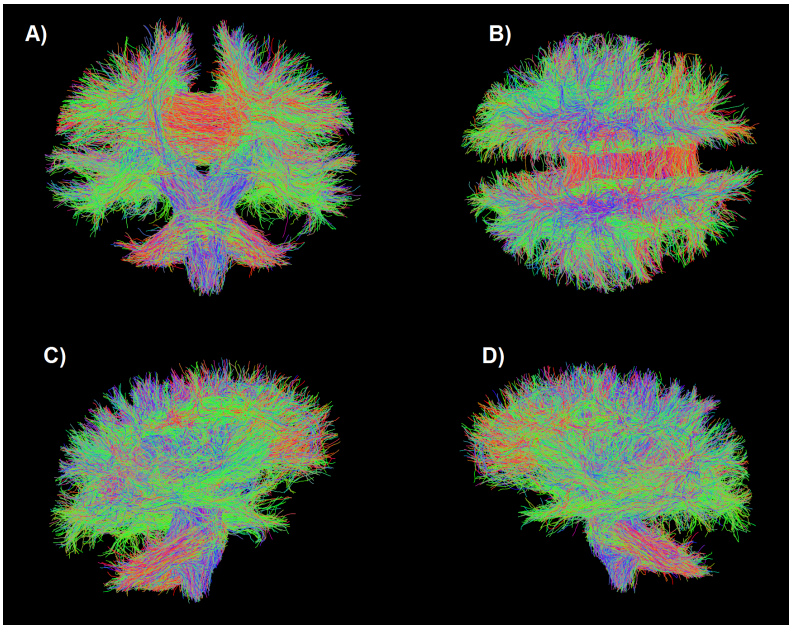

Figure 1.7: *A) Coronal B) Horizontal and Sagittal C) right and D) left views of a tractogram in a healthy human brain.*

1.3 Transcranial magnetic stimulation and electroencephalography

1.3.1 An overview of electroencephalography

Electroencephalography (EEG) is a technique for the direct recording of electrical activity in the brain through a set of electrodes placed on the scalp. Electrical activity was first recorded on the human scalp nearly a century ago [29]. The biological origin of the EEG signal is complex and has multiple components. For an in-depth review into neuronal polarization and EEG in general, the reader is referred to [30]. Excitatory and inhibitory post-synaptic potentials at pyramidal neurons in the cortex are thought to be the primary contributors to the EEG signal, which is thought to reflect thousands of neurons' synchronous activity (Fig. 1.8).

The rate, height, and length of the EEG signal vary in different parts of the brain, and each individual has a unique and characteristic pattern. The EEG is typically described in terms of [31] rhythmic activity. The rhythmic activity is divided into bands by frequency. These designations arose because

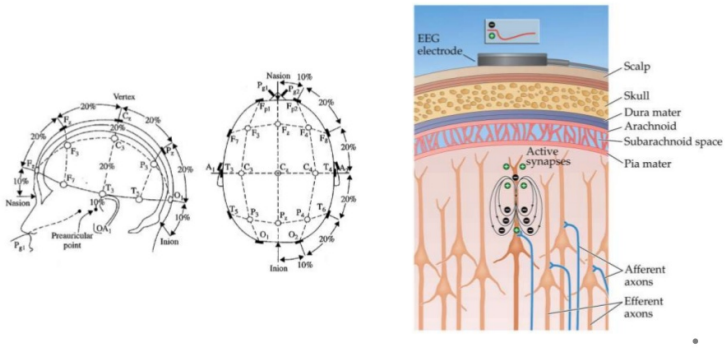

Figure 1.8: *Right) EEG results from the combined activity of a large number of similarly oriented pyramidal neurons. It reflects the synchronous post-synaptic activity of large neuronal ensembles. Left) EEG is recorded from electrodes placed on the surface of the scalp. The* $10-20$ *position system ensures consistent placement of the electrodes across the surface of the scalp independent of head size and shape, by using anatomical landmarks to determine specific distances across the head. Adapted from [31].*

rhythmic activity within a certain frequency range was noted to have a certain distribution over the scalp or a certain biological significance. Most of the recorded waves in a normal adult's EEG are the occipital alpha waves (8 to 13 Hertz). The beta waves (16 to 31 Hertz), obtained from the central and front parts of the head, are more closely related to the sensory-motor parts of the brain. In a normal EEG the frequencies are predominately within the range of alpha and beta rhythms at the rate of 1 to 30 hertz.

A common goal, known as source localization, is to identify the origin of signals within the head. Reconstructing the source of neural activity requires a number of key assumptions. The first, which is well established, is that a neural source can be approximated as an equivalent current dipole [32]. Next, a model must be chosen to approximate the geometry of the subject's head as well as the position of the electrodes. Once the head model is built, the next step is to construct a leadfield matrix to relate voltage values on the scalp with current sources in the brain. Constructing the leadfield is known as the forward problem.

Next, using the leadfield, algorithms are used to estimate the most likely configuration of sources that could produce the known scalp voltage profile. The inverse problem is analytically ill-posed, meaning that there is no unique correct solution. Algorithms must attempt to find the best possible solution given the data and adopted model. In inverse approaches, the model refers

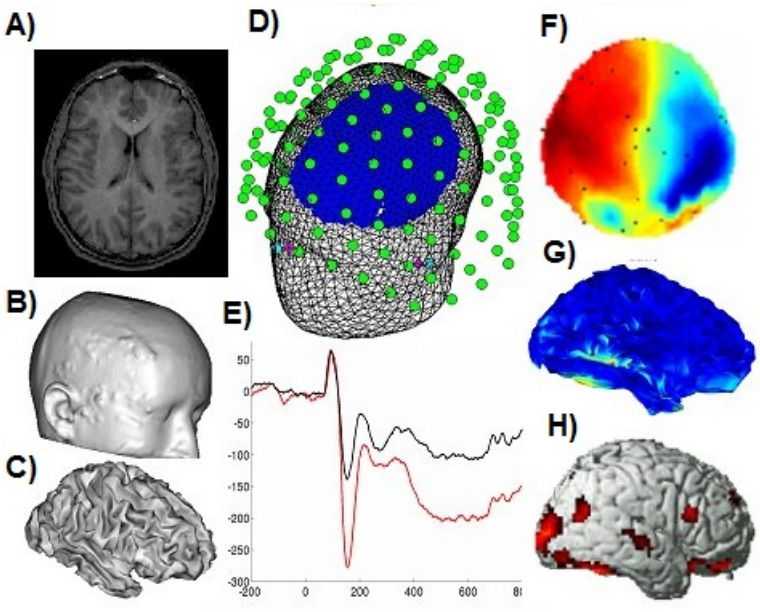

Figure 1.9: *Flowchart of source localization using EEG signal and MR images. A conductive head volume is modeled by adapting the individual MRI A) to the corresponding canonical meshes B,C); the EEG response in the cerebral cortex is then modeled as a three-dimensional grid of N fixed dipoles D,F) oriented normally to cortical surface; finally, the single trial distribution of electrical sources in the brain is estimated E) and statistical testing to avoid spurious or artifactual sources G,H) is carried out. Adapted from [31].*

to the number and type (e.g. varying orientation and/or amplitude and/or position) of dipoles that the algorithm will try to fit. Inverse solutions can be divided into two categories: parametric, in which the locations of one or more dipoles are estimated, and non-parametric, in which dipole locations are fixed and their amplitude and orientation are estimated [33] (Fig. 1.9).

1.3.2 Combining magnetic pulses with EEG

Transcranial magnetic stimulation (TMS) is a method for non-invasively activating the brain by modulating the voltage over the membranes of cortical neurons, by means of electromagnetic induction [34]. In TMS, short current pulses are driven through a coil, which is placed against the subject's head [35]. These magnetic pulses induce secondary ionic currents in the brain that penetrate the membranes of the neurons, resulting in an action potential or excitatory/inhibitory post-synaptic potential. The stimulating effect is

strongest at the cortical surface [36]. As the magnetic field falls off rapidly with distance from the coil [37], it only directly activates neural elements superficially (that is, on the surface of the cortex) or in the white matter underneath the stimulation site, limiting the number of brain structures one can reach. Afterwards, From the site of cortical stimulation, the neuronal signal then propagates along intra- and inter-hemispheric association fibers to other cortical areas and to deeper neural structures.

Combined with magnetic resonance imaging and EEG, TMS is developing towards a brain research method in which stimulation is navigated into a desired brain area [38, 39] and the concurrently recorded scalp potentials are processed into source images of the TMS-evoked neuronal activation [40]. EEG allows to study the instantaneous neuronal effects of TMS in the brain with a millisecond time scale, which is presently not possible with any brain imaging method.

EEG, with excellent temporal resolution, provides a complementary method for mapping TMS-evoked activation. In addition, EEG has appeared to be a remarkably sensitive measure of the brain effect of TMS [41]. However, while TMS systems have been available for a long time, EEG amplifiers have not been compatible and recording artefact-free response was impossible. EEG amplifiers have then been equipped with sample and-hold circuits to prevent the recording of the powerful TMS-related artefact. This allowed recording the TMS evoked potentials response with milliseconds time scale, which reliably reflects the state of excitability of underlying cortical circuits [42] (Fig. 1.10).

Researchers interested in human cognition have widely adopted TMS as a tool to disturb neuronal processing within selected cortical regions, thus enabling them to deduce the importance of the disturbed area on task performance [43]. Combined with data from functional imaging studies, this information may provide some inference about the causality between distinct task-related activations within the network of activated brain areas.

The avail of TMS-EEG for the study of connectivity arises from an utterly different perspective: in the resting brain, one cortical region is stimulated and the spreading of the neuronal activity is traced based on EEG signals and their source reconstructions. TMS-EEG endows one with the possibility of mapping cortical connectivity with the implicit knowledge about causal

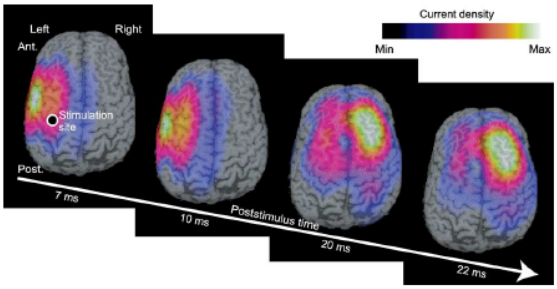

Figure 1.10: *Minimum-norm current-density estimates displayed above cortical surface segmented from a 3D magnetic resonance image set, illustrating the spreading of neuronal activation after stimulation of the primary motor cortex, for one subject. The black circle in the first image indicates the stimulation site. Activation spread from the stimulation site first to the neighboring cortical areas, mainly parieto-temporally. Contralateral activation emerged at 20 ms and was strongest at 22 ms at frontal regions. The studied latency range was 730 ms poststimulus. Note that the colors of individual images are auto-scaled so that the amplitudes of current density are not directly comparable. Ant. = anterior; Post. = posterior. Adpated from [42].*

relations of the evoked activations; the causality between the detected activations is readily evident through their temporal sequence, as long as the temporal resolution of EEG is sufficient to detect the neural phenomena.

To trace the spreading of TMS evoked neuronal activity, the minimum-norm estimate [45] has been applied for the assessment of cortical current density [41]. Stimulation of the sensorimotor regions of the cortex evoked activity in the vicinity of the coil within 7 ms poststimulus (earlier activity could not be detected because of the gating settings used in the recordings; [46]). The initial activity spread to the surrounding cortical areas as well as to the contralateral cortex, reflecting the area-to-area connectivity of the brain.

How are these activation patterns then related to neuroanatomical connectivity? The intrahemispheric spread of activity from the sensorimotor region near the hand area of M1 is possible via its extensive connections to the supplementary motor area, the premotor cortex, and the primary and secondary somatosensory cortices [47]. The interhemispherically conducted activity, initially peaking over frontal areas close to the midline, can be explained with commissural pathways from M1 to the homologous contralateral cortical regions, to the contralateral supplementary motor area, and the premotor cortex [48] (Fig. 1.11).

The endeavor of the TMS-EEG studies has appeared twofold. One focus

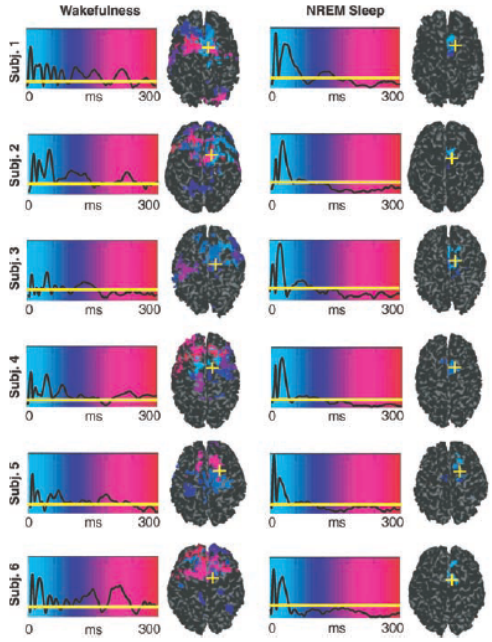

Figure 1.11: *Spatiotemporal TMS-induced cortical current maps during wakefulness and NREM sleep in all six subjects. Black traces represent the global mean field powers, and the horizontal yellow lines indicate significance levels. For each significant time sample, maximum current sources were plotted and colorcoded according to their latency of activation (light blue, 0 ms; red, 300 ms). The yellow cross marks the TMS target on the cortical surface. Adapted from [44].*

has been to describe the nature of the TMS-evoked potentials, to extend the understanding of the activation mechanisms of TMS. The other objective has been to confirm the potential of TMS/EEG as a tool for basic neurophysiological research and possibly for diagnostic purposes [42]. TMS-EEG seems to be a promising tool to assess brain functions in both healthy subjects and pathological conditions [37]. Specifically, its utility in the assessment of non communicative patients will be discussed in Chapter 3.

2 BRAIN CONNECTIVITY: AN INTRODUCTION.

Although graph theory has been around since the 18th century, the field of network science is more recent and continues to gain popularity, particularly in the neuroimaging community. Quantitative analysis based on network scientific methods have become more commonly used to study the brain as a network, giving rise to the area of research so called Brain Connectivity. This chapter will review this progressive shift from graph theory towards brain connectivity, pointing out the main differences between functional connectivity (FC) and structural connectivity (SC) brain models.
***Keywords**: Graph theory, network science, brain connectivity, functional connectivity, structural connectivity.*

2.1 *From network science to brain networks*

Networks are everywhere in the physical world. The first mathematical formulation of real problems using network theory roots back in the past. In 1736, Euler showed that it was impossible to pass through the seven bridges of the city of Königsberg exactly once and return to the starting point (Fig.2.1).

To prove this hypothesis, Euler represented the problem as a graph, and his work [50] is considered to be the origin of a new area of mathematics: graph theory. Nowadays, graph theory spreads over many areas of science, boosted by to the dual discoveries of small-worldness (i.e. the presence of high-degree nodes or hubs [51]) and scale-free [52] distribution in social and natural networks (Fig. 2.2).

The rise of network science [53] and mathematical advances in graph theory has improved our understanding in the characterization of the structure and function in a network. Nonetheless, only in the past 2 decades, the developments in the quantitative analysis of complex networks have been finally

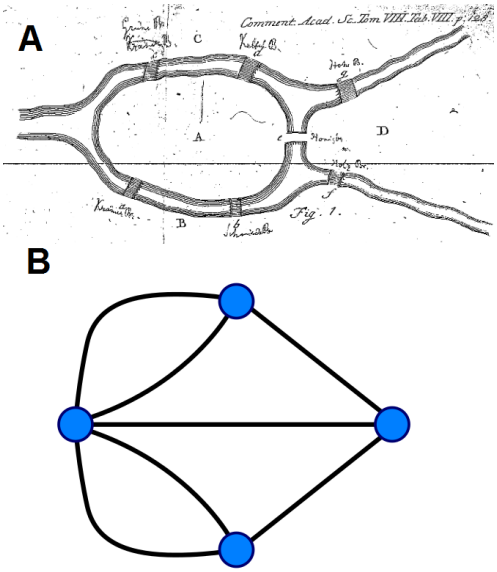

Figure 2.1: *A) Map of Königsberg in Euler's time showing the actual layout of the seven bridges, highlighting the river Pregel and the bridges. B) Graph representation of the seven bridges problem: one replaces each land mass with an abstract vertex, i.e. a node, and each bridge with an abstract connection, i.e. an edge. Adapted from [49].*

applied to studies of brain network organization, first in animals, then in humans [54, 55].

As a matter of fact, the human brain may be seen as a very efficient network, in which a huge number of different regions with different functions are unceasingly exchanging information with each other [56].

2.2 *Structural networks in the human brain*

The anatomical configuration of brain networks has always been of great interest in neuroscience. Structural brain networks can be represented as graphs comprised of nodes (vertices) symbolizing neural elements (e.g. brain regions) and edges denoting physical connections (e.g. axonal bundles) [49].

For graphical analysis of tract-tracing data on large-scale axonal projections between regions of mammalian cortex, nodes have usually been defined cytoarchitectonically as Brodmann areas [57]. In some of the early graphical studies of human neuroimaging data, an approximately equivalent convention was followed to define nodes [58]. Each individuals brain image was coregistered with an anatomically parcellated template image, and the

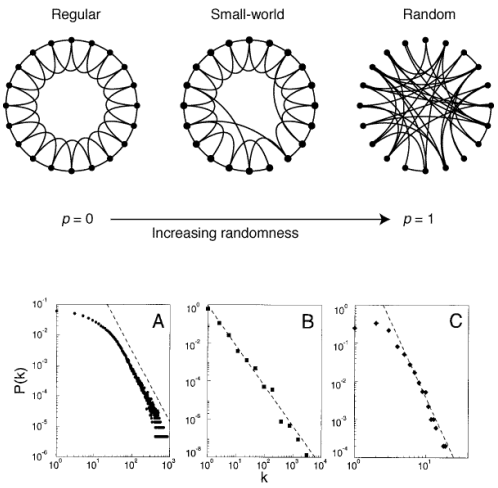

Figure 2.2: *Two seminal results of modern network science. Top) The rewiring procedure used by Watts and Strogatz [51] for interpolating between a regular ring lattice and a random network, without altering the number of vertices or edges in the graph. They started with a ring of n vertices, each connected to its k nearest neighbours by undirected edges. With probability p, they reconnected this edge to a vertex chosen uniformly at random over the entire ring. Three realizations of this process are shown, for different values of p. For $p = 0$, the original ring is unchanged; as p increases, the graph becomes increasingly disordered until for $p = 1$, all edges are rewired randomly. One of their main results was that for intermediate values of p, the graph is a small-world network, i.e. highly clustered like a regular graph, yet with small characteristic path length, like a random graph. Adapted from [51]. Bottom) Exploring several large databases describing the topology of large networks that span fields as diverse as the (A) Actor collaboration, (B) WWW and (C) Power grid data, Barabasi and Albert [52] showed that, independent of the system and the identity of its constituents, the probability $P(k)$ that a vertex in the network interacts with k other vertices decays as a power law. This result indicated for the first time that large networks self-organize into a scale-free state. Adapted from [52].*

mean signal over all voxels in each region of the template image was taken as the nodal value at that anatomical location. Several similar but not identical template images are available and have been used for this purpose. The main advantage of using an anatomically defined template for nodal parcellation of neuroimaging data is that it can support direct comparison of results to prior neuroimaging or primate neuroanatomy studies using the same or a similar template (Fig. 2.3).

The main disadvantage, which is probably more significant, is that the size of different template regions can vary considerably. Nodal values obtained by averaging across many voxels in larger regions will be less noisy

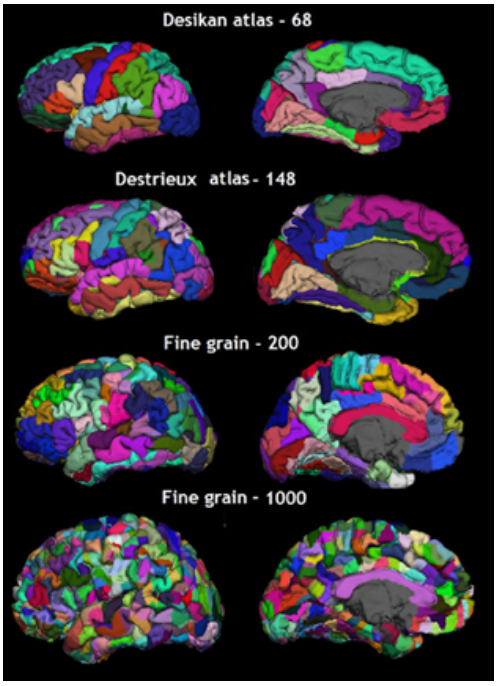

Figure 2.3: *Different possibilities of parcellation schemes for brain connectivity analysis: the Freesurfer Desikan atlas [59] of* 68 *brain regions and the Destrieux atlas of* 148 *[60]; the fine grained of* 200 *and* 1000 *regions as in [61]. Adapted from [61].*

than nodal values estimated by averaging across smaller regions, leading to a bias in favor of stronger statistical associations between larger regions of the template image [62].

Once defined the nodes, anatomical connectivity edges can be defined in different ways. For diffusion weighted imaging, it is possible to assign a probability of axonal connection between any pair of gray matter regions on the basis of tractographic analysis of an individual dataset. The association between two nodes i and j may be defined as simple count of the tracts passing through the two nodes, which can be normalized by the surface of each node to avoid the bias across smaller regions, or the mean FA value along the tract, or even the mean fiber lenght (in mm) separating the two nodes [63].

In the last decades several studies have been trying to map the structural networks of the human brain (i.e. the human connectome [64]) at the scale of cortical regions, by means of diffusion imaging and tractography. In the seminal work of 2008, Hagmann et al. [65] demonstrated the existence of modules, hubs and a structural core in the human anatomical network de-

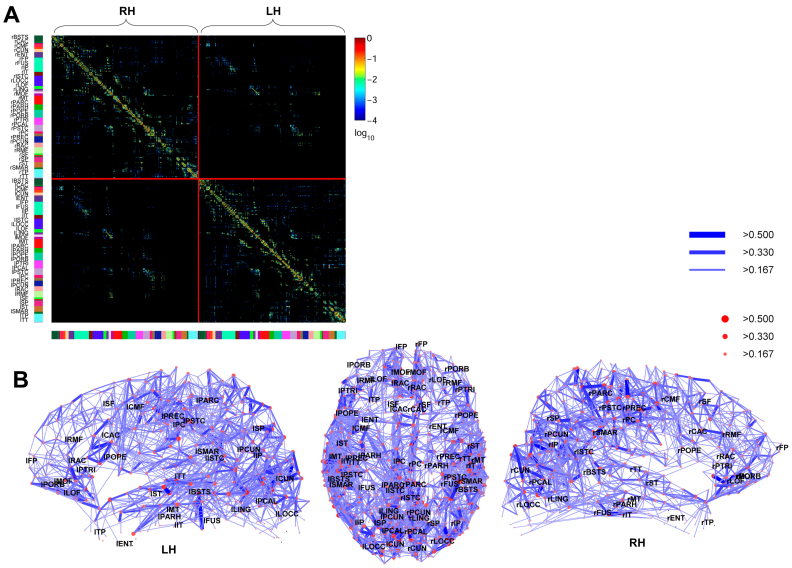

Figure 2.4: *The structural core of human cortex (i.e. the connectome).(A) Matrix of fiber densities (connection weights) between all pairs of n = 998 cortical regions of interest (ROIs). ROIs are plotted by cerebral hemispheres, with right-hemispheric ROIs in the upper left quadrant, left-hemispheric ROIs in the lower right quadrant, and interhemispheric connections in the upper right and lower left quadrants. All connections are symmetric and displayed with a logarithmic color map. (B) Dorsal and lateral views of the connectivity backbone. Adapted from [65].*

rived from DWI, suggesting the emergence of complex cognitive operations from the structural organization of distributed brain networks (Fig. 2.4).

Other studies mapping white matter pathways of cortical and basal brain grey matter areas [66, 67] showed that the precuneus, the insula, the superior parietal cortex and the superior frontal cortex, appear to have highly connected nodes, and thus to constitute putative hubs.

Despite being a rising field, the structural connectivity analysis of the human brain already helped neuroscientists to identify several highly connected and highly central regions, stressing the importance of the network hubs and their connections in the integration of information for an efficient communication in the brain.

2.3 *Functional networks in the human brain*

Even though structural connectivity helps to understand the basic core of anatomical connections, it is worth to investigate functional networks in or-

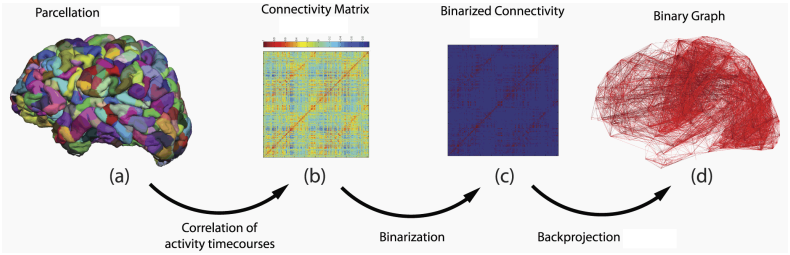

Figure 2.5: *Whole-brain functional connectivity pipeline: first, data are derived from fMRI timecourses in cortical areas (a), and calculation of a correlation matrix between every pair of these regions is carried out (b). The matrix is then thresholded (c), and transformed into a binary graph. Adapted from [68].*

der to elucidate how this architecture supports neurophysiological dynamics. Functional neuroimaging studies have provided a huge amount of information about the role of functionally interacting brain regions in the human brain.

Given a multivariate time series like an fMRI dataset (or EEG recordings), the first step is to describe the statistical association between each nodal time series. In general, we estimate the pairwise association $a_{i,j}$ between the ith and jth nodes, $i = j = 1, 2, 3, ..., N$ and compile these statistics for all possible pairs in a N N interregional association matrix, A. Many measures of association could be used for this purpose, and they can be categorized by various criteria (Fig. 2.5).

A functional connectivity statistic measures the extent to which two processes behave similarly over time as the temporal dependence of neuronal activity patterns of anatomically separated brain regions [69]. Thus, the association matrix generated by estimating the functional connectivity between each pair of nodes will be symmetric, whereas the association matrix generated by an effective connectivity analysis need not be. Some measures of functional connectivity, such as the correlation coefficient, will only capture linear interactions between time series, whereas other measures, such as the mutual information [70] or synchronization likelihood [71], are sensitive to both linear and nonlinear interactions. Some measures are sensitive to association between nodal time series subtended by a specific frequency interval, such as the wavelet correlation [72] or coherence in the frequency domain [73]. Some measures, such as the partial correlation [74] or partial coherence [73], are particularly sensitive to the specific association between each pair

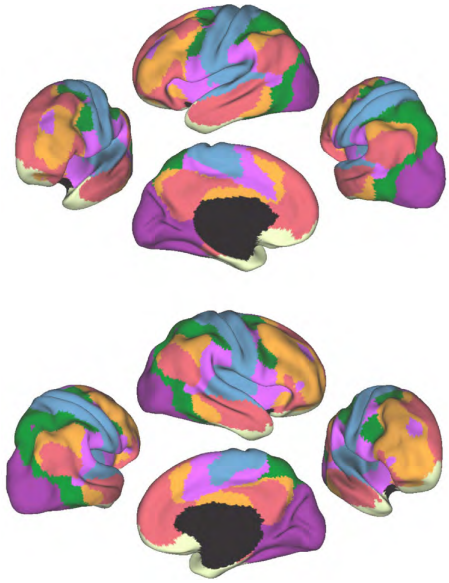

Figure 2.6: *A coarse (7-network) parcellation of the human cerebral cortex based on* 1000 *subjects. To provide the best estimates of the* 7 *cortical networks, clustering was performed on the fMRI data of the full* 1000 *subjects. A salient feature is the separation of the early sensory and late motor cortices (blue and purple) from the association cortex. The association networks converged and extended on networks previously described in the resting state literature, including the dorsal attention (green), ventral attention (violet), frontoparietal control (orange), lymbic (cream) and default networks (red). Adapted from [77].*

of nodes and will discount third-party effects, such as shared inputs from a third node or global mode of covariation.

To date, almost all graphical analyses of fMRI data have been based on a symmetric association matrix generated by some measure of functional connectivity between nodes. Studies have been shown the feasibility of examining co-activations of functional MRI time-series measured during task or rest [13]. On longer timescales of seconds to minutes, correlations between spontaneous fluctuations in brain activity form functional networks that are particularly robust (e.g. the default mode network) [75, 76, 77] (Fig. 2.6).

To examine whole-brain connectivity patterns, several model-free methods have been suggested and successfully applied to resting-state time-series, including principal component analysis (PCA) [78], independent component analysis (ICA) [79], Laplacian [80] and normalized cut clustering [81]. ICA-based methods [82, 83] are perhaps the most commonly used and have been

reported to show a high level of consistency [84]. ICA methods are designed to search for a mixture of underlying sources that can explain the resting state patterns, looking for the existence of spatial sources of resting-state signals that are maximally independent from each other. ICA methods for resting-state fMRI are powerful methods as they can be applied to whole-brain voxel-wise data and as the temporal signals of the independent resting state components can be easily selected for further examination of possible group differences between healthy controls and patients. For example, group ICA resting-state fMRI studies have consistently reported the formation of the so called default mode network during rest [82, 84], which have been extensively confirmed by the other methodologies.

Recently, other methods to investigate brain functional systems have recently been developed, including mathematical models of dynamic and directed connectivity between regions. Dynamic functional connectivity analysis has been proposed to quantify changes in functional connectivity metrics over time scales shorter than the whole fMRI acquisition period [85]. Directed, (or effective, following Friston [86]) connectivity models, such as dynamic causal modelling [86] or Granger causality [87], involve estimating the extent to which one process can be predicted or explained by the other. All these different methods aim to enrich the understanding of large-scale network activity. Even if the field of dynamic and directed FC is presently exploratory, it may represent an extraordinary new frontier in the study of brain connectivity.

2.4 *Structure-function relations in the human brain*

In which way structural connectivity is shaping functional connectivity patterns in the brain? From a network perspective, the functionality of a node is partly constrained by its structural connections with other nodes in the network [88]. Resting state functional networks provide a way to study the interaction between function and structure in the brain. Direct matching of structural and functional connectivity in healthy volunteers [89, 90] suggest that structural connections are highly predictive of functional connections (Fig. 2.7).

Computational models may give new insights on the structurefunction

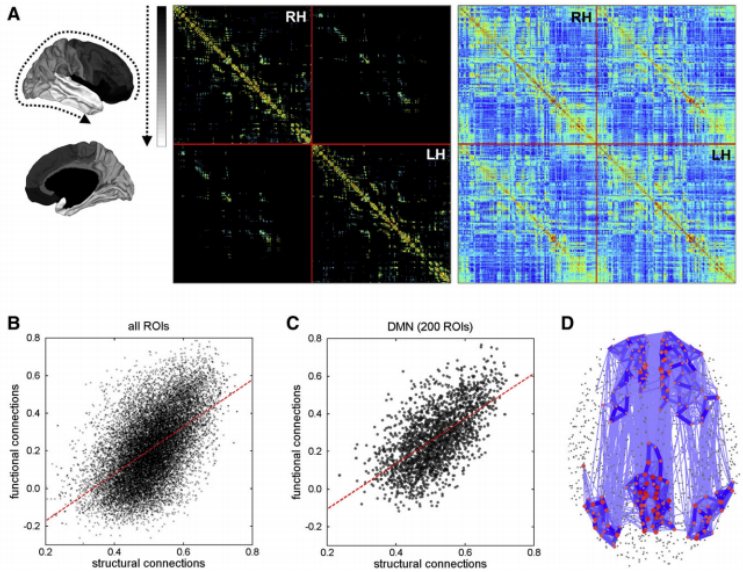

Figure 2.7: *Direct comparison of structural and functional connectivity in the human brain. (A) Structural connectivity derived from diffusion imaging and resting-state functional connectivity derived with functional neuroimaging, from the same dataset of [65]. Maps show connectivity among* 998 *cortical regions of interest (ROIs) in an anteriorposterior-ortemporal arrangement to emphasize spatial organization. (B) Scatter plot of structural connections and corresponding functional connections (correlation* $r = 0.54$*). (C) Scatter plot of structural connections and corresponding functional connections (correlation* $r = 0.61$*) for the* 200 *ROIs that form the default mode network (DMN). (D) Location of the* 200 *DMN ROIs and their structural interconnections. Adapted from [89]*

relations in brain networks. Simulation studies of large-scale cortical networks showed the rising of realistic patterns of modeled BOLD resting-state correlations that depend on the topology [91] and time delays [92] of the structural coupling matrix. These findings indicate that the brains structural and functional networks are intimately related and share common topological features, such as modules and hubs, even though the relationship is not clearly assessed yet [93].

2.5 *Brain connectivity in neurological diseases*

One application of direct clinical impact of brain connectivity may be to provide new measures to quantify differences in the functional or structural patterns of brains with neurological disorders (an example is shown in Fig. 2.8). Several studies have found that brain networks derived from fMRI or struc-

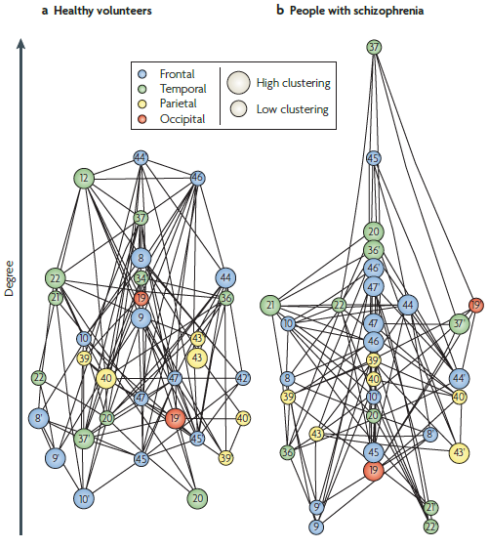

Figure 2.8: *Graphical visualization of brain networks in healthy volunteers (a) and people with schizophrenia (b). Nodes are ordered according to their degree (y-axis). Size of nodes indicates greater than (large) or less than (small) average clustering. Color of the nodes indicates lobe location: frontal (blue), temporal (green), parietal (black), or occipital (red). Lettering indicates approximate Brodmann area, and the denotes left-sided regions. Note that highly clustered nodes are concentrated at the bottom, which is dominated by highly connected nodes (many of them frontal) with low clustering; conversely, in people with schizophrenia, highly clustered nodes are more evenly distributed in terms of their degree, and frontal hubs are less prominent. Adapted from [98].*

tural MRI data are disrupted in patients with schizophrenia or alzheimers disease (aD) [94, 95]. In an fMRI study of aD, clustering was significantly reduced at a global level (in whole-brain networks operating at frequencies below 0.1 Hz) and global clustering was able to discriminate aD patients from age-matched comparison subjects with high specificity and sensitivity [96]. In the same way, the small-world properties of low-frequency functional networks derived from fMRI data were shown to be impaired in patients with schizophrenia [97, 98](Fig. 2.8).

The task of separating patient groups in neurological disorders through networks features has been made complicated by the clinical heterogeneity of the samples and of the analytic methods employed. Nonetheless, the number of studies attempting to map network differences in several neurological disorders and conditions (such as epilepsy [99], attention-deficit hyperactivity disorder [100] or spinal cord injury [101]) is continuously growing. In the last

decade, brain connectivity methodology has been also applied for investigating pathological and pharmacological modifications of levels of consciousness. The current state of the art of the field will be extensively reviewed in the next chapter.

BRAIN CONNECTIVITY AND CONSCIOUSNESS: STATE OF THE ART.

3

The last 15 years witnessed a growing interest in the investigation of brain function in survivors to severe brain injuries with disorders of consciousness (DOC) as well as in induced alterations of levels of consciousness. At the same time, the use of neuroimaging as a new tool to detect different states of consciousness has boosted this line of research, with particular attention devoted to brain connectivity studies. This chapter will review the state of the art of several brain connectivity methods and correspondent main findings in the exploration of different levels of consciousness.
***Keywords**: Brain connectivity, DOC patients, consciousness*

3.1 *An operational definition of levels of consciousness*

A proper definition of consciousness is still argument of debate for both the scientific and philosophical communities [102]. When scientifically approaching the matter, it is worth to clarify the difference between levels and the contents of consciousness [103]. Levels of consciousness refers to the ability to perceive anything [104]: this ability ranges from coma to complete wakefulness [105]. The contents of consciousness refer to any of the particular perceptions that can be experienced during a normal wakefulness state [106]. Here, we will focus on the operational definition of levels of consciousness, and its two main features, awareness and wakefulness (or arousal [107]) [108].

Awareness is defined as the capability to perceive the self and its surroundings [109]. Wakefulness describes the state of arousal [110]. Wakefulness generally correlates with awareness; an enhance in arousal is usually followed by an augment of the conscious experience. For example, during coma and anesthesia, awareness and wakefulness decline simultaneously:

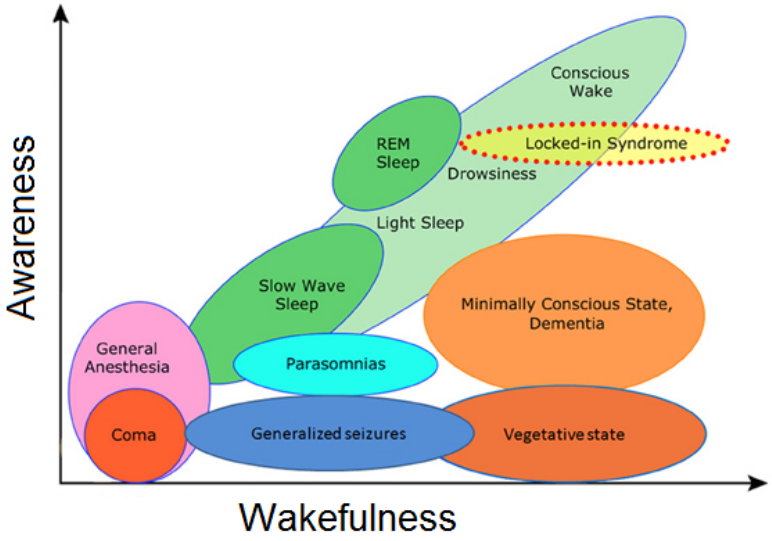

Figure 3.1: *Oversimplified illustration of the two major dimensions of consciousness: arousal or wakefulness and awareness or experience. Adapted from [110].*

the drowsier one becomes, the less aware of his surroundings and himself [107] (Fig. 3.1).

The definition of levels of consciousness as a combination of awareness and wakefulness comes in handy when facing disorders of consciousness (DOC). This devastating spectrum of clinical conditions characterized by the massive breakdown in global conscious states due to severe brain injury.

Indeed, in some cases of DOC, arousal and awareness are dissociated. Patients with unresponsive wakefulness syndrome/vegetative state (UWS) show no signs of awareness but do have an altered sleep and wake cycle; patients in a minimally conscious state (MCS) retain minimal non-reflexive and highly fluctuating signs of awareness. When patients regain functional object use and/or reliable communication they are referred to as emerging from MCS (EMCS) [111, 112]. A particular outcome is represented by patients with a locked-in syndrome (LIS), who have no means of producing speech, limb or facial movements (except mostly for eye movement and/or blinking) but are still awake and fully conscious [113].

To date, the diagnosis of DOC patients is mainly behavioral [108]. The

distinction between these pathological levels of consciousness can be very challenging, as the boundaries between these entities are often uncertain and ambiguous. However, in the last decade, the progress of neuroimaging techniques has given important insights into the pathophysiology of DOC and shown that altered states of consciousness are related to a complex disruption in the functional and structural architecture of the brain [106, 107].

In next sections we will review the state of the art of brain connectivity assessment in different pathological (i.e. DOC) and pharmacologically-induced (i.e. anesthesia) levels of consciousness.

3.2 *Brain connectivity in disorders of consciousness*

In the last decades, different methods have been developed that may be used to investigate connectivity in patients with disorders of consciousness (DOC). Brain connectivity in DOC can be studied at both the structural [114] and functional [115, 116] levels.

3.2.1 *Diffusion imaging studies*

Structural imaging studies have shown diverse lesion patterns in DOC, suggesting that no specific brain region can be unequivocally related to awareness [117]. Nonetheless, recent studies demonstrated that cognitive impairment after traumatic brain injury results from the disconnection of network hubs by traumatic axonal injury, confirming the relevance of the use of diffusion imaging as biomarkers for consciousness recovery after TBI and support the possible use of these biomarkers for early classification of patients (Fig. 3.2). Furthermore, widespread diffuse axonal injury and thalamic damage have been observed in UWS patients following traumatic brain injury [118], supporting the role of the thalamus and cerebral cortex in the genesis of awareness.

3.2.2 *fMRI studies*

In the past years most of the functional connectivity analysis in DOC patients has mainly focused on the default mode network (DMN) assessment, suggesting this network as crucial for the proper functioning of conscious awareness [75, 119]. Resting state fMRI studies have detected reduced con-

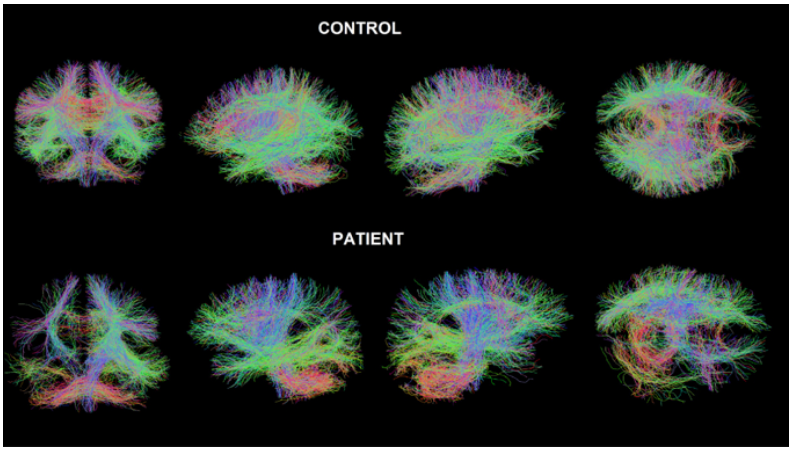

Figure 3.2: *Comparison between tractograms of a healthy control (top) and a patient in MCS (bottom) confirms the structural damage which is evident in the temporo-parietal regions of the right hemisphere. Colors indicate directionality of the fiber pathway: red = left-right; green = anterior-posterior; blue = superior-inferior.*

nectivity in the DMN of patients in coma, UWS and MCS [120]. This decrease of connectivity was correlated to the level of consciousness, mostly affecting the precuneus, a brain area considered to be a critical hub within this network with a massive degree of interconnectivity [121]. Nevertheless, coherent DMN connectivity has also been observed in UWS [122]. This suggests that the role of the DMN in consciousness is highly complex. Concurrent with decreasing DMN connectivity, a recent study reported increased connectivity in deep structures of the limbic system in DOC patients, greater in UWS than in MCS patients [123].

A recent study of resting state functional connectivity in DOC patients [124] investigated changes in seed-based correlation on six functional networks (default, frontoparietal, salience, auditory, sensorimotor and visual). The authors showed that the functional network with the most discriminative capacity for separating MCS patients with UWS ones encompassed auditory and visual cortices. Functional connectivity in these areas is referred to as cross-modal interaction, and it appears to be crucial for top-down multisensory integration of higher-order regions in healthy subject [125, 126]. This corroborates the hypothesis that loss consciousness might also correlate with the disruption of primary sensory areas and higher-order associative cortices, which are thought to be required for conscious perception [127] (Fig. 3.3).

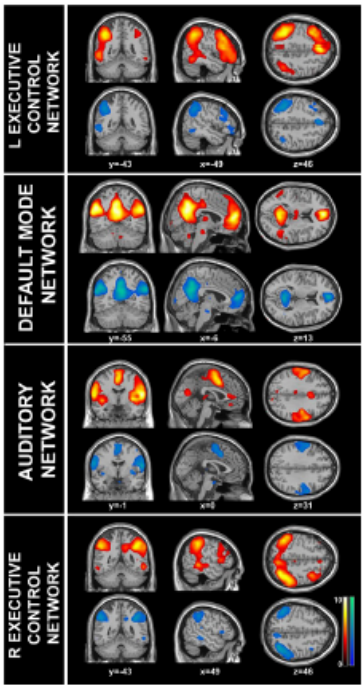

Figure 3.3: *System-level fMRI resting state functional connectivity is reproduced across healthy controls (red color-scaled areas) and shows consciousness level-dependent decreases ranging from healthy subjects, to patients in MCS and UWS (blue color-scaled areas) in several resting state networks. Statistical maps are thresholded at FDR for multiple comparisons $p < 0.05$ and are rendered on a structural $T1$ magnetic resonance template (x, y and z values indicate Montreal Neurological Institute coordinates of represented sections, neurological convention).*

However, loss of functional connectivity is, therefore, not necessarily the only sign of impaired consciousness, but only a single aspect of a more intricate dysfunction in the whole-brain network. In fact, recent studies showed decreasing anti-correlation between the fronto-parietal and DMN networks as one goes towards the deepest unconsciousness, such as in UWS patients [122]. Particularly, Di Perri et al. [128] showed that negative connectivity between DMN and salience/control/attentional network was significantly different between patients and healthy controls. Indeed, UWS and MCS patients showed a pathological positive connectivity between these two networks, whereas patients exiting from MCS exhibited a negative connectivity in the same direction of that observed in controls. The maintenance of anti-correlation between these networks seem then to be a core constituent of

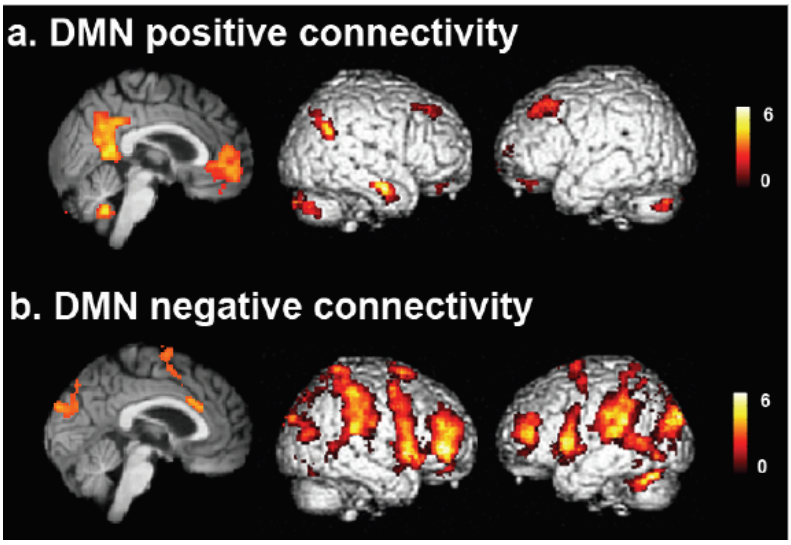

Figure 3.4: *a) Brain regions where the positive connectivity within the DMN shows a significant (FDR $p < 0.05$) linear relation across groups with progressively different level of consciousness. b) Brain regions where the negative connectivity between the DMN and salience/control/attentional network shows a significant (FDR $p < 0.05$) linear relation across groups with progressively different level of consciousness. Adapted from [128].*

conscious cognition [107, 108] (Fig. 3.4).

3.2.3 TMS/EEG studies

Recently, TMS-EEG has been proposed as a tool to investigate effective connectivity at the bedside of DOC patients [129]. In this category of patients, TMS-EEG may be especially useful, because it does not rely on the subject's ability to process sensory stimuli, to understand and follow instructions, or to communicate. Also, the study of TMS evoked potentials has increased the understanding of cortical processing in DOC [130]. Stimulation of a superficial region of the cerebral cortex of UWS patients with TMS has been shown to either induce no response or trigger a simple, local EEG response, indicating a breakdown of effective connectivity [131], similar to that observed in deep sleep [44]. In contrast, in MCS patients, TMS triggered complex EEG activations which sequentially involved distant cortical areas, similar to activations recorded in locked-in patients, in healthy awake subjects and during vivid dreams [44, 132]. Interestingly, an MCS patient assessed during a period of no responsiveness still showed complex and widespread brain re-

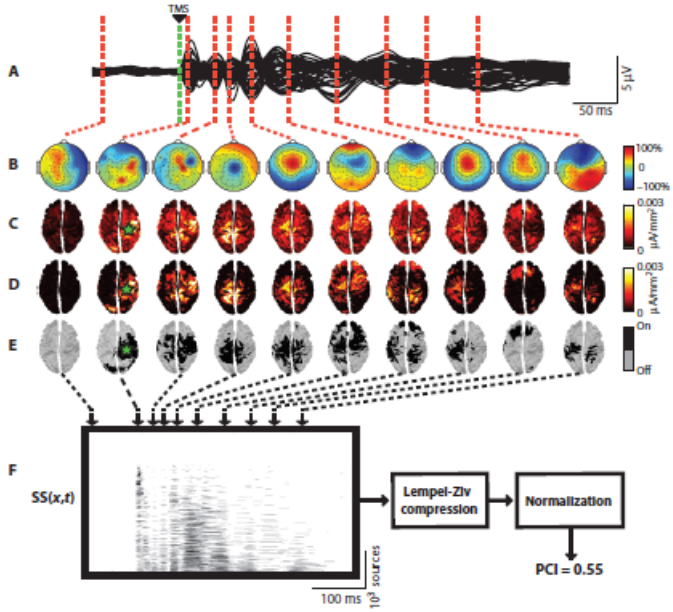

Figure 3.5: *Perturbational complexity index (PCI) calculation. A) The black traces show the superposition of the averaged TMS-evoked potentials* (150 *trials) recorded from all EEG channels (butterfly plot of* 60 *channels) in one representative subject during wakefulness. (B) The color-coded maps show the instantaneous voltage distributions at selected latencies [auto-scaled between the maximum* (100%) *and the minimum* (100%) *instantaneous voltages]. (C) The corresponding distributions of cortical currents are calculated by means of a weighted minimum norm inverse solution applied to a three-sphere BERG forward model. (D) Significant TMS-evoked cortical currents are estimated by applying a nonparametric bootstrap-based statistical procedure at the source level. (E) A binary spatiotemporal distribution of significant sources (SS) is extracted:* $SS(x,t) = 1$ *for significant sources* (x) *and time samples* (t)*;* $SS(x,t) = 0$ *otherwise. The sources in the matrix* $SS(x,t)$ *are sorted, from bottom to top, on the basis of their total activity during the post-stimulus period. (F) The information content of* SS *is estimated by calculating the Lempel-Ziv complexity measure. PCI is defined as the information content of* SS*, normalized by the correspondent source entropy. Green star, site of TMS stimulation. Adapted from [133].*

sponses to TMS, even though no conscious behavior could be observed at the bedside [131].

Furthermore, from compressing the information given by TMS, Casali et al. defined an empirical measure of brain complexity, i.e. the perturbational complexity index (PCI). They demonstrated that this index can reliably discriminate between different physiological, pharmacological, and pathological levels of consciousness [133] (Fig. 3.5).

Transcranial magnetic stimulation combined with EEG (TMS-EEG) seems

then to be a promising approach to study connectivity across different levels of consciousness. Nonetheless, a better understanding of the neurophysiological mechanism of TMS-induced cortical excitability is needed (e.g. how the perturbation propagates through the cortex, and how it is constrained and shaped by brain structure). To shed light on the huge variety of information contained in the functional response generated by TMS will definitely boost the efficacy and the applications of this technique to the DOC patients' population.

3.3 *Brain connectivity in anesthesia*

General anesthesia is a reversible state of unconsciousness. As the dosage can be controlled, it provides a unique opportunity to modulate the levels of wakefulness and awareness. General anesthesia is induced by pharmacological drugs that provoke loss of consciousness, immobilization and analgesia with concomitant stability of the autonomic, cardiovascular, respiratory, and thermoregulatory systems [134]. To date, no consensus has been reached on how the anesthetics cause modifications of consciousness. However, it has recently been shown that anesthetic agents act on specific brain sites in a dose-dependent manner [135]. Also, anesthetic agents might generate widespread decreases of resting cerebral metabolism as well as reduced brain activations in response to external stimuli in the cortex, thalamus, and midbrain [136, 137].

Among the anesthetic agents, the most extensively studied is propofol [138]. fMRI studies have demonstrated that propofol-induced anesthesia is associated with decreased cortico-cortical and thalamo-cortical connectivity in higher-order brain networks including fronto-parietal networks (i.e., executive control network and DMN) and the salience network [139, 140]. In addition, both DMN activity and cross-modal interaction between auditory and visual networks could be correlated to the level of consciousness. These results suggest that propofol induces a breakdown in brain functional integration, modifying both within- and between-network connectivity [139] (Fig. 3.6).

Besides decreasing activity in higher-order brain areas of the cortex, increase of connectivity has also been observed in other brain regions during

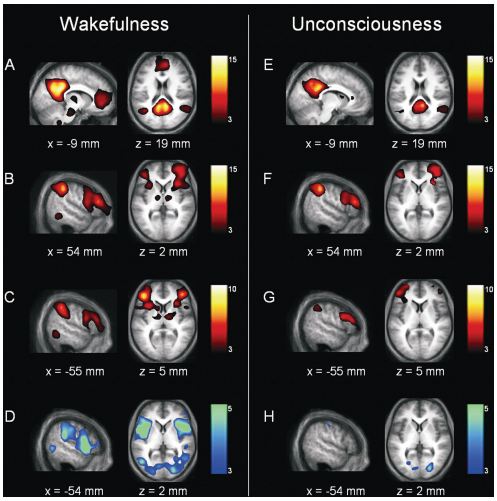

Figure 3.6: *Large-scale network connectivity is partially preserved during propofol-induced unconsciousness. (Left) Normal wakefulness resting-state networks connectivity in default network (A), right executive control network (B), left executive control network (C), and anticorrelations between default network and lateral frontoparietal cortices (D). (Right) Connectivity patterns in default network (E), right executive control network (F), left executive control network (G), and anticorrelations between default network and lateral frontoparietal cortices (H) during deep sedation with clinical unconsciousness. For display purposes, results are thresholded at false discovery rate corrected $p < 0.05$ and are shown on the mean structural $T1$ magnetic resonance scan of the subjects. Adapted from [139].*

sedation [141], as already observed in patients with DOC. Specifically, increased connectivity between the thalamus and auditory, insular and sensorimotor cortex has been reported under propofol induced anesthesia [140]. Altogether, these findings support the hypothesis of a complex brain connectivity architecture in the emergence of consciousness, and demonstrates the importance of considering functions of a brain region in terms of both functional integration and segregation [142].

INVESTIGATION OF FUNCTIONAL CO-ACTIVATION PATTERNS IN ANESTHESIA

4

Recent studies have been shown that functional connectivity of cerebral areas is not a static phenomenon, but exhibits spontaneous fluctuations over time. There is also evidence that fluctuating connectivity is an intrinsic phenomenon of brain dynamics that persists during anesthesia. Lately, point process analysis applied on functional data has revealed that much of the information regarding brain connectivity is contained in a fraction of critical time points of a resting state dataset. The study presented in this chapter extends this methodology for the investigation of functional connectivity changes during propofol-induced modulation of consciousness, with the aim of extracting new insights on brain networks consciousness-dependent fluctuations.
***Keywords**: functional connectivity, point process analysis, propofol, anesthesia*

4.1 *Overview*

As already mentioned in Chapter 3, functional connectivity studies of resting state networks in induced sedation through anesthesia, have shown widespread changes in fronto-parietal networks, compared with the relative preservation of sensory networks, suggesting a major role of higher-order frontoparietal associative network activity in the loss of consciousness phenomena [139, 142]. Moreover, functional impairment of highly connected frontoparietal areas seems to have greater repercussions on global brain function than on less centrally connected sensorimotor areas [143, 144].

Additionally, recent studies have been shown that functional connectivity of cerebral areas is not a static phenomenon, but exhibits spontaneous fluctuations over time [85, 145, 146]. Previously, fluctuations of functional connectivity have been thought to reflect changing levels of vigilance, task switching or conscious processing. There is evidence that fluctuating connectivity is an intrinsic phenomenon of brain dynamics that persists even during anesthe-

sia [85]. Fluctuations of functional connectivity within an attention network in macaques have been demonstrated and interpreted as mechanistically important network information [147]. Still, the relationship between changes of consciousness and network dynamics is not understood yet.

Lately, a new approach in exploring functional brain connectivity, using point process analysis, has been proposed by Tagliazucchi et al. [148]. The main idea in this work is that important features of brain functional connectivity at rest can be obtained from BOLD fluctuations, isolating the periods in which the signal crosses some amplitude threshold. In this way the study of the dynamics of a continuous BOLD time series is reduced to the exploration of a discretized one (a point process), defined by time and location of BOLD signal threshold crossings. Through point process analysis, Tagliazucchi and colleagues showed that much of the information regarding a specific RSN is actually contained in a fraction of critical time points (i.e. BOLD signal peaks) of a resting state dataset. This idea has next been adopted by Liu et al. [149], in a study showing that seed-based RSNs extracted from fMRI BOLD signal are averages of multiple distinct spatial co-activations patterns (CAPs) at different time points, and that the analysis of these patterns might provide more fine-grained information on brain functional network organization.

In the present study we want to extend and apply this methodology for the investigation of fMRI resting state spatial pattern changes during propofol-induced modulation of consciousness, with the central aim of extracting new information regarding brain networks consciousness-dependent fluctuations.

4.2 *Methods*

Eighteen healthy right-handed volunteers participated in the study. Propofol was infused through an intravenous catheter placed into a vein of the right hand or forearm.

The subject was asked to strongly squeeze the hand of the investigator. She/he was considered fully awake or to have recovered consciousness if the response to verbal command (squeeze my hand) was clear and strong (Ramsay 2), in sedation if the response to verbal command was clear but slow (Ramsay 3), and in unconsciousness if there was no response to verbal command (Ramsay 5-6). For each consciousness level assessment, Ramsay

scale verbal commands were repeated twice. Functional MRI acquisitions consisted of resting-state functional MRI volumes repeated in four clinical states: normal wakefulness (Ramsay 2), sedation (Ramsay 3), unconsciousness (Ramsay 5), and recovery of consciousness (Ramsay 2). The typical scan duration was half an hour in each condition. The number of scans per session (197 functional volumes) was matched in each subject to obtain a similar number of scans in all four clinical states.

The fMRI data were preprocessed using Statistical Parametric Software (SPM8), performing the typical preprocessing steps of functional connectivity analysis [150]. These steps included motion correction, spatial smoothing (FWHM = 8 mm), temporal filtering with a bandpass filter (0.005 to 0.1 Hz), and the removal of linear and quadratic temporal trends. In addition, the brain-averaged signal, the time series of regions of interest in the white matter and cerebrospinal fluid, and six affine motion parameters were regressed out from the dataset. The fMRI data of each subject was first spatially coregistered to high-resolution anatomical images and then to the 152-brain Montreal Neurological Institute (MNI) space. Additionally, the preprocessed fMRI data were resampled to $3 \times 3 \times 3$ mm^3 in the MNI space, and the signal of each voxel was demeaned and normalized by its temporal standard deviation (SD).

4.2.1 *Co-activation patterns construction*

After preprocessing, the dataset was reduced to a spatio-temporal point process [148] by selecting time points in the seed region at which the signal is higher than a given threshold. In this work we used a $6 \times 6 \times 6$ mm^3 cube centered at the posterior cingulate cortex (i.e. PCC, [0, 53, 26] in MNI coordinates, identical to Liu et al. [149]). CAPs construction can then be summarized in three steps (the MATLAB code employed is freely available at the github page `https://github.com/CyclotronResearchCentre/CAPsToolbox`):

1. First, we collected all the points in the normalized PCC time course where the BOLD signal was above threshold. For each of these points in the PCC, and for each of the 4 levels of consciousness, we collected the relative spatial maps (Fig. 4.1). These spatial maps, or time frames

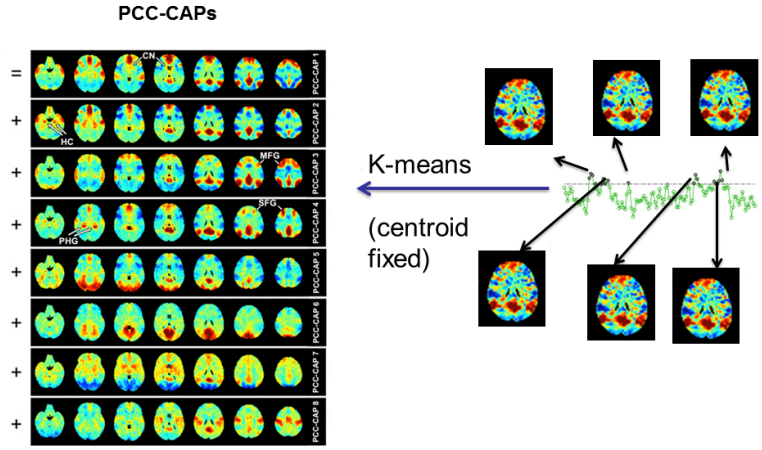

Figure 4.1: *Co-activation patterns (CAPs). The approach is similar to the ones proposed in [149] and [148]. After the extraction of a seed region, in this case Posterior Cingulate Cortex (PCC), a threshold equal to 1 standard deviation(SD) was applied, as to consider only the time points corresponding to peaks in the BOLD signal; next, the spatial maps (namely, time frames), associated with these time points are collected and clusterized using k-means, with a number of clusters fixed to 8. The centroids were kept fixed as well, to allow cluster comparison between the different clinical conditions. The within-cluster time frames were then averaged to obtain 8 spatial PCC-related co-activation patterns. Finally, the computation was iterated over the 4 different states of consciousness (wakefulness, sedation, unconsciousness, recovery), obtaining 8 PCC-related co-activation patterns for each state.*

[149], represent whole-brain patterns of functional activations correlated to PCC BOLD peaks, previously extracted using this thresholding approach.

2. In order to achieve a spatio-temporal mapping of correlated activity we clustered all the time frames which were significantly co-activated with PCC, in the same way as described in [149]. The sorting of the time frames was performed by K-means clustering, a machine learning classification method able to group unlabeled data into clusters [151]. We performed K-means (number of clusters fixed at 8) over all the spatial maps collected to classify the time frames based on their spatial similarity, and then averaging them within-cluster to extract 8 different spatial PCC-related co-activation patterns (i.e. CAPs [149]). With the purpose of obtaining a robust benchmark baseline against which

to track modifications related to level of consciousness, we first ran k-means clustering over the PCC time frames collected on an independent dataset from the 1000 Functional Connectome Project (FCP, `www.nitrc.org/projects/fcon\_1000/`), which includes wakefulness resting-state functional magnetic resonance imaging (fMRI) collected at multiple sites (247 subjects), as used by Liu and colleagues [149].

3. The eight PCC-CAPs centroids obtained from the clustering of the 1000 Functional Connectome Project dataset (FCP,`www.nitrc.org/projects/fcon\_1000/`) were then kept fixed, and spatial clustering on the PCC time frames extracted from our propofol dataset, for each condition (i.e. wakefulness, sedation, unconsciousness, recovery), was then performed around these centroids, averaging the within-cluster spatial maps to obtain 8 different PCC-CAPs for each level of consciousness. The clustering with centroid fixed allowed us to compare PCC-CAPs between states (i.e. CAP1 in wakefulness with CAP1 in sedation, etc.), and to follow thus the fluctuation of each PCC-CAP over the course of consciousness modulation.

All statistical analyses were carried out using SPM8. For each CAP, individual time frames were entered in a second-level analysis, corresponding to a random effects model in which subjects are considered random variables. These second-level analyses consisted of analyses of variance (repeated measures analysis of variance) with the four clinical conditions as factors: normal wakefulness, sedation, unconsciousness, and recovery of consciousness. A linear one-tailed T contrast was computed for each CAP, searching for a linear relationship between PCC co-activation patterns and the level of consciousness of the subjects across the four conditions (i.e., normal wakefulness, sedation, unconsciousness, and recovery of consciousness, SPM contrast [1.5 -0.5 -1.5 0.5], as previously described in [139]). It should here be noted that during the recovery of consciousness subjects showed residual plasma propofol levels and lower reaction times scores (table 1 in [139]). Therefore we fixed different SPM contrast values for wakefulness (1.5) and recovery (0.5).

Results were considered significant at $p<0.05$, corrected for multiple comparisons with False Discovery Rate (FDR), as in [139].

4.3 Results

We studied PCC-CAPs in our 18 subjects fMRI resting state dataset, for all the 4 different states of consciousness acquired, i.e. normal wakefulness, sedation, unconsciousness, recovery.

Some regions are no longer co-activated with the PCC in states of propofol-reduced consciousness. As to better quantify this phenomenon we decided to use a contrast that correlates with levels of consciousness. The regions in each PCC-CAP where activity follows consciousness modulation are depicted in Fig. 4.2. Interestingly, results show several region specific drops in CAPs activation that we are able to differentiate thanks to the employed methodology, some of them already shown in literature, some others not. In Fig. 4.2, CAP 1, 2 5 and 7 show drop in the prefrontal cortex, CAP 3 and 7 isolates the thalamic drop, the auditory and motor cortex decreases come up in CAP 8 and 5, drop of the visual area in CAP 6.

4.4 Discussion

With the aim to investigate changes in global and local brain activity, in this study we assessed propofol-induced changes in PCC co-activation functional patterns, during wakefulness, sedation, unconsciousness, and wakefulness recovery. Our results contribute to a growing literature addressing the changes in functional connectivity accompanying the loss of consciousness [139, 152, 153].

The approach proposed, based on the clustering of instantaneous PCC-related spatial maps, helps in the refinement and the differentiation in the spatial modulation of the default mode network when switching from wakefulness to unconsciousness.

Also, this approach adds new information on region specific drops in connectivity between the seeds in the DMN area and whole brain connectivity, correlating with levels of consciousness (Fig. 4.2): prefrontal drops (CAP 1, 2, 5, 7) are in line with previous findings in the field, showing widespread changes in prefrontal connectivity [139, 143, 144]: at the cortical level, hypnotic anesthetic agents have traditionally been considered to decrease activity in a widespread bilateral frontoparietal network. The primary action of hypnotic anesthetic agents would be to functionally disconnect different

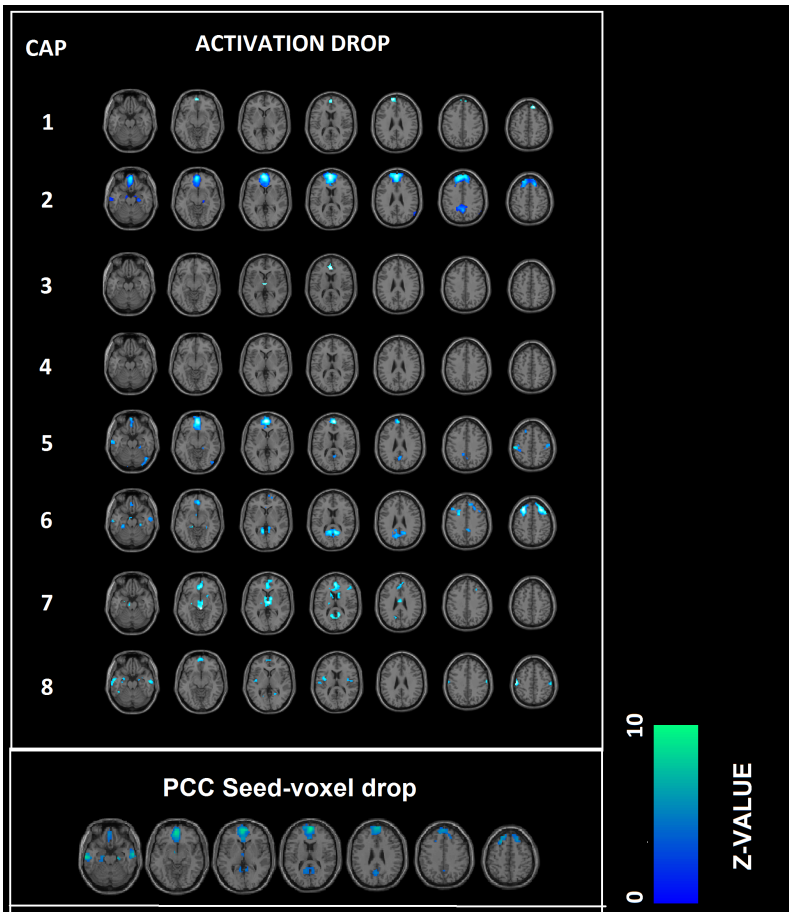

Figure 4.2: *Decreases in CAPs. This figure shows the local decreases in co-activation from wakefulness to unconsciousness, using the same t-contrast as in [139]. All the images report contrast which are significant at p<0.05, FDR corrected.The seven slices shown in the maps are at Z= -21, -9, 3, 15, 27, 39, 51, respectively. CAPs consciousness-dependent deactivations appear in mesial prefrontal cortex (MPC), CAPs 1, 2, 5 (see Z=15); superior fontal gyrus (SFG) in CAP 2 (Z=39 and 51); thalamus (THA) in CAPs 3 and 7 (Z=3); mesencephalon (MP) in CAP 7 (Z=-9); motor area (MA) in CAP 5 and CAP 8 (Z=51); parahippocampal gyrus (PHG) in CAPs 2, 5, 6 (Z=-21); caudate nucleus (CN) in CAP 7 (Z=15); visual area (VA) in CAP 6 (Z=15); auditory cortex (AC) in CAP 8 (Z=15) and precuneus (PC) in CAP 2 (Z=39). Note how this approach adds novel information to the functional changes due to propofol sedation when compared with the standard PCC-seed voxel map (below).*

parts of the cortex, which would probably impair the ability to integrate information [142, 152].

The disconnection of the thalamic area, already noted in [154, 155], is highlighted in CAP 3 and 7 (Fig. 4.2). Using positron emission tomography, thalamic metabolism has been shown to decrease significantly during anesthesia-induced unconsciousness [153]. Furthermore, a model has been suggested in which the thalamus orchestrates the commonly observed increased and coherent alpha frequency activity in the frontal cortex during propofol-induced unconsciousness. This steady thalamic alpha rhythm could impede conduction and thus responsiveness to external stimuli [156].

Decrease of activation in the visual area (CAP 6) during anesthesia has previously been studied in monkeys [157, 158], where it has been shown how local and global processing in the visual area might depend gradually on the depth of anesthesia. It may also critically depend on information integration mechanisms that function properly only in the awake and perceiving animal [157]. Here, this disconnection is shown in fMRI resting state on humans: thus, this approach seem to enlighten instantaneous spatial connectivity changes between DMN and other external areas, unlikely to be seen with other commonly used correlation analysis (e.g. seed-based functional connectivity, Fig. 4.2).

Similarly, the PCC-related primary motor disconnection is pointed out here (CAP 5 and 8, Fig. 4.2) on fMRI resting state data. These results are in line with previous transcranial magnetic stimulation (TMS) and electroencephalographic (EEG) studies, that indicate intracortical inhibition of central motor circuitry during incremental suppression by a potentiator of GABA agonist (propofol) in a dose-dependent manner [159, 160].

The decrease in auditory cortex PCC-coactivation (CAP8) is in agreement with previous findings, in animals [161] and humans [162]. Our finding of decreased auditory cortex co-activation could be related to the hypothesis that propofol bilaterally attenuates the auditory-induced BOLD signal activation of the auditory cortex in a dose-dependent manner [163].

A limitation to this approach is the choice of the seed, that needs to be based on a strong priori hypothesis: whole brain connectivity analysis can improve research in this direction. Finally, since it has recently been shown that EEG directional connectivity shows characteristic changes during propofol-

induced unconsciousness [164], the nature of BOLD peaks and their correlation with cortical activity needs to be explored using combined fMRI-EEG recordings.

In conclusion, our results show that functional changes in the brain associated to propofol-induced modulation of consciousness can be efficiently revealed by tracking the patterns of co-activation in the Posterior Cingulate Cortex, an area with a central role in the dynamical connectivity at rest. This methodology, based on point process analysis, can help in refining the characterization of local functional disconnections following the partial or total loss of consciousness.

TRACKING FUNCTIONAL CONNECTIVITY CHANGES IN THE BRAIN AFTER TMS

5

Transcranial magnetic stimulation (TMS) in combination with neuroimaging techniques allows to measure the effects of a non-invasive and direct perturbation of the brain. When coupled to high density electroencephalography (TMS/hd-EEG), TMS pulses revealed the electrophysiological signatures of different cortical modules in health and disease. However, the neural underpinnings of these signatures remain unclear. In the study described in this Chapter a novel methodology for multimodal analyses of cortical response to TMS recordings and diffusion magnetic resonance imaging (dMRI) tractography will be presented. Results from the investigation of the relationship between functional and structural features of different cortical modules in a cohort of awake healthy volunteers will also be outlined and examined.

***Keywords**: TMS/EEG, dMRI, directed functional connectivity, structural connectivity, structure-function, brain directed functional connectivity*

5.1 *Overview*

We have already stressed (Chapter 1) how TMS/EEG recordings can provide new and reliable insights [130] on the whole brain cortical excitability with reasonable spatial and excellent temporal resolution [165].

Indeed, the amount of information contained in the hd-EEG response to TMS has appeared to contain inner signatures of the functional organization in a brain network. Two recent studies [166, 167] in healthy awake subjects showed that TMS can also induce EEG oscillations at different frequencies. The TMS pulse gives rise to different connected cortical regions in the brain, generating a complex EEG pattern composed of strong fluctuations at the "natural" frequency of the stimulated area. These oscillations are thought to reflect neurophysiological activity that is transiently elicited by the TMS pulse and possibly engaged through brain connections [166, 168, 169].

The purpose of this study was to investigate EEG changes of directed functional connectivity in the brain induced by TMS from both a functional and structural perspective, using multimodal modeling of source reconstructed TMS/hd-EEG recordings and dMRI tractography. The study of functional connectivity changes after the perturbation can possibly help in understanding the structure-function modulation caused by TMS (i.e. the extent to which TMS-induced EEG dynamics is constrained by white matter pathways) and the specific frequency bands of the involved brain regions. Functional and structural connectivity in the brain are known to be closely correlated [49, 89, 170], but their interactions remain only poorly understood [171].

Taking the aforementioned recent findings as a starting point, we aimed to assess: 1) if the extent to which functional changes in a cortical region, as a consequence of the induced perturbation, is related to the number of fiber pathways passing through it [170]; 2) whether the temporal variability of the response to TMS has specific spectral EEG signatures [166]; 3) the role of these "natural frequencies" in the flow spread during TMS and in the structure-function interactions [44, 133, 166].

5.2 Methods

5.2.1 TMS/hd-EEG recordings

TMS/EEG data were acquired and analyzed similarly to previous studies ([133]). 14 healthy adults (6 males and 8 females, age range 23–37 years) were enrolled in the experiment. Stimulation was performed using a TMS figure-of-eight coil driven by a mobile stimulator unit (eXimia TMS Stimulator, Nexstim Ltd., Finland), stimulating two of the chosen areas (left precuneus (PCC) and left premotor (PreMot)) for at least 200 trials. The intensity was chosen as to assure an induced electrical field at the cortical level between 100 and 140 V/m. TMS trials containing noise, muscle activity, or eye movements were automatically detected and rejected. EEG data were average referenced, downsampled at half of the original sampling rate (from 725 Hz to 362 Hz), and bandpass filtered (2 to 80 Hz). Source reconstruction was performed as in [133]. Briefly, conductive head volume was modeled according to the 3-spheres BERG method [172] and constrained to the cerebral cortex that was modeled as a three-dimensional grid of 3004 fixed dipoles ori-

ented normally to cortical surface. This model was adapted to the anatomy of each subject using the Statistical Parametric Mapping software package (SPM8, freely available at: `http://www.fil.ion.bpmf.ac.uk/spm`) as follows: binary masks of skull and scalp obtained from individual MRIs were warped to the corresponding canonical meshes of the Montreal Neurological Institute (MNI) atlas. Then, the inverse transformation was applied to the MNI canonical mesh of the cortex for approximating to real anatomy. Finally, the single trial distribution of electrical sources in the brain was estimated by applying the empirical Bayesian approach as described in [173, 174].

In order to summarize significant functional measures over anatomically and/or functionally identifiable brain regions, the time courses of the 3004 reconstructed sources were then averaged into the specific 90 cortical and subcortical areas of the Automated Anatomical Labeling (AAL) [175] parcellation (Fig.5.1), according to their position on the cortical mesh.

5.2.2 *Diffusion magnetic resonance imaging data*

Diffusion volumes were analysed using typical preprocessing steps in DTI [178]. Eddy current correction for each participant was achieved using FDT, v2.0, the diffusion toolkit within FSL 5.0 (http://www.fmrib.ox.ac.uk/fsl). Rotations applied to the diffusion-weighted volumes were also applied to the corresponding gradient directions [179]. A fractional anisotropy (FA) image was estimated using weighted linear least squares fitted to the log-transformed data for each subject. We segmented each subject's T1-weighted image into whole-brain white matter (WM), grey matter (GM), and cerebrospinal fluid (CSF) masks using FAST, part of FSL (FMRIB Software Library v 5.0). The corresponding white matter mask image was registered without resampling to the relevant DWI series (target image = thresholded FA image (FA > 0.2)) using FLIRT, v5.5, 12 degrees of freedom, nearest neighbour interpolation, mutual information cost function [180]. The registration was performed without resampling in order to mantain the high spatial resolution of the structural image in the diffusion space. As previously stated, the 90 cortical and subcortical nodes comprising the automated anatomical labeling (AAL) template [175] were used as candidate atlas. The atlas was first registered to the T1 space using linear (FSL flirt) and non-linear warping (FSL FNIRT) in order to achieve the best registration into each subject's

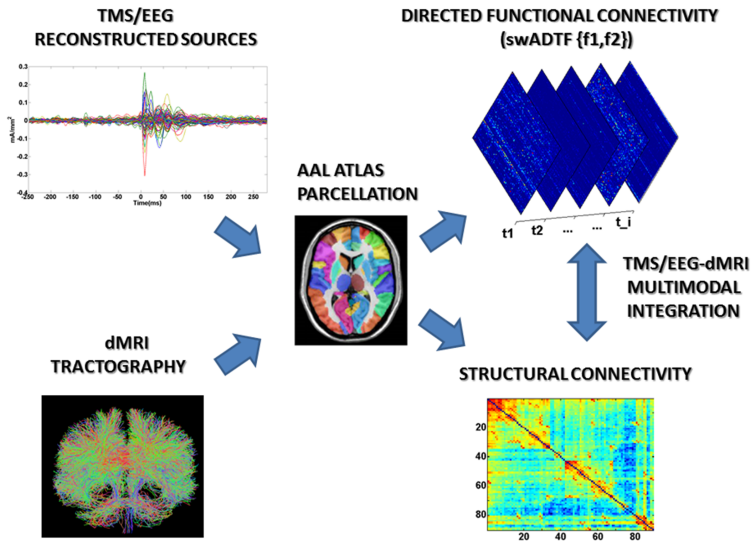

Figure 5.1: *Flow chart of TMS/EEG-dMRI modeling. Up: the time courses of the* 3004 *reconstructed dipoles were averaged into the parcels of the Automated Anatomical Labeling (AAL) atlas [175], consisting of* 90 *unique brain regions (cerebellar regions were excluded from the analysis). The* 90 *time courses obtained were modeled using spectrum-weighted adaptive directed transfer function (swADTF)[176, 177]. swADTF returns the causal interactions between the cortical regions (*$90x90$ *time varying directed functional connectivity matrices) at a specific frequency interval (f1,f2). Bottom: for each dMRI dataset whole-brain probabilistic tractography was performed using a combination of FSL and MRTRIX (see* ***Materials and methods****). The AAL atlas was then used to segment the fiber bundles between each pair of ROIs. Next, we determined the percentage of tracts between each pair of regions of the AAL template, resulting in a* $90x90$ *structural connectivity matrix.*

space. Then, the single subject AAL template was finally registered without resampling to the dwi space using the affine transform resulting from the WM registration. This transformation matrix was also applied to the T1-derived GM mask which was used as termination mask for the tractography analysis. Probabilistic tractography was performed using randomly placed seeds within subject-specific white matter masks, registered as mentioned in the latter. Fiber tracking settings were as follows: number of tracks = 10 million, FOD magnitude cutoff for terminating tracks = 0.1, minimum track length = 5 mm, maximum track length = 200 mm, minimum radius of curvature = 1 mm, tracking algorithm step size = 0.5 mm. Streamlines were terminated when they extended out of the WM-GM mask interface, or could not progress along a direction with an FOD magnitude or curvature radius

higher than the minimum cutoffs. The streamlines obtained were mapped to the relevant nodes defined by the AAL parcellation registered in the subject's dwi space, using MRtrix [63]. Each streamline termination was assigned to the nearest grey matter parcel within a 2 mm search radius.The resulting connectome was finally examined by determining the fiber density between any two regions of the AAL template, as in [178]. This correction was needed to account for the variable size of the cortical ROIs of the AAL template [65].

5.2.3 *TMS/hd-EEG directed functional connectivity estimation*

We evaluated directed functional connectivity using a multivariate model of spectral coefficients, i.e. the directed transfer function (DTF) [181, 182, 183]. In order to cope with the non-stationary nature of the signals under study, we used the adaptive directed transfer function (ADTF) [184, 185]. Specifically, we adopted the spectrum-weighted adaptive directed transfer function (swADTF)[177], which has been successfully used for connectivity modeling of epileptic intracranial EEG data [176, 177].

A time-variant multivariate autoregressive (TVAR) model is built from the TMS/hd-EEG sources by using the Kalman filtering algorithm [176, 186, 187]. The time-variant connectivity measure, the swADTF, is calculated from the coefficients of the TVAR model as follows:

$$swADTF_{ij}(t) = \frac{\sum_{f=f_1}^{f_2} |H_{ij}(f,t)|^2 \sum_{k=1}^{K} |H_{jk}(f,t)|^2}{\sum_{l=1}^{K} \sum_{f'=f_1}^{f_2} |H_{il}(f',t)^2 \sum_{s=1}^{K} |H_{ls}(f',t)|^2} \tag{5.1}$$

where $H_{ij}(f,t)$ in eq. 5.1 is the time-variant transfer matrix of the system describing the directed functional connectivity from signal j to i at frequency f at time t, for each of the K signals. Each term $H_{ij}(f,t)$ is weighted by the autospectrum of the sending (in this case j) signal.

The swADTF allows us to investigate the causal relation between all the signals at a predefined frequency band over time. The measure weighs all outgoing directed functional connectivity present in the terms $H_{ij}(f,t)$ by the power spectrum of the sending signal j. Each swADTF value corresponds to the directed time-variant strength of the directed functional connectivity between two nodes. This dynamic interaction between nodes can also be represented as a series of time-varying directed matrices (see also Fig.5.1).

The swADTF is normalized so that the sum of incoming directed functional connectivity into a channel at each time point is equal to 1:

$$\sum_{k=1}^{K} swADTF_{ik}(t) = 1 \tag{5.2}$$

5.2.4 *TMS/EEG-dMRI multimodal integration*

We computed directed functional connectivity (swADTF) on the brain network defined by the anatomical atlas (AAL) reconstructed sources for each subject. A detailed discussion on the implementation and the setup of the parameters can be found in [176].

The swADTF was calculated in 3 frequency bands: α (8-12 Hz), β (13-20 Hz), $\beta 2/\gamma$ (21-50 Hz). This choice followed the evidence that TMS on healthy awake subjects consistently evoked dominant EEG oscillations in different cortical areas [166].

In order to track modulations of directed functional connectivity due to TMS, we considered 2 different non-overlapping windows of 300 ms: a "baseline", pre TMS stimulus, extended from 500 ms to 200 ms before the TMS pulse; a "post stimulus", directly after TMS, which captures the dynamics from 20 to 320 ms after the pulse (the first 20 ms were discarded to minimize the effect of possible artifacts occurring at the time of stimulation, [166, 188]).

We obtained the mean global outgoing flow from a region j before and after the stimulation by averaging the swADTF time courses in each of the two time windows and by summing the average amount of directed connectivity transferred from j to each node of the network. In network terms, this quantity is called Outdegree. In our case, for each frequency band and window (i.e. baseline or post stimulus):

$$Outdegree_j = \sum_{k=1}^{K} C_{jk}, \quad \forall\, k,\, j = 1...K, \tag{5.3}$$

where $K = 90$ in our case (i.e. the number of AAL regions), and C is the connectivity matrix constructed by averaging the swADTF time courses within each window. All self-edges were set to 0. By using this procedure we aimed to obtain an illustrative snapshot of the total directed functional con-

nectivity from a region j at a specific stage of the TMS process (i.e. baseline or post stimulus).

In order to detect significant group changes in the Outdegree before and after the stimulation, a two-sample t-test of the post stimulus Outdegree against the correspondent baseline Outdegree was performed in each region. Post stimulus Outdegree values were considered significant at $p \leq 0.05$, False Discovery Rate (FDR) corrected for multiple comparisons (i.e. for $K = 90$ independent tests).

For each subject, the structural degree of a node j (SCdegree) was simply calculated from the structural connectivity matrix S by summing over its columns.

$$SCdegree_j = \sum_{k=1}^{K} S_{jk}, \quad \forall\, j = 1...K, \tag{5.4}$$

5.2.5 *Structure-function correlations and statistical assessment*

The dynamic interaction between regions modeled by swADTF can be represented as a series of time-varying directed connectivity matrices (see also Fig.5.1). In each frequency band, dynamic spatial correlation was defined as the mean row-by-row Pearson's correlation at each time point between each subject's directed functional connectivity matrix and the correspondent structural connectivity matrix. The 95% confidence intervals for the Pearson's correlation distribution at the baseline were calculated by using a non-parametric bootstrap procedure [189].

5.3 *Results*

The significant differences in directed functional connectivity across cortical regions after TMS perturbation are illustrated by projecting the OutDegree onto the anatomical template (Fig.5.2). The two sites of stimulation have peaks in the Outdegree at different frequency bands. In particular, the precuneus area has a maximum of directed functional connectivity in the β band in proximity of the stimulation site, whereas the premotor has a maxima in the $\beta 2/\gamma$ band, more spread towards the controlateral hemisphere. These findings are in line with previous studies [166, 167], where the authors

Figure 5.2: *Directed functional connectivity across cortical regions after TMS. Snapshot of differences between baseline and post TMS stimulus directed functional connectivity (i.e. Outdegree) at $p < 0.05$, FDR corrected across cortical regions, for the three predefined frequency bands (α, β, $\beta 2/\gamma$ [166]), obtained by averaging the swADTF time courses from 20 to 320 ms after the pulse. The red circles represent the stimulation site. Note that the precuneus area has a maximum of directed functional connectivity in the β band in proximity of the stimulation site, whereas the premotor has a maxima in the $\beta 2/\gamma$ band, more spread towards the hemisphere controlateral to the stimulation site. These brain images were obtained using BrainNet Viewer [190].*

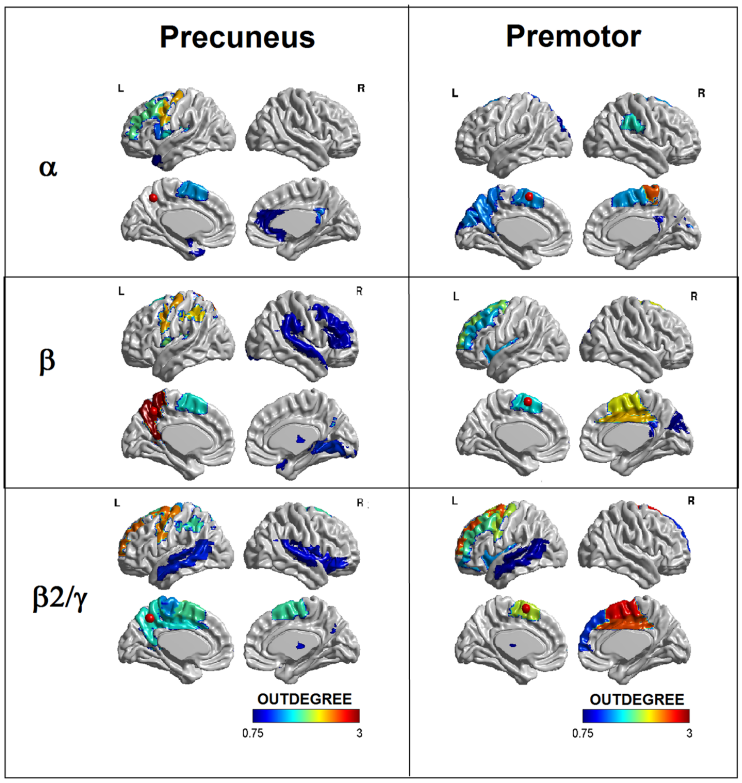

showed that TMS on healthy awake subjects consistently evokes EEG oscillations with dominant frequencies that depend on the site of stimulation. In particular, precuneus was shown to respond to TMS in the β band and premotor in $\beta 2/\gamma$. The peaks in directed functional connectivity at different frequencies in the areas depicted in Fig.5.2 confirm the hypothesis that different brain regions might be normally tuned to oscillate at a characteristic rate (i.e. natural frequency)[166, 167].

The dynamic spatial correlation between the directed functional connectivity (swADTF) and the connectome, for the two different sites of stimula-

tion (i.e. left precuneus and left premotor) and for each of the three chosen frequency bands (i.e. α, β, $\beta 2/\gamma$) deviates from baseline directly after the TMS pulse (Fig.5.3). This global network behavior does not depend on the subject or the stimulation site. The stable baseline configuration is then recovered after 200-300 ms, depending on the frequency band. The evidence that different brain area can be normally tuned by TMS to oscillate at a characteristic rate (i.e. natural frequency) might also explain the drop in structure-function correlation depicted in Fig.5.3. In fact, assuming that each of the 90 AAL cortical regions respond to TMS by oscillating at its peculiar natural frequency, the emergence of this complex between-band interaction might generate a consequent deflection in the within-band structure-function correlation (Fig.5.3). Specifically, this TMS-induced modulation of EEG rhythms over the brain network is more pronounced (i.e. higher deviation from the baseline correlation) and faster in the $\beta 2/\gamma$ and β bands, while the return to baseline is slower and less pronounced in the α band. This effect might be due to the region-specific variability in the intensity and the duration of the cortical response to TMS at the different natural frequencies, but it might also depend on the degree to which each recruited region is structurally connected to the rest of the network.

To further investigate this hypothesis, we evaluated the local dynamic spatial correlation between the directed functional connectivity (swADTF) for the cortical regions near to the stimulation site and the connectome, for both sites of stimulation (Fig.5.4). Notably, the structure-function correlation significantly increases over time in the right premotor area after TMS, when its natural frequency band (i.e. $\beta 2/\gamma$) is taken into consideration. This effect is not reproduced in the precuneus area (Fig.5.4).

5.4 Discussion

In this work we studied the interplay between directed functional connectivity computed from TMS reconstructed EEG sources and the connectome extracted from whole-brain dMRI tractography.

Our analysis on peaks of significant changes in directed functional connectivity and local structure-function interactions at different frequency bands corroborated the hypothesis that TMS evokes dominant oscillation in differ-

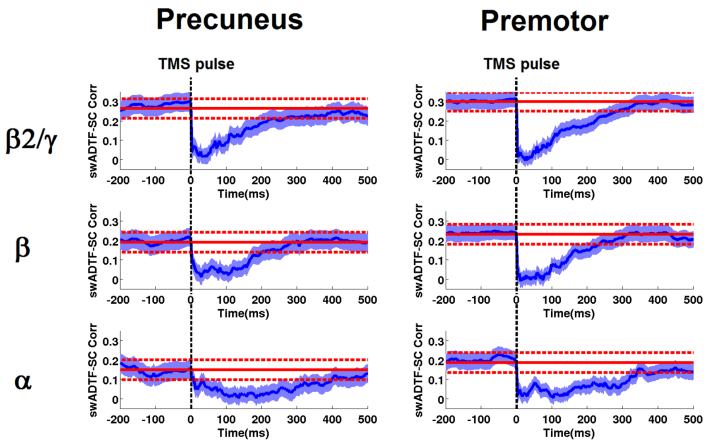

Figure 5.3: *Time-varying spatial correlation between directed functional connectivity and structural connectivity. Each plot shows the average over subjects of the dynamic spatial correlation between the directed functional connectivity (swADTF) matrices and the structural connectivity (SC) in function of time (blue line, standard error in shaded blue), for the three different frequency bands (α, β, $\beta 2/\gamma$, [166]). The red line indicates the mean baseline value, the dashed lines represent 95% confidence interval of the empirical baseline distribution. Note the TMS-induced decrease in the observed structure-function correlation, for both stimulation sites and in each frequency band.*

ent cortical areas at a characteristic rate [166]. Each stimulated area appeared to mainly respond to the stimulation by being functionally elicited in specific "natural" frequency bands, i.e. β for precuneus and $\beta 2/\gamma$ for premotor (Fig. 5.2).

We compared structural and directed functional connectivity at the whole network level for different EEG bands (α, β, $\beta 2/\gamma$). We observed a temporary decrease in the correlation between directed connectivity and structural connectivity after TMS. In particular, we showed that, after stimulation, precuneus responds mostly in the β band, whereas premotor has peaks of directed functional connectivity in the $\beta 2/\gamma$ band (Fig 5.2). Assuming that the each region in the brain reacts to the perturbation at a characteristic operating frequency, then the decrease in function-structure correlation in each frequency (Fig.5.3) might be caused by the complex pattern of between-frequency interactions rising after TMS in the whole-brain network. The return to baseline might then depend on two things: one is the temporal duration of the functional activation of the elicited area; the second is the extent

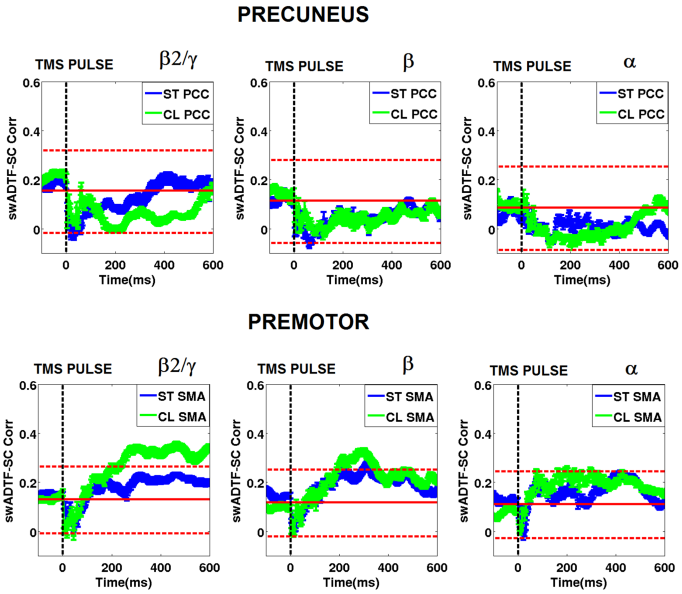

Figure 5.4: *Time-varying spatial correlation for the stimulated cortical regions. Figure shows the average over subjects of the dynamic spatial correlation (blue and green line, standard error in shaded blue and green) between the directed functional connectivity (swADTF) and structural connectivity (SC) for the AAL ROIs comprising left and right premotor areas (stimulated and controlateral) respectively, for the three different frequency bands (i.e. α, β, $\beta 2/\gamma$ respectively [166]). The continuous red line indicates the mean baseline value, the dashed lines represent 95% confidence interval of the empirical baseline distribution. Note the constant increase over time in the structure–function correlation for the controlateral supplementary motor area (SMA) following the TMS pulse, when taking into account its natural frequency (i.e. $\beta 2/\gamma$, Fig.5.2). This effect is not reproduced when stimulating the precuneus area.*

to which it is related to its structural connectivity pattern.

These considerations brought us to explore the link between the "natural" frequency response of the stimulated cortical areas and their structural architecture. Interestingly, for the premotor area controlateral to the stimulation site the correlation between directed functional connectivity at the natural frequency and structural connections increases after the stimulation and reveals a long-lasting effect over time (Fig.5.4). The fact that this effect is not reproduced for precuneus might be due to a number of reasons. First, the precuneal area is located deeper in the cortex then the premotor area, and thus more difficult to elicit. Secondly, it is possible that the different

frequency responses in each cortical area might reflect different anatomical background. Indeed, recent studies have reported that there is a strong correlation between cytoarchitecture and anatomical and functional connectivity in cat, macaque and humans [191, 192], with precuneus showing both a different cytoarchitecture as well as a different connectivity architecture than supplementary motor regions [193]. This might explain why the functional activation at specific resonant frequencies is related to the structural coupling (i.e. the amount of tracts connecting them) differently depending on the anatomical architecture of the specific brain region.

These results lead to three main concluding remarks. First, this work confirms the hypothesis that different rhythms in the brain emerge after TMS, and that this modulation is influenced by the structural connectivity among regions. This dynamic interaction at different natural frequencies seems to reflect intrinsic properties of cortical regions, and the way those are interconnected [166, 168].

Secondly, our analysis permitted to evaluate the dynamic interactions between directed functional connectivity and anatomical connectivity, before and after TMS (Fig.5.3, Fig. 5.4). The interplay between directed functional connectivity and structural connectivity at baseline is in line with findings reported in recent fMRI-dMRI studies [89, 194], where the rich repertoire of brain states do not necessarily correlate with the structural pattern. Here, our directed connectivity approach also allowed the investigation of the causal effects of systematic TMS-induced perturbations of the system, extending the insight on the relationship between structure and function. We showed that the way directed functional connectivity changes due to TMS at the natural frequency might depend on the different structural architecture of the specific cortical region (Fig. 5.4).

Thirdly, our multimodal whole-brain approach gives new insight on how TMS causally interferes with the brain network in healthy controls. More specifically, our study points out the importance of taking into account the major role played by different cortical oscillations when investigating the mechanisms for integration and segregation of information in the human brain [133, 195, 196].

Given the intrinsic limitations of the EEG in terms of spatial resolution, it is important to stress that the patterns of connectivity detected by TMS/hd-

EEG are necessarily coarse. Even though TMS-evoked potentials are characterized by a good test-retest reproducibility [197], the inter–individual reproducibility of the outgoing flow of information could be improved by a better computation of the electric field induced by TMS. More advanced models (boundary, or finite, element models) could improve the accuracy of the source localization [198].

Another limitation of our study concerns the relatively small sample size and the inter-subject variability at the tractography level. In addition, it has been shown that there are many brain regions with complex fiber architecture, also referred to as crossing fibers [63, 199]. In this context, tractography approaches based on more advanced diffusion models [199], or on more refined anatomical constraints [28] may provide more accurate anatomical connectivity patterns of brain networks. Therefore, our approach works best for studying large scale interactions than fine scale, local dynamics.

Finally, a b-value of 1000 s/mm^2 is lower than the optimal one for performing probabilistic tractography, about 2500-3000 s/mm^2 [200]. However, despite of a low b-value, with a sufficient amount of directions crossing fibers can be reliably modeled and the result is still significantly better than with a simple DTI-based model, e.g. see [201] for a successful application.

MAPPING THE FUNCTIONAL TRAITS OF LEVELS OF CONSCIOUSNESS

6

Examining resting state functional connectivity (FC) in the human brain offers insights on how spontaneous integration and segregation of information relate to human cognition, and how this organization may be altered in different conditions, and neurological disorders. In this chapter a novel data-driven methodology will be presented, namely connICA, which implements Independent Component Analysis (ICA) for the extraction of robust independent FC patterns (FC-traits) from a set of individual functional connectomes, without imposing any a priori data stratification into groups. The application of connICA to FC data from patients in disorders of consciousness (DOC) will also be presented and discussed.
***Keywords**: fMRI, resting state functional connectivity, Network Science, DOC patients, consciousness*

6.1 *Overview*

In Chapters 2 and 3 we have discussed the potential of functional connectivity (FC) in particular and brain connectivity in general in exploring the diseased human brain as a network going through systemic changes. However, there is still no clear way to accomplish two critical steps of great clinical importance. First, separate underlying FC patterns representing different functional mechanisms and, second, relate those FC patterns or subsequent network features to individual cognitive performance or clinical evaluations. This is specially the case when studying a continuum of states, where the stratification of the cohort-subjects into categories or groups is inappropriate and/or poorly defined. In this study we implemented a novel data-driven methodology, connICA, which consists of the extraction of robust independent patterns (traits) from a set of individual functional connectomes (see scheme in Figure 6.2). Here we applied connICA to investigate the link between cognitive/clinical features that define states of consciousness and

resting-state functional connectivity (FC) data. The method allows the assessment of individual FC patterns (or FC layers) in a joint data-driven fashion providing as outputs multivariate independent FC-traits, which model independent sources or phenomena present in the input. In a final step, we assess the predictability of the weights (fingerprints) of each FC-trait on each subject from demographic and consciousness related variables, allowing for a continuous mapping of levels of consciousness within functional connectomes.

6.2 Methods

6.2.1 Data acquisition and processing

The cohort studied here consists of 88 subjects with different levels of consciousness. From those, 32 were healthy controls (mean age 44 years $\pm$ 15 years, 21 males, 11 females), and 56 patients. Out of the 56, 39 were patients with disorders of consciousness (2 coma, 17 UWS, 20 MCS), 13 EMCS and 4 LIS. 28 out of 56 patients had traumatic brain injury (TBI), and 31 were sedated during the fMRI acquisition. To assess the level of consciousness, we used the scores obtained from the JFK Coma Recovery Scale-Revised (CRS-R) [202, 203] assessment for each DOC patient. The CRS-R is the most sensitive and validated [204] scale to fully characterize and monitor DOC patients and provide a global quantification of their levels of consciousness. In particular, CRS-R integrates 25 arranged items that comprise 6 sub-scales addressing auditory, visual, motor, oromotor, communication, and arousal processes. Scoring is based on the presence or absence of specific behavioral responses to sensory stimuli administered in a standardized manner. The reader can refer to [202, 203] for a detailed description of the scale. Each subject underwent structural MRI and a 10 minute fMRI resting-state (task-free) session. Data processing was performed by combining functions from FSL [205] and in-house developed Matlab (MATLAB 6.1, The MathWorks Inc., Natick, MA, 2000) code. The individual functional connectomes were modeled in the native BOLD fMRI space of each subject. Structural images were first denoised to improve the signal-to-noise ratio [206], bias-field corrected, and then segmented (FSL FAST) to extract white matter, grey matter and cerebrospinal fluid (CSF) tissue masks. These masks were warped in each individual sub-

jects functional space by means of subsequent linear and non-linear registrations (FSL flirt 6dof, FSL flirt 12dof and fnirt). BOLD fMRI functional volumes were processed according to the steps recommended by [150, 207]. Briefly, these steps included: slice timing correction; motion correction; normalization to mode 1000, demeaning and linear detrending; inclusion of 18 regressors consisting of 3 translations [x,y,z], 3 rotations [pitch, yaw, roll], and 3 tissue regressors (mean signal of whole-brain, WM and CSF), and the 9 corresponding derivatives; a scrubbing procedure censoring high motion volumes [150]; a bandpass first-order Butterworth filter in forward and reverse directions [0.001 Hz, 0.08 Hz]. After that, the 3 principal components of the BOLD signal in the WM and CSF tissue were regressed out of the GM signal. A whole-brain data-driven functional parcellation based on 278 regions, as obtained by Shen and colleagues [208], was first warped into each subjects T1 space (FSL flirt 6dof, FSL flirt 12dof and finally fnirt) and then into each subjects fMRI space. To improve the registration of the structural masks and the parcellation to the functional volumes FSL boundary-base- registration was also applied. Individual functional connectivity matrices (FC) were then estimated by means of pairwise Pearson correlations between the averaged signals of the regions of the parcellation, excluding the censored volumes as determined by the above-mentioned scrubbing procedure. Finally, the resulting FC matrices were ordered according to 7 resting-state sub-networks (RSNs) as proposed by Yeo and colleagues [77], see also Fig. 2.6 in Chapter 2). For completeness, we added two more sub-networks: an 8th sub-network representing the subcortical regions and a 9th sub-network representing the cerebellum (Fig. 6.1).

6.2.2 *ConnICA: Independent component analyses of sets of individual functional connectomes*

The input of ConnICA consists of all the individual FC profiles embedded into a dataset matrix where each row contains all the entries of the upper triangular part of the FC matrix for each subject (given the symmetry of FC) and hence provides an individual FC pattern. Note that this includes all FC matrices from all subjects, without any a priori information or any stratification of the data into groups (see scheme at Fig. 6.2). With this input, ICA decomposition of the FC patterns was applied by running fastICA algorithm

Figure 6.1: *Illustrative example of ordering individual FC matrices by resting state networks. A) The individual FC matrix of a subject. B) The same FC matrix ordered according to the resting-state sub-networks (RSNs) scheme in C) proposed by Yeo and colleagues ([77], see also Fig. 2.6 in Chapter 2). For completeness, we added two more sub-networks: an 8th sub-network representing the subcortical regions and a 9th sub-network representing the cerebellum (see C)). Note how in B), after reordering, the 9 within-network connectivity blocks pop up on the main diagonal; the off diagonal entries represent instead the between-network connectivity interaction.*

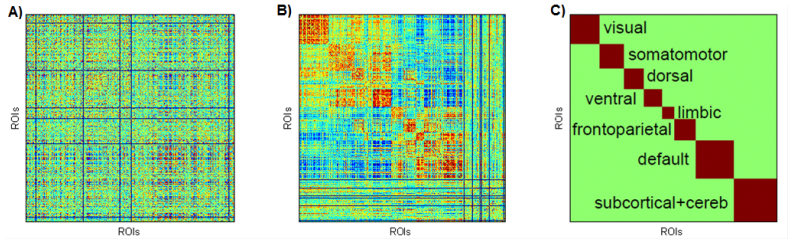

[209] and setting the number of independent components to 15. The output of connICA consists of two vectors per component. The first output vector will be referred to as FC-trait, which represents an independent pattern of functional connectivity. Interestingly, this vector can be represented back to its spatial form, i.e. a square symmetric matrix with brain regions in rows and columns. While the values here express connectivity units, they are not Pearson correlation coefficients and hence not restricted tothe [-1,1] range. The second output vector is the weight of the FC-trait on each subject, which quantifies the prominence or presence of the trait in each individual FC matrix (note that this value can be positive or negative). In that sense, connICA is maximizing the individual variance explained by the multilinear regression of the obtained collection of FC-traits and subsequent subject weights.

Given the non-deterministic nature of ICA decomposition into components, we selected only the most robust ones (from now on simply denominated FC-traits), i.e. only those independent patterns that are frequently observed during the ICA decomposition of the FC data. To do so, instead of analyzing the connICA components from a single run, we evaluated the similarity of the connICA components over 100 runs. For an FC-trait to be robust, it has to appear (correlation of 0.75 or higher across runs) in at least 75% of the runs. This criterion resulted in 5 robust FC-traits. Each of these traits is obtained by averaging the correspondent representations found along the runs. The subject weights associated to each assessed FC-traits were then used as response in an incremental multi-linear regression model with up to

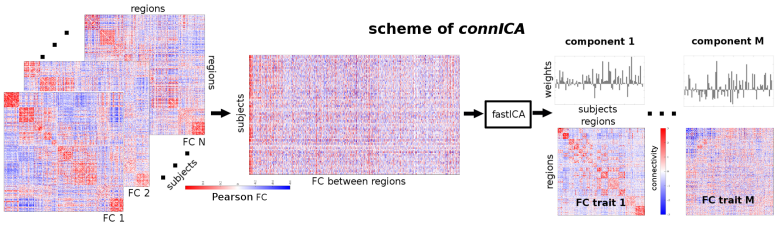

Figure 6.2: *Workflow scheme of the proposed Connectivity Independent Component Analysis (ConnICA). The N individual functional connectivity (FC) matrices (left) are concatenated into a matrix where rows are the subjects and columns are the functional connectivity entries in the FC matrix). The ICA algorithm extracts the M independent components (i.e. functional traits) associated to the whole population and their relative weights across subjects. Colorbars indicate positive (red) and negative (blue) connectivity values, being Pearson correlation coefficient values in the case of individual FC matrices (left side of scheme), and unitless connectivity weights in the case of FC-traits (right side of the scheme).*

7 predictors. The 7 predictors included the Coma Recovery Scale Revised (30) clinical subscores of each patient (Arousal, Auditory, Communication, Motor, Oromotor, Visual), and the sum of these scores. The control population was assumed to have the highest scores for each of the subscales. The following nuisance variables were also included in model: age, gender, etiology (1 for TBI, 0 otherwise), sedation (1 for sedated subjects, 0 otherwise) and the inverse of the time since the insult (in days), as we assumed healthy subjects time since onset to be infinite and hence corresponds to zero in our codification. We then identified the FC-traits whose presence (weights) in individual FCs was significantly explained by a cognitive predictor (statistical significance set at p-value ≤ 0.05, Fig. 6.3G, 6.3H, 6.3I). The aim was to extract the connectivity patterns or traits associated to clinical features that go from wakefulness to the deepest level of unawareness.

6.2.3 *Modularity analyses*

Modularity is a measure of the strength of division of a network into modules or communities. Networks with high modularity have dense connections between the nodes within modules but sparse connections between nodes in different modules. The Newman-Girvan quality function Q is a way of quantifying network modularity. It is defined as the fraction of edges that fall within modules minus the expected number of edges for a random graph with the same node degree distribution as the given network [210].

Particularly, we here used the extension of Q for signed undirected networks proposed by Mucha et al. [211], and inspired by [212, 213]. To investigate the functional organization properties of the FC-traits extracted with connICA, we first assessed the similarity of each trait with Yeos partitions using Newman-Girvan modularity function Q for signed undirected networks [211]. In other words, we wanted to evaluate to what extent each FC-trait can be well-separated into communities based on a partition based on RSNs. We then assessed the community structure of each FC-trait by using the Louvain method for identifying communities in large networks [214]. In order to improve the stability of the community detection procedure, we performed consensus clustering [215] out of a set of 100 partitions obtained by the Louvain method. Consensus clustering is a technique that seeks for a median (or consensus) partition, i.e. the partition that is most similar, on average, to all the input partitions. The similarity can be measured in several ways, for instance co-occurrence of the nodes in the clusters of the input partitions [215]. This consensus partition was finally selected as the most robust one.

6.3 *Results*

Following individual subject BOLD fMRI data processing and subsequent modeling of the individual task-free functional connectomes, connICA (see scheme Fig. 6.2) was run on the cohort of 88 subjects (32 conscious controls and 56 severely brain-damaged patients at different levels of consciousness) without imposing any a priori information or stratification into groups. The procedure included 100 runs of connICA and allowed us to identify a total of 5 robust FC-traits. Three of them were correlating with the CRS-R scores of the subject. The dominant FC-trait extracted using connICA (i.e. the one with the highest explained FC variance in the cohort) is shown in Figure 6.3D. Interestingly, it conforms to all the connectivity blocks or modules of the resting-state functional networks (RSNs, see Fig. 6.1) as introduced by Yeo and colleagues [77]. For this reason, this FC-trait was denominated the RSNs trait. An incremental multi-linear model predicting the weight or quantity of the RSNs trait on each subject (see Figure 6.3A) was used, based on up to 7 predictors (see Figure 6.3G). A significant association with arousal, a subscore of the Coma Recovery Scale-Revised (CRS-R) [202, 203], was found,

after controlling for age, gender, traumatic brain injury (TBI), sedation, onset and CRS-R total score (with none of them being significant terms). In other words, the more aroused the subject (Figure 6.3G), the higher the subject-weight associated to the RSNs trait and hence the higher the presence of such trait. The other two FC-traits linked to cognitive features associated with levels of consciousness (i.e. the CRS-R total score and the communication subscore [202, 203]) are shown in Figure 6.3E and 6.3F. In particular, the FC-trait depicted in Figure 6.3E mainly captures changes of intra-hemispheric functional connectivity in the visual and sensory motor networks across subjects in different levels of consciousness. We will refer to it as the VIS-SM trait. A significant link with the CRS-R communication subscore [202, 203] was found, as well as with three other variables previously added to the multilinear model (precisely with TBI, sedation and onset, see Figure 6.3H).

The positive sign of the beta coefficient associated to the communication subscore indicates that the trend of the linear fit follows the correspondent individual weights of the FC trait. In other words, the higher the communication subscore of a subject, the higher the contribution or presence of the VIS-SM trait in his/her functional connectome (Figure 6.3B). Interestingly, when adding etiology, sedation and time since onset (quantified here as the inverse of the days since the insult, see Methods), the explained variance of the model significantly increased. The negative sign of the associated beta coefficients for the three nuisance variables indicates a negative slope in the fit with the FC individual weights. That is, in the case of etiology, TBI patients have a lower amount of the VIS-SM trait in their functional connectomes; in the case of sedation, sedated patients have a lower contribution of the trait on their individual FC patterns; in the case of time since onset, the more recent the insult, the lower the prominence of the VIS-SM trait on the individual FC of the patient. The trait shown in Figure 6.3F mainly captures modifications in the connectivity between DMN and fronto-parietal networks (hence denominated FP-DMN trait). Interestingly, the FP-DMN trait is linked to the CRS-R sum of scores, but also to the CRS-R communication subscore, even when the sum of scores is already added to the multilinear model (Figure 6.3I). The positive sign of the beta coefficient associated to these two predictors indicates that the higher the CRS-R sum of scores (communication subscore) for a subject, the higher the presence of the FP-DMN trait on his

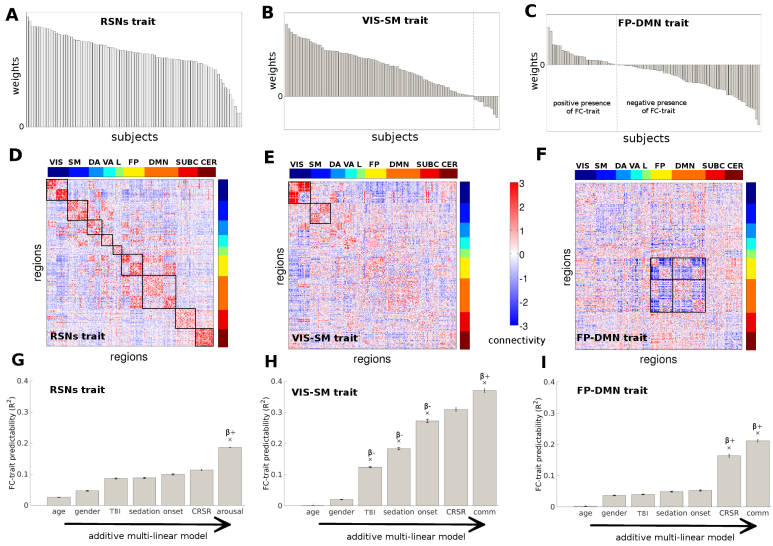

Figure 6.3: *Mapping of the three main functional traits and their predictability by consciousness features. A-C) Quantified presence of each FC-trait on each individual functional connectome. Subject weights are sorted from greater to smaller on each FC-trait. D-F) Visualization of the three FC-traits associated to consciousness features. The brain regions are ordered according to Yeo [77] functional RSNs as indicated : Visual (V), Somato-Motor (SM), Dorsal Attention (DA), Ventral Attention (VA), Limbic system (L), Fronto-Parietal (FP), Default Mode Network (DMN), and for completeness, also subcortical regions (SUBC) and cerebellum (CER). G-I) Bar-plot of the FC-traits predictability based on additive multi-linear regression models when predictors are sequentially introduced in the following order: age, gender, trauma, sedation, inverse of the time since onset, Coma Recovery Scale-Revised (CRS-R) total scores and the CRS-R communication subscore. Error bars show the standard error across the 100 ICA runs. Crosses on the top of a bar indicate that the inclusion of the correspondent predictor significantly increased the predictability of the model. The sign of the beta coefficient associated to each significant variable is shown below each asterisk, indicating whether there is a negative or positive trend with respect to the weights of the FC traits.*

functional connectome. Notably, as one goes lower in the levels of consciousness, the contribution of the FP-DMN trait on the FC of a subject flips sign from negative to positive (see the sorted individual weights associated to FP-DMN trait, Figure 6.3C, 6.3F). There is an analogous effect in a few subjects for the VIS-SM trait (Figure 6.3B, 6.3E). Further analyses were performed on VIS-SM and FP-DMN traits to assess the presence of communities (Figure 6.4) by using consensus clustering [215] over 100 modularity solutions computed using the Louvain algorithm [214] with quality function Q extended to signed networks [211] (see Methods). For both traits, the highest modularity was associated to partitions of three modules. The most influential module (the highest within-module average) for the VIS-SM trait appears to be the one comprising the occipital cortex and higher order visual areas. Notably, the latter is strongly decoupled from the DMN module (highest between-modules negative connectivity, Figure 6.4B), suggesting that in a healthy brain these two modules are negatively correlated. This modular configuration is then altered after modifications of levels of consciousness. The modular organization of FP-DMN trait revealed a substantial division of the brain in two hemispheres. The between-modules average weight shows that the most antagonistic communities encompass the two different hemispheres (Figure 6.4D), indicating that in normal consciousness the hemispheres are also anti-correlated. This decoupling or negative inter-module connectivity might change (i.e. it turns to positive, Figure 6.3C, 6.3F) following loss of consciousness.

6.4 *Discussion*

In this work we applied a novel data-based methodology, connICA, to the field of Brain Connectomics. Our approach is based on extracting independent connectivity traits from a set of individual functional connectomes to extract and map robust independent mechanisms or processes that explain the FC patterns of an entire cohort of subjects, without setting any a priori stratification into groups. We used the connICA framework to assess rsfMRI in 88 subjects with different levels of consciousness: 32 conscious controls and 56 severely damaged patients (2 coma, 17 UWS, 20 MCS, 13 EMCS, 4 LIS) of different etiology and duration, 31 of whom were acquired while re-

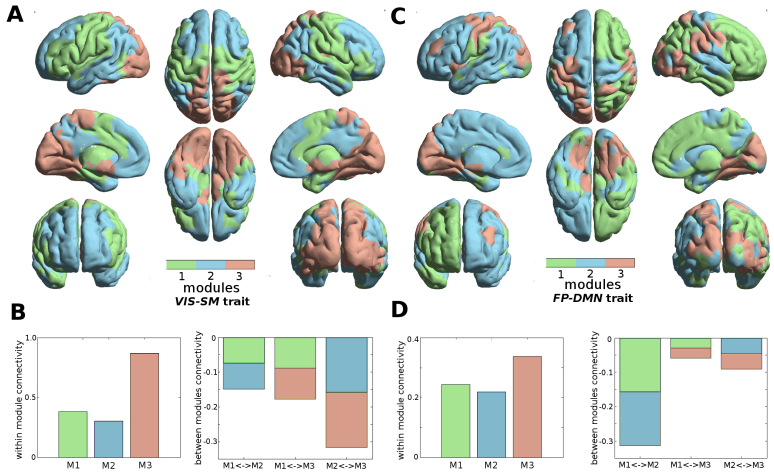

Figure 6.4: *A) Brain render of the modules obtained on VIS-SM trait (see Materials and Methods). Each color represents region membership in a module. B) Left: bar plot of the average weight within each module in VIS-SM trait. Right: bar plot of the average between-module weight in VIS-SM trait. C) Brain render of the modules obtained on FP-DMN trait. D) Left: bar plot of the average weight within each module in FP-DMN trait. Right: bar plot of the average between-module weight in FP-DMN trait.*

ceiving sedative drugs to control for movement artifacts. We investigated the functional connectivity traits underlining specific sensorimotor/cognitive capacities related to consciousness.

We showed how these traits separate the FC data into network subsystems with significant associations to levels of consciousness. Notably, this methodology allowed us to map and match the most meaningful functional traits to consciousness-related predictors taken at the patients bedside. This approach established the link between the alteration of levels of consciousness and the connectivity core associated to it.

The connICA framework provides a multiplex data-driven way to extract and compact (dimensionality reduction) the most meaningful multivariate information contained in the functional connectomes in a relatively small set of connectivity traits. In this work we showed how the modification of levels of consciousness is associated to specific connectivity disruptions using as reference seven widely accepted RSNs (i.e., visual, somatomotor, dorsal attention, ventral attention, limbic system, fronto-parietal, default mode network [77], and for completeness, also subcortical regions (SUBC) and cerebellum (CER), see Figure 6.1C). One additional advantage of this

approach is that the dimensionality of the output is significantly reduced, both in the number of the robust components extracted with respect to the initial population size (in the study analyzed here, 5 FC-traits starting from 88 FC matrices) and in the number of variables to be encoded in the multi-linear models, hence notably decreasing number of multiple comparisons. As opposed to univariate approaches mapping up to N(N-1)/2 functional connections and their subsequent multi-linear models (N being the number of brain regions), the multi-layered output of connICA allows to focus on a small subset of robust FC-traits (by definition, a subset smaller or equal to the number of components set). This dimensionality reduction does not compromise but rather considerably facilitates the interpretability of the results, by compressing the individual variability into the most meaningful independent functional cores. It is noteworthy that most if not all the traits would have been missed with a standard group-average analysis of the functional connectomes.

By using connICA, we extracted three independent functional connectivity traits linked to cognitive features of levels of consciousness. The RSNs trait (Figure 6.3D) is the closest to the Yeos RSNs organization [77]. It seems mainly associated to a global drop in the functional connectivity within each of the networks, and correlates with the CRS-R arousal subscore. We might think of this trait as the one of an awake resting brain. It reflects the connectivity organization of a functioning brain, which might be at least partially driven by its underlying structural connectivity [91, 216].

The VIS-SM trait seems more associated to the effect of the pathology (i.e. etiology, time since onset) and the sedation level (Figure 6.3H). It shows a more prominent disruption in the occipital and sensorimotor areas as the level of consciousness decreases (Figure 6.3E), and it also correlates with functional communication (Figure 6.3H). Interestingly, the modularity analysis suggests that visual areas and DMN are anti-correlated in normal wakefulness (Figure 6.4A, 6.4B), stressing the importance of the interaction between the so called sensory slave regions [217] and higher order cognitive regions as the DMN, for consciousness and functional communication [218].

However, the recovery of this connectivity pattern seems not a sufficient condition for the restoration of levels of consciousness. Another independent functional trait appears to be linked to behavioral assessment of levels of con-

sciousness, particularly to both the CRS-R total score and the communication subscore (FP-DMN trait, Figure 6.3F). The FP-DMN trait captures changes in the anti-correlation between the FP-DMN networks. Notably, as one goes towards the deepest unconsciousness, the FP-DMN anti-correlation decreases, until the point where it flips to positive correlation, (see Figure 6.3C, 6.3F). This is in line with a recent study [128], showing that negative connectivity between DMN and FP networks was significantly different between patients and healthy controls. In this respect, the fact that the FP-DMN trait is strongly correlated to the communication subscore corroborates the idea that recovery of the FP-DMN between-network negative connectivity is prerequisite in order to regain functional communication.

Notably, the modularity analysis on FP-DMN trait reveals that the decoupling between the two hemispheres (Figure 6.4C) represents a healthy way of communication between left and right brain areas. The anti-correlation between hemispheres tends to disappear (i.e. goes towards zero or even positive correlation, see the individual weights of FP-DMN trait in Figure 6.3C) as levels of consciousness decrease. Indeed, in this study we show that the interaction between specialized modules, as the VIS-SM interaction with DMN or the FP-DMN between-networks negative connectivity, is crucial for the emergence of consciousness. Perhaps this laterality enhances the complexity of ongoing brain processes and facilitates demanding cognitive processes such as consciousness of the self and the surrounding.

Taken together, these findings suggest that the connectivity core which differentiates across levels of consciousness is a combination of positive and negative interactions between functional sub-networks. This evidence stresses the importance of a whole-brain network modulation between coherent and non-coherent functional states. The disruption of the equilibrium between these two might lead to changes in levels of consciousness and, ultimately, to reduced levels of consciousness.

CONCLUDING REMARKS

During my 4 years of PhD work I have implemented and tested novel methods to assess brain connectivity in different levels of consciousness, by means of different neuroimaging techniques. Below is a concluding summary of the findings.

Study I (Chapter 4, Appendix A)

Resting-state fMRI volumes on 18 healthy subjects were acquired in four clinical states during propofol injection: wakefulness, sedation, unconsciousness, and recovery. The dataset was reduced to a spatiotemporal point process by selecting time points in the Posterior Cingulate Cortex (PCC) at which the signal is higher than a given threshold (i.e. BOLD intensity above 1 standard deviation).

Spatial clustering on the PCC time frames extracted was then performed (number of clusters=8), to obtain 8 different PCC co-activation patterns (CAPs) for each level of consciousness.

The current analysis showed that the core of the PCC-CAPs throughout consciousness modulation seems to be preserved.

Nonetheless, this methodology enabled to differentiate region-specific propofol-induced deactivations in PCC-CAPs, some of them already present in the literature (e.g. disconnections of the prefrontal cortex, thalamus, auditory cortex), some others new (e.g. motor cortex and visual area deactivations).

Study II (Chapter 5, Appendix B)

Directed functional connectivity interactions between cortical areas from the source reconstructed TMS/hd-EEG recordings were computed on a cohort of 14 healthy volunteers and correlated them with the correspondent structural connectivity matrix extracted from dMRI tractography,

in three different frequency bands (alpha, beta, gamma) and two sites of stimulation (left precuneus and left premotor).

Each stimulated area appeared to mainly respond to TMS by being functionally elicited in specific frequency bands, i.e. beta for precuneus and gamma for premotor. A temporary decrease in the whole-brain correlation between directed functional connectivity and structural connectivity after TMS in all frequency bands was observed.

Notably, when focusing on the stimulated areas only, we found that the structure-function correlation significantly increases over time in the premotor area contralateral to TMS.

These results shed further light on the link between structure and function of human cortical networks in health and might pave the way for a novel and non-invasive approach to study neurological and psychiatric conditions.

Study III (Chapter 6, Appendix C)

A novel data-driven methodology, connICA, was presented. ConnICA implements Independent Component Analysis (ICA) for the extraction of robust independent FC patterns (FC-traits) from a set of individual functional connectomes, without imposing any a priori data stratification into groups.

connICA was applied to investigate associations between network-traits derived from task-free FC and cognitive/clinical features that define levels of consciousness. Three main independent FC-traits were identified and linked to consciousness-related clinical features.

The first one represents the functional configuration of an awake resting brain, and is associated to the level of arousal. The second FC-trait reflects the disconnection of the visual and sensory-motor connectivity patterns and relates to the ability of communicating with the external environment. The third FC-trait isolates the connectivity pattern encompassing the fronto-parietal and the default-mode network areas as well as the interaction between left and right hemisphere, which are also associated to the awareness of the self and its surroundings.

Each FC-trait represents a distinct functional process with a role in the degradation of conscious states in functional brain networks, shedding further light on the functional sub-circuits that get disrupted in severe brain-damage.

Future work

There are several different avenues to explore for extending this PhD work. In short:

- In my first study I have shown that functional changes in the brain associated to propofol-induced modulation of consciousness can be efficiently revealed by tracking the patterns of co-activation in the Posterior Cingulate Cortex. A partially preserved co-activation core, probably reflecting the structural connectivity present in a living (albeit anesthetized) brain was also observed. A future line of research will involve the investigation of the co-activation patterns in patients with disorders of consciousness following severe brain injury, where the brain structure might be damaged or disrupted.

- In my second study I have implemented a novel multimodal whole-brain approach to evaluate the dynamic interactions between directed functional connectivity and anatomical connectivity, before and after transcranial magnetic stimulation. An interesting follow up of this study would indeed be to look at differences in structure-function interactions either when the cognitive function is pharmacologically modulated (i.e. anesthesia), or following pathology, damage or disruption in structural connections (i.e. disorder of consciousness).

- In my third study I have presented a novel data-based methodology, connICA to extract independent connectivity traits from a set of individual functional connectomes. Future work can be extended to the use of connICA for structural connectivity patterns, hence identifying SC-traits within a population of subjects. This approach is not limited to assessing consciousness, but has the potential of studying other progressive diseases and disorders, drug-induced effects (i.e. anesthesia), and also differences based on aging or gender. When associating

traits with cognitive/clinical features, multi-linear models employed here can be expanded by allowing for non-linear terms and interactions, which could capture more complex associations between connectivity patterns and cognition.

PAPER I

A

Posterior Cingulate Cortex-Related Co-Activation Patterns: A Resting State fMRI Study in Propofol-Induced Loss of Consciousness

Amico E., Gomez F., Di Perri, C.,
Vanhaudenhuyse, A., Lesenfants, D., Boveroux, P.,
Bonhomme, V., Brichant, J.F., Marinazzo, D., Laureys, S.

PLoS One, 2014, 9(6):e100012.

OPEN ACCESS Freely available online

PLOS ONE

Posterior Cingulate Cortex-Related Co-Activation Patterns: A Resting State fMRI Study in Propofol-Induced Loss of Consciousness

Enrico Amico[1,2]*, Francisco Gomez[1], Carol Di Perri[7], Audrey Vanhaudenhuyse[1,6], Damien Lesenfants[1], Pierre Boveroux[1,4], Vincent Bonhomme[1,4,5], Jean-François Brichant[4], Daniele Marinazzo[2], Steven Laureys[1,3]

1 Coma Science Group, Cyclotron Research Centre, University of Liège, Liège, Belgium, **2** Faculty of Psychology and Educational Sciences, Department of Data Analysis, Ghent University, Ghent, Belgium, **3** Department of Neurology, University of Liège, Liège, Belgium, **4** Department of Anesthesia and Intensive Care Medicine, CHU Sart Tilman Hospital, University of Liège, Liège, Belgium, **5** Department of Anesthesia and Intensive Care Medicine, CHR Citadelle, University of Liège, Liège, Belgium, **6** Department of Algology and Palliative Care, CHU Sart Tilman Hospital, University of Liège, Liège, Belgium, **7** Department of Neuroradiology, National Neurological Institute C. Mondino, Pavia, Italy

Abstract

Background: Recent studies have been shown that functional connectivity of cerebral areas is not a static phenomenon, but exhibits spontaneous fluctuations over time. There is evidence that fluctuating connectivity is an intrinsic phenomenon of brain dynamics that persists during anesthesia. Lately, point process analysis applied on functional data has revealed that much of the information regarding brain connectivity is contained in a fraction of critical time points of a resting state dataset. In the present study we want to extend this methodology for the investigation of resting state fMRI spatial pattern changes during propofol-induced modulation of consciousness, with the aim of extracting new insights on brain networks consciousness-dependent fluctuations.

Methods: Resting-state fMRI volumes on 18 healthy subjects were acquired in four clinical states during propofol injection: wakefulness, sedation, unconsciousness, and recovery. The dataset was reduced to a spatio-temporal point process by selecting time points in the Posterior Cingulate Cortex (PCC) at which the signal is higher than a given threshold (i.e., BOLD intensity above 1 standard deviation). Spatial clustering on the PCC time frames extracted was then performed (number of clusters = 8), to obtain 8 different PCC co-activation patterns (CAPs) for each level of consciousness.

Results: The current analysis shows that the core of the PCC-CAPs throughout consciousness modulation seems to be preserved. Nonetheless, this methodology enables to differentiate region-specific propofol-induced reductions in PCC-CAPs, some of them already present in the functional connectivity literature (e.g., disconnections of the prefrontal cortex, thalamus, auditory cortex), some others new (e.g., reduced co-activation in motor cortex and visual area).

Conclusion: In conclusion, our results indicate that the employed methodology can help in improving and refining the characterization of local functional changes in the brain associated to propofol-induced modulation of consciousness.

Citation: Amico E, Gomez F, Di Perri C, Vanhaudenhuyse A, Lesenfants D, et al. (2014) Posterior Cingulate Cortex-Related Co-Activation Patterns: A Resting State fMRI Study in Propofol-Induced Loss of Consciousness. PLoS ONE 9(6): e100012. doi:10.1371/journal.pone.0100012

Editor: Yong He, Beijing Normal University, Beijing, China

Received February 27, 2014; **Accepted** May 21, 2014; **Published** June 30, 2014

Funding: This research was supported by the Belgian Funds for Scientific Research (FRS), European Commission (DECODER), Belgian Science Policy (CEREBNET), McDonnell Foundation, European Space Agency, Wallonia-Brussels Federation Concerted Research Action Mind Science Foundation, University of Liège. The funders had no role in study design, data collection and analysis, decision to publish, or preparation of the manuscript.

Competing Interests: Daniele Marinazzo is a PLOS ONE Editorial Board member. This does not alter the authors' adherence to PLOS ONE Editorial policies and criteria.

* Email: eamico@ulg.ac.be

Introduction

Functional magnetic resonance imaging (fMRI) technique has been widely used in the investigation of brain connectivity patterns at rest [1,2]. Blood-oxygen-level dependent (BOLD) signal activity at rest is organized in correlated spatial patterns, which are called "resting state networks" (i.e. RSNs). These networks have been increasingly investigated and their modulation or disruption has been associated to several pathophysiological conditions [3,4], together with the importance of these RSNs to provide information about brain dynamic organization, as a complement to structural information.

In particular, in altered states of consciousness it's important to see which functional connections remain unaltered and which ones are modified or disrupted [5,6]. In this regards, functional connectivity studies of RSNs in induced sedation through anesthesia, have shown widespread changes in fronto-parietal networks, compared with the relative preservation of sensory networks, suggesting a major role of higher-order frontoparietal associative network activity in the loss of consciousness phenom-

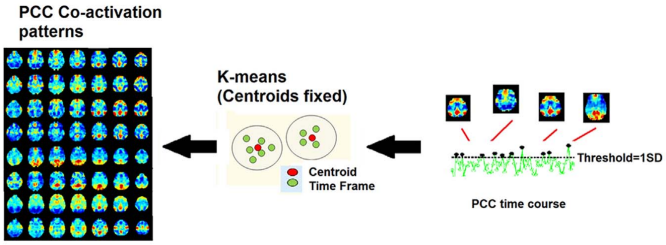

Figure 1. Co-activation patterns (CAPs). The approach is similar to the ones proposed in [16] and [15]. After the extraction of a seed region, in this case Posterior Cingulate Cortex (PCC), a threshold equal to 1 standard deviation(SD) was applied, as to consider only the time points corresponding to peaks in the BOLD signal; next, the spatial maps (namely, time frames), associated with these time points are collected and clusterized using k-means, with a number of clusters fixed to 8. The centroids were kept fixed as well, to allow cluster comparison between the different clinical conditions. The within-cluster time frames were then averaged to obtain 8 spatial PCC-related co-activation patterns. Finally, the computation was iterated over the 4 different states of consciousness (wakefulness, sedation, unconsciousness, recovery), obtaining 8 PCC-related co-activation patterns for each state.
doi:10.1371/journal.pone.0100012.g001

ena [7,8]. Moreover, functional impairment of highly connected frontoparietal areas seems to have greater repercussions on global brain function than on less centrally connected sensorimotor areas [9,10].

Additionally, recent studies have been shown that functional connectivity of cerebral areas is not a static phenomenon, but exhibits spontaneous fluctuations over time [11–13]. Previously, fluctuations of functional connectivity have been thought to reflect changing levels of vigilance, task switching or conscious processing. There is evidence that fluctuating connectivity is an intrinsic phenomenon of brain dynamics that persists even during anesthesia [11]. Fluctuations of functional connectivity within an attention network in macaques have been demonstrated and interpreted as mechanistically important network information [14]. Still, the relationship between changes of consciousness and network dynamics is not understood yet.

Lately, a new approach in exploring functional brain connectivity, using point process analysis, has been proposed by Tagliazucchi et al. [15]. The main idea in this work is that important features of brain functional connectivity at rest can be obtained from BOLD fluctuations, isolating the periods in which the signal crosses some amplitude threshold. In this way the study of the dynamics of a continuous BOLD time series is reduced to the exploration of a discretized one (a point process), defined by time and location of BOLD signal threshold crossings. Through point process analysis, Tagliazucchi and colleagues showed that much of the information regarding a specific RSN is actually contained in a fraction of critical time points (i.e. BOLD signal peaks) of a resting state dataset. This idea has next been adopted by Liu et al. [16], in a study showing that seed-based RSNs extracted from fMRI BOLD signal are averages of multiple distinct spatial co-activations patterns (CAPs) at different time points, and that the analysis of these patterns might provide more fine-grained information on brain functional network organization.

In the present study we want to extend and apply this methodology for the investigation of fMRI resting state spatial pattern changes during propofol-induced modulation of consciousness, with the central aim of extracting new information regarding brain networks consciousness-dependent fluctuations.

Materials and Methods

Ethics Statement

The study was approved by the Ethics Committee of the Medical School of the University of Liège (University Hospital, Liège, Belgium). The subjects provided written informed consent to participate in the study.

Clinical Protocol

The present work is a reanalysis of previous published data [7,8]. Eighteen healthy right-handed volunteers participated in the study. Subjects fasted for at least 6 h from solids and 2 h from liquids before sedation. During the study and the recovery period, electrocardiogram, blood pressure, pulse oxymetry (SpO2), and breathing frequency were continuously monitored (Magnitude 3150M; Invivo Research, Inc., Orlando,FL). Propofol was infused through an intravenous catheter placed into a vein of the right hand or forearm. An arterial catheter was placed into the left radial artery. Throughout the study, the subjects breathed spontaneously, and additional oxygen (5 l/min) was given through a loosely fitting plastic facemask. The level of consciousness was evaluated clinically throughout the study with the scale used by Ramsay et al. [17].

The subject was asked to strongly squeeze the hand of the investigator. She/he was considered fully awake or to have recovered consciousness if the response to verbal command (squeeze my hand) was clear and strong (Ramsay 2), in sedation if the response to verbal command was clear but slow (Ramsay 3), and in unconsciousness if there was no response to verbal command (Ramsay 5–6). For each consciousness level assessment, Ramsay scale verbal commands were repeated twice. Functional MRI acquisitions consisted of resting-state functional MRI volumes repeated in four clinical states: normal wakefulness (Ramsay 2), sedation (Ramsay 3), unconsciousness (Ramsay 5), and recovery of consciousness (Ramsay 2). The typical scan duration was half an hour in each condition. The number of scans per session (197 functional volumes) was matched in each subject to obtain a similar number of scans in all four clinical states. Functional images were acquired on a 3 Tesla Siemens Allegra scanner (Siemens AG, Munich, Germany; Echo Planar Imaging sequence using 32 slices; repetition time = 2460 ms, echo time = 40 ms, field of view = 220 mm, voxel size = $3.45 \times 3.45 \times 3$ mm^3, and matrix size = $64 \times 64 \times 32$).

Table 1. Stereotactic coordinates of peak voxels in clusters of PCC-CAPs showing a linear correlation with propofol-induced changes in consciousness.

CAP 1	**x**	**y**	**z**	**Z-value**	**FDR-p**
Right Superior Frontal Gyrus	18	42	48	5.41	0.002
Left Superior Medial Frontal Gyrus	−9	60	30	5.12	0.002
Left Mid Orbital Gyrus	0	57	−9	4.65	0.004
Right Superior Medial Frontal Gyrus	9	57	36	4.06	0.016
CAP 2	**x**	**y**	**z**	**Z-value**	**FDR-p**
Left Superior Medial Frontal Gyrus	−3	60	9	6.55	<0.001
Left Superior Frontal Gyrus	−15	60	24	6.55	<0.001
Right Precuneus	3	−54	36	5.54	<0.001
Left Middle Cingulate Cortex	0	−36	39	3.09	0.011
Right ParaHippocampal Gyrus	24	−21	−18	4.47	<0.001
Right Angular Gyrus	60	−63	33	3.97	<0.001
Left Middle Temporal Gyrus	−63	−15	−24	3.38	0.005
CAP 3	**x**	**y**	**z**	**Z-value**	**FDR-p**
Left Anterior Cingulate Cortex	0	39	15	5.23	0.003
Thalamus	0	−12	0	4.48	0.012
CAP 5	**x**	**y**	**z**	**Z-value**	**FDR-p**
Right Superior Medial Frontal Gyrus	3	57	12	6.55	<0.001
Left Superior Medial Frontal Gyrus	0	57	3	6.55	<0.001
Left Precentral Gyrus	−39	−18	60	5.47	<0.001
Right Cerebellum	27	−33	−33	5.053	<0.001
Hippocampus	15	−33	−9	3.47	0.011
Right Precuneus	3	−57	21	4.83	<0.001
Left Middle Temporal Gyrus	−66	−15	−21	4.75	<0.001
Right Inferior Occipital Gyrus	48	−81	−6	4.03	0.002
Left Superior Frontal Gyrus	−21	30	48	4.51	<0.001
Right Postcentral Gyrus	57	−15	48	4.28	<0.001
Right Precentral Gyrus	48	−15	60	3.64	0.006
Left Precuneus	−9	−45	39	3.61	0.007
CAP 6	**x**	**y**	**z**	**Z-value**	**FDR-p**
Left Middle Frontal Gyrus	−24	30	54	7.52	<0.001
Right Superior Frontal Gyrus	27	27	54	7.11	<0.001
Right Middle Frontal Gyrus	45	18	48	5.68	<0.001
Right Precuneus	9	−54	15	6.12	<0.001
Left Hippocampus	−15	−33	−6	5.09	<0.001
Left Middle Temporal Gyrus	−57	−18	−24	5.55	<0.001
Right Fusiform Gyrus	30	−27	−21	4.71	<0.001
Right ParaHippocampal Gyrus	30	−36	−9	3.69	0.005
CAP 7	**x**	**y**	**z**	**Z-value**	**FDR-p**
Left Thalamus	6	−12	9	5,48	<0.001
Right Thalamus	6	−12	0	5,48	<0.001
Left Anterior Cingulate Cortex	0	48	9	5,25	<0.001
Left Precuneus	−15	−60	21	4,67	0,001
Right Precuneus	12	−51	15	4,43	0,002
Right Calcarine Gyrus	12	−60	15	4,37	0,002
Right Middle Frontal Gyrus	33	30	45	4,19	0,003
Right Superior Frontal Gyrus	24	33	54	3,61	0,012
Right Inferior Temporal Gyrus	54	3	−39	3,93	0,006

Table 1. Cont.

CAP 7	x	y	z	Z-value	FDR-p
Left Middle Cingulate Cortex	0	−33	48	3,86	0,007
Hippocampus	−24	−9	−21	3,84	0,007
Right Inferior Frontal Gyrus	48	39	15	3,74	0,009
Right Inferior Parietal Lobule	51	−51	57	3,47	0,016
CAP 8	**x**	**y**	**z**	**Z-value**	**FDR-p**
Left Postcentral Gyrus	−54	−18	54	6,58	<0.001
Right Postcentral Gyrus	63	−12	42	4,86	0,001
Right Precentral Gyrus	48	−6	60	3,91	0,011
Right Middle Temporal Gyrus	60	−12	−24	4,76	0,002
Left Superior Medial Frontal Gyrus	0	57	6	3,82	0,013
Left Anterior Cingulate Cortex	−12	45	0	3,65	0,018
Left Middle Temporal Gyrus	−57	−6	−18	4,43	0,005
Left Rolandic Operculum	−39	0	15	4,32	0,005
Left Insula Lobe	−42	−9	3	3,84	0,012
Right Rolandic Operculum	48	−12	21	4,15	0,007
Left Amygdala	−27	−3	−24	3,95	0,011
Right Hippocampus	30	−3	−24	3,95	0,011

doi:10.1371/journal.pone.0100012.t001

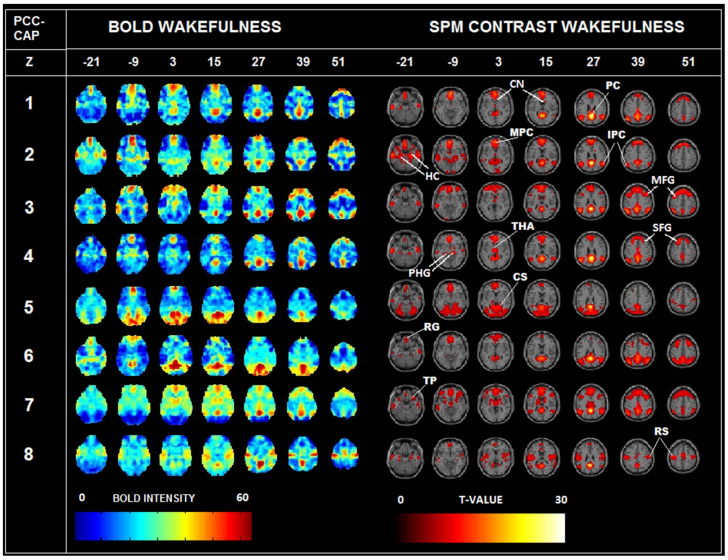

Figure 2. PCC-CAPs in wakefulness. Left: PCC co-activation patterns in wakefulness (colormap normalized by BOLD intensity), current dataset (18 subjects). Note the similarity of these patterns with the ones showed in Fig. 2 of [16]. Right: t-test on the same CAPs in the awake state showing statistically significant PCC co-activations. The seven slices shown in the maps are at Z = −21, −9, 3, 15, 27, 39, 51, respectively. The activation of precuneus (PC) appears in all 8 CAPs (see Z = 27); superior frontal gyrus (SFG) is co-activated in CAPs 1, 2, 3, 4, 6, 7 (Z = 39 and 51); the mesial prefrontal cortex (MPC) in CAPs 1, 2, 3, 4, 5, 6, 7 (Z = 3); rectus gyrus (RG) in CAPs 1, 2, 3,4, 5, 6, 7 (Z = −21); thalamus(THA) in CAPs 4 and 7 (Z = 3); caudate nucleus (CN) in CAPs 1, 3, 7 (Z = 15); temporal pole (TP) in all CAPs (slice Z = −21); hippocampus(HC) in CAPs 2, 4, 6, 8 (Z = −21); parahippocampus gyrus(PHG) in CAPs 2 and 4 (Z = −9); intraparietal cortex(IPC) all CAPs (Z = 27); medial frontal gyrus(MFG) in CAPs 3, 6, 7 (Z = 39); cuneus(CS) in CAPs 4 and 5 (Z = 3); rolandic stripe(RS) in CAPs 5 and 8 (Z = 51). Note how all these region-specific PCC co-activations survive to the t-test (e.g. HC for CAPs 2, 4, 6, 8; MFG for CAPs 3, 6, 7; PHG for CAPs 2, 4 etc.)
doi:10.1371/journal.pone.0100012.g002

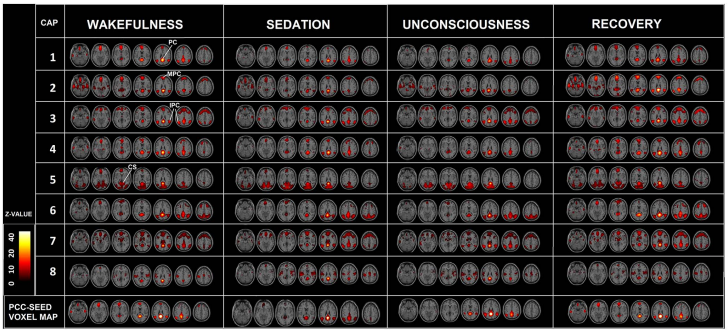

Figure 3. CAPs at different levels of consciousness. Co-activation patterns (t-contrast) in wakefulness (left), sedation (middle-left), unconsciousness (middle-right), recovery (right), corrected at FDR $p<0.05$. Lower panel shows PCC seed-voxel correlation maps for each state. The seven slices shown in the maps are at $Z=-21, -9, 3, 15, 27, 39, 51$, respectively. Spatial patterns in wakefulness and recovery do not significantly differ from each other. Precuneal (PC) activations are preserved in all CAPs in all conditions ($Z=27$ and $Z=39$); mesial prefrontal (MPC) cortical activity is preserved in CAPs 1, 2, 3, 4 and 7 during wakefulness, sedation and recovery ($Z=27$); intraparietal cortex (IPC) activation is preserved in CAPs 1, 2, 3, 4, 6 and 7 in all conditions ($Z=39$); cuneus(CS) in CAPs 4 and 5 in all conditions ($Z=3$). Note that PCC-CAPs add spatial region-specific information to the network characterization across the different stages of consciousness, when compared to the equivalent PCC seed-based contrast (last row), which exhibit a prominent drop of frontal activation during sedation and unconsciousness.
doi:10.1371/journal.pone.0100012.g003

fMRI preprocessing

The fMRI data were preprocessed using Statistical Parametric Software (SPM8), performing the typical preprocessing steps of functional connectivity analysis. These steps included motion correction, spatial smoothing (FWHM = 8 mm), temporal filtering with a bandpass filter (0.005 to 0.1 Hz), and the removal of linear and quadratic temporal trends. In addition, the brain-averaged signal, the time series of regions of interest in the white matter and cerebrospinal fluid, and six affine motion parameters were regressed out from the dataset. The fMRI data of each subject was first spatially coregistered to high-resolution anatomical images and then to the 152-brain Montreal Neurological Institute (MNI) space. It has recently been shown that even after standard motion correction, residual head movements can still inflate connectivity measures [18]. In order to evaluate the extent of these residual motion artifact in CAPs, for each subject and for each state of consciousness, we computed the two indices proposed by [18], i.e. Framewise Displacement (FD) and DVARS: D referring to temporal derivative of timecourses, VARS referring to root mean square (RMS) variance over voxels. FD is a scalar quantity that expresses instantaneous head motion, while DVARS is a measure of how much the intensity of a brain image changes in comparison to the previous timepoint [18]. Secondly, we defined as motion corrupted the frames in which FD and DVARS values were both above 0.5 mm for FD and 0.5% Bold for DVARS, as suggested in the same paper. Next, for each state of consciousness, we checked if there were corrupted time frames in our PCC-CAPs, and the percentage of these frames over the whole sample (see also Figure S4). We noticed that the percentage of corrupted time frames in wakefulness was 5% of the total number of frames collected; in sedation 3%; in unconsciousness 8%; in recovery 1%. However, there was no significant difference between CAPs calculated with or without artifact removal. Additionally, the preprocessed fMRI data were resampled to $3\times3\times3$ mm^3 in the MNI space, and the signal of each voxel was demeaned and normalized by its temporal standard deviation (SD).

Co-activation patterns construction

After preprocessing, the dataset was reduced to a spatio-temporal point process [15] by selecting time points in the seed region at which the signal is higher than a given threshold. In this work we used a $6\times6\times6$ mm^3 cube centered at the posterior cingulate cortex (i.e. PCC, [0, 53, 26] in MNI coordinates, identical to Liu et al. [16]). We chose PCC as seed to study default mode network (DMN) variability during consciousness modulation, since PCC is widely known as a central node in the DMN [19,20]. CAPs construction can then be summarized in three steps (Fig. 1):

1. First, we collected all the points in the normalized PCC time course where the BOLD signal was above threshold. In our study we fixed the threshold at 1 SD, roughly the 15% of the whole dataset. This percentage did not significantly vary across the four levels of consciousness. For each of these points in the PCC, and for each of the 4 levels of consciousness, we collected the relative spatial maps (Fig. 1). These spatial maps, or time frames [16], represent whole-brain patterns of functional activations correlated to PCC BOLD peaks, previously extracted using this thresholding approach.
2. In order to achieve a spatio-temporal mapping of correlated activity we clustered all the time frames which were significantly co-activated with PCC, in the same way as described in [16]. The sorting of the time frames was performed by K-means clustering, a machine learning classification method able to group unlabeled data into clusters. Once that the desired number of clusters has been fixed, K-means iteratively optimizes the position of the centers in order to minimize the total variance within each cluster [21]. We performed K-means (number of clusters fixed at 8) over all the spatial maps collected to classify the time frames based on their spatial similarity, and then averaging them within-cluster to extract 8 different spatial PCC-related co-activation patterns (i.e. CAPs [16]). Here, since we also aimed to compare different PCC-CAPs between different conditions (i.e. 4 different levels of consciousness), we added an extra step. With the purpose of

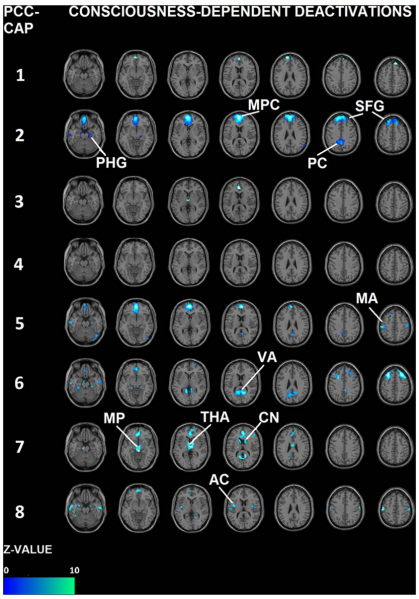

Figure 4. Decreases in CAPs. This figure shows the local decreases in co-activation from wakefulness to unconsciousness, using the same t-contrast as in [7]. All the images report contrast which are significant at $p<0.05$, FDR corrected. The seven slices shown in the maps are at $Z = -21, -9, 3, 15, 27, 39, 51$, respectively. CAPs consciousness-dependent deactivations appear in mesial prefrontal cortex (MPC), CAPs 1, 2, 5 (see $Z = 15$); superior fontal gyrus (SFG) in CAP 2 ($Z = 39$ and 51); thalamus (THA) in CAPs 3 and 7 ($Z = 3$); mesencephalon (MP) in CAP 7 ($Z = -9$); motor area (MA) in CAP 5 and CAP 8 ($Z = 51$); parahippocampal gyrus (PHG) in CAPs 2, 5, 6 ($Z = -21$); caudate nucleus (CN) in CAP 7 ($Z = 15$); visual area (VA) in CAP 6 ($Z = 15$); auditory cortex (AC) in CAP 8 ($Z = 15$) and precuneus (PC) in CAP 2 ($Z = 39$). For details see also Fig. 5 and Table 1.
doi:10.1371/journal.pone.0100012.g004

obtaining a robust benchmark baseline against which to track modifications related to level of consciousness, we first ran k-means clustering over the PCC time frames collected on an independent dataset from the 1000 Functional Connectome Project (FCP, *www.nitrc.org/projects/fcon_1000/*), which includes wakefulness resting-state functional magnetic resonance imaging (fMRI) collected at multiple sites (247 subjects), as used by Liu and colleagues [16].

3. The eight PCC-CAPs centroids obtained from the clustering of the 1000 Functional Connectome Project dataset (FCP, *www.nitrc.org/projects/fcon_1000/*) were then kept fixed, and spatial clustering on the PCC time frames extracted from our propofol dataset, for each condition (i.e. wakefulness, sedation, unconsciousness, recovery), was then performed around these centroids, averaging the within-cluster spatial maps to obtain 8 different PCC-CAPs for each level of consciousness. The clustering with centroid fixed allowed us to compare PCC-CAPs between states (i.e. CAP1 in wakefulness with CAP1 in sedation, etc.), and to follow thus the fluctuation of each PCC-CAP over the course of consciousness modulation.

Statistical analysis

All statistical analyses were carried out using SPM8. For each CAP, individual time frames were entered in a second-level analysis, corresponding to a random effects model in which subjects are considered random variables. These second-level analyses consisted of analyses of variance (repeated measures analysis of variance) with the four clinical conditions as factors: normal wakefulness, sedation, unconsciousness, and recovery of consciousness. The error covariance was not assumed to be independent between regressors, and a correction for non-sphericity was applied. We used one-sided T contrasts, as implemented in Statistical Parametric Mapping software, to test for significant effects in all our analyses. After model estimation, a first T contrast searched for areas co-activated with the PCC during normal wakefulness, sedation, unconsciousness and recovery. Afterwards, in a second analysis a linear one-tailed T contrast was computed for each CAP, searching for a linear relationship between PCC co-activation patterns and the level of consciousness of the subjects across the four conditions (i.e., normal wakefulness, sedation, unconsciousness, and recovery of consciousness, SPM contrast [1.5 −0.5 −1.5 0.5], as previously described in [7]).

It should here be noted that during the recovery of consciousness subjects showed residual plasma propofol levels and lower reaction times scores (table 1 in [7]). Therefore we fixed different SPM contrast values for wakefulness (1.5) and recovery (0.5).

Results were considered significant at $p<0.05$, corrected for multiple comparisons with False Discovery Rate (FDR [22]), as in [7].

Results

We studied PCC-CAPs in our 18 subjects fMRI resting state dataset, for all the 4 different states of consciousness acquired, i.e. normal wakefulness, sedation, unconsciousness, recovery (see **Material and Methods** section for details). Fig. 2 shows the CAPs obtained in our study, before and after t-contrast on the significant co-activations. These spatial patterns are well reproduced in our smaller cohort (compared to the one obtained from the 1000 Functional Connectome Project dataset, depicted in Fig. 2 of [16]), and they also appear to be statistically significant(see Legend Fig. 2 for details).

Fig. 3 illustrates significant PCC co-activations in wakefulness, sedation, unconsciousness and recovery. The coarse core of the patterns throughout the consciousness modulation seem to be preserved (see Legend Fig. 3 for details). The comparison with the common seed-voxel analysis (bottom) helps to understand the advantage of this methodology, that is the ability to differentiate spatially the activation, adding fine grained information [16].

Preserved CAPs aside, some regions are no longer co-activated with the PCC in states of propofol-reduced consciousness. As to better quantify this phenomenon we decided to use a contrast that correlates with levels of consciousness. Fig. 4 illustrates the regions in each PCC-CAP where activity follows consciousness modulation. Interestingly, results show several region specific drops in CAPs activation that we are able to differentiate thanks to the employed methodology, some of them already shown in literature, some others not. In Fig. 4, CAP 1, 2 5 and 7 show drop in the prefrontal cortex, CAP 3 and 7 isolates the thalamic drop, the auditory and motor cortex decreases come up in CAP 8 and 5, drop of the visual area in CAP 6 (see also Fig. 5 and Table 1 for details).

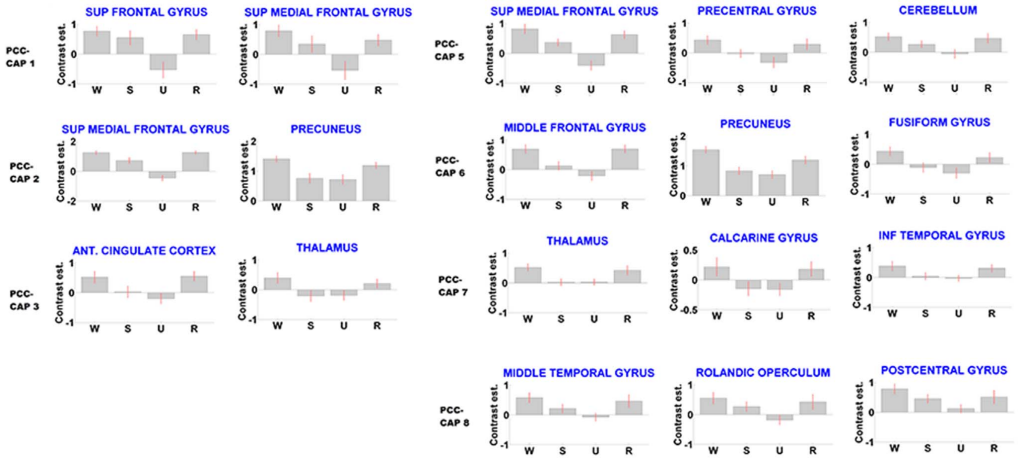

Figure 5. Region specific consciousness modulation in CAPs. Parameters estimates for the t-contrast employed, identical as in [7], for some indicative regions where PCC-related activation correlates with propofol-induced changes in consciousness. (mean ± SE; x axis labels: W = wakefulness; S = sedation; U = unconsciousness; R = recovery). Note how PCC co-activation in these regions significantly follows consciousness modulation (see also Table 1).
doi:10.1371/journal.pone.0100012.g005

Discussion

With the aim to investigate changes in global and local brain activity, in this study we assessed propofol-induced changes in PCC co-activation functional patterns, during wakefulness, sedation, unconsciousness, and wakefulness recovery. Our results contribute to a growing literature addressing the changes in functional connectivity accompanying the loss of consciousness [23–26]. The approach proposed, based on the clustering of instantaneous PCC-related spatial maps, helps in the refinement and the differentiation in the spatial modulation of the default mode network when switching from wakefulness to unconsciousness.

Two key aspects of the methodology proposed in [16], and extended here, are worth discussing. One is the choice of the threshold, that is a crucial step for the construction of a spatio-temporal point process from BOLD time series. We decided to fix our threshold at 1 SD, as in [15], rather than address the threshold in terms of time frame similarity with the seed-based correlation map (see Fig. 1B in [16]). The hypothesis behind this choice is that BOLD signal point processing can help in the spatial characterization of functional connectivity patterns, better than standard correlation analysis (see also Figure S2 and S3). This data-driven evidence is independent of the assumption that BOLD signal peaks may or may not reflect cortical activations [15,27]. In this study we simply focused on spatial clustering of point processed BOLD time series, which allowed us to better characterize functional spatial interaction with the PCC during modulation of consciousness. On the other hand, the employed point process methodology is not purely dominated by hemodynamics. Indeed, co-activations patterns obtained after deconvolving the hemodynamic response function (HRF) at rest as in [27], are not qualitatively different from the ones presented in Fig. 2 (see also Figure S1).

Furthermore, the results from our PCC coactivation patterns seem in line with the ones obtained by Liu [16], in a different cohort and with a different choice of the threshold. This comes out on the side of point process methodology and of the importance of these BOLD signal peaks in spatial differentiation of network co-activations. Also, the use of clustering with centroid fixed, that is new with respect to the approach proposed in [16], can be an useful benchmark for statistical comparison of functional changing patterns between conditions (conscious states in this case, but it could also be used in pathological conditions, etc.).

A primary result is that the core of PCC-CAPs is preserved in anesthesia (Fig. 3). This is in line with other studies [7,14], where, using standard seed-based functional connectivity, the preservation of a core network of correlated regions independent on the level of consciousness was confirmed. The origin of these functional networks could be related to the fixed structural connection present in the awake brain, albeit anesthetized. This partial preservation of functional connectivity in the absence of consciousness has been suggested to possibly reflect preserved anatomical connections dissociated from higher cognitive functions [28].

Also, this approach adds new information on region specific drops in connectivity between the seeds in the DMN area and whole brain connectivity, correlating with levels of consciousness (Fig. 4 and Fig. 5): prefrontal drops (CAP 1, 2, 5, 7) are in line with previous findings in the field, showing widespread changes in prefrontal connectivity [7,9,10]: at the cortical level, hypnotic anesthetic agents have traditionally been considered to decrease activity in a widespread bilateral frontoparietal network. The primary action of hypnotic anesthetic agents would be to functionally disconnect different parts of the cortex, which would probably impair the ability to integrate information [8,23,29]. A recent electroencephalography study similarly suggests the presence of some anterior-posterior functional uncoupling in the brain, during anesthesia-induced loss of consciousness [30].

The disconnection of the thalamic area, already noted in [31,32], is highlighted in CAP 3 and 7. Using positron emission tomography, thalamic metabolism has been shown to decrease

significantly during anesthesia-induced unconsciousness [24]. Furthermore, a model has been suggested in which the thalamus orchestrates the commonly observed increased and coherent alpha frequency activity in the frontal cortex during propofol-induced unconsciousness. This steady thalamic alpha rhythm could impede conduction and thus responsiveness to external stimuli [33].

Decrease of activation in the visual area (CAP 6) during anesthesia has previously been studied in monkeys [34,35], where it has been shown how local and global processing in the visual area might depend gradually on the depth of anesthesia. It may also critically depend on information integration mechanisms that function properly only in the awake and perceiving animal [34]. Here, this disconnection is shown in fMRI resting state on humans: thus, this approach seem to enlighten instantaneous spatial connectivity changes between DMN and other external areas, unlikely to be seen with other commonly used correlation analysis (e.g. seed-based functional connectivity).

Similarly, the PCC-related primary motor disconnection is pointed out here (CAP 5 and 8) on fMRI resting state data. These results are in line with previous transcranial magnetic stimulation (TMS) and electroencephalographic (EEG) studies, that indicate intracortical inhibition of central motor circuitry during incremental suppression by a potentiator of GABA agonist (propofol) in a dose-dependent manner [36,37]. The decrease in auditory cortex PCC-coactivation (CAP8) is in agreement with previous findings, in animals [38] and humans [39]. Our finding of decreased auditory cortex co-activation could be related to the hypothesis that propofol bilaterally attenuates the auditory-induced BOLD signal activation of the auditory cortex in a dose-dependent manner [40]. However, it should be noted that activation studies and resting state acquisitions offer different assessments of the underlying neurophysiological activity, in response to external stimulation or during resting conditions, respectively.

A limitation to this approach is the choice of the seed, that needs to be based on a strong priori hypothesis: whole brain connectivity analysis can improve research in this direction. Finally, since it has recently been shown that EEG directional connectivity shows characteristic changes during propofol-induced unconsciousness [41], the nature of BOLD peaks and their correlation with cortical activity needs to be explored using combined fMRI-EEG recordings.

In conclusion, our result show that functional changes in the brain associated to propofol-induced modulation of consciousness can be efficiently revealed by tracking the patterns of co-activation in the Posterior Cingulate Cortex, an area with a central role in the dynamical connectivity at rest. This methodology, based on point process analysis, can help in refining the characterization of local functional disconnections following the partial or total loss of consciousness.

Supporting Information

Figure S1 CAPs from BOLD and deconvolved BOLD signal. To avoid the possibility that the PCC-coactivation patterns were only due to different hemodynamic response functions in the different areas of the brain, we applied the approach proposed in Wu et al. [27], where point process is used to deconvolve the HRF at rest from the BOLD signal. As shown above, the CAPs obtained from the BOLD signal reported in the manuscript are confirmed when obtained from the deconvolved BOLD, suggesting a connection between spatial functional co-activations and neuronal brain response.
(TIF)

Figure S2 CAPs from negative BOLD peaks. CAPs obtained using positive threshold crossing (left) and negative threshold crossing (right), during wake resting state (CAPs colormap in absolute Z-value, to make patterns comparable). After the clustering, the specificity of the spatial patterns obtained using positive peaks in BOLD is not reproducible using negative peaks; positive BOLD peaks allow to reconstruct a richer variety of patterns.
(TIF)

Figure S3 Sliding window correlation vs CAPs. PCC co-activation patterns in wakefulness (left) compared to the 8 patterns obtained after spatial clustering of the N PCC-correlation maps computed using sliding window correlation, with window size varying from 5 time points (i.e. 12 s window, TR = 2.46 s) to 20 time points (i.e. 50 s window). Note that the region-specific patterns obtained with point process on the BOLD peaks are not recovered by using sliding window correlation. This approach seems to add more refined information in the spatial differentiation of functional networks.
(TIF)

Figure S4 Motion correction in CAPs. Example of the procedure discussed in **Materials and Methods**, for one subject, for each level of consciousness (i.e. wakefulness, sedation, unconsciousness, recovery). In order to evaluate the extent of these residual motion artifact in CAPs, for each subject and for each state of consciousness, we computed the two indices proposed by [18], i.e. Framewise Displacement (FD) and DVARS. FD is a scalar quantity that expresses instantaneous head motion, while DVARS is a measure of how much the intensity of a brain image changes in comparison to the previous time point [18]. Secondly, we defined as motion corrupted the frames (ArtFrames in the figure) in which FD and DVARS values were both above 0.5 mm for FD and 0.5.
(TIF)

Author Contributions

Conceived and designed the experiments: DM SL EA. Performed the experiments: AV DL PB JB VB CD. Analyzed the data: EA FG. Wrote the paper: EA DM SL.

References

1. Greicius MD, Krasnow B, Reiss AL, Menon V (2003) Functional connectivity in the resting brain: a network analysis of the default mode hypothesis. Proceedings of the National Academy of Sciences 100: 253–258.
2. Fox MD, Snyder AZ, Vincent JL, Corbetta M, Van Essen DC, et al. (2005) The human brain is intrinsically organized into dynamic, anticorrelated functional networks. Proceedings of the National Academy of Sciences of the United States of America 102: 9673–9678.
3. Fox MD, Raichle ME (2007) Spontaneous uctuations in brain activity observed with functional magnetic resonance imaging. Nature Reviews Neuroscience 8: 700–711.
4. Fox MD, Greicius M (2010) Clinical applications of resting state functional connectivity. Frontiers in systems neuroscience 4: 19–24.
5. Boly M, Tshibanda L, Vanhaudenhuyse A, Noirhomme Q, Schnakers C, et al. (2009) Functional connectivity in the default network during resting state is preserved in a vegetative but not in a brain dead patient. Human brain mapping 30: 2393–2400.
6. Vanhaudenhuyse A, Noirhomme Q, Tshibanda LJF, Bruno MA, Boveroux P, et al. (2010) Default network connectivity reects the level of consciousness in non-communicative brain-damaged patients. Brain 133: 161–171.
7. Boveroux P, Vanhaudenhuyse A, Bruno MA, Noirhomme Q, Lauwick S, et al. (2010) Breakdown of within-and between-network resting state functional

magnetic resonance imaging connectivity during propofol-induced loss of consciousness. Anesthesiology 113: 1038–1053.
8. Schrouff J, Perlbarg V, Boly M, Marrelec G, Boveroux P, et al. (2011) Brain functional integration decreases during propofol-induced loss of consciousness. Neuroimage 57: 198–205.
9. Martuzzi R, Ramani R, Qiu M, Rajeevan N, Constable RT (2010) Functional connectivity and alterations in baseline brain state in humans. NeuroImage 49: 823–834.
10. Deshpande G, Kerssens C, Sebel PS, Hu X (2010) Altered local coherence in the default mode network due to sevourane anesthesia. Brain research 1318: 110–121.
11. Hutchison RM, Womelsdorf T, Allen EA, Bandettini PA, Calhoun VD, et al. (2013) Dynamic functional connectivity: Promises, issues, and interpretations. NeuroImage 80: 360–368.
12. Allen EA, Damaraju E, Plis SM, Erhardt EB, Eichele T, et al. (2012) Tracking whole-brain connectivity dynamics in the resting state. Cerebral Cortex : bhs352.
13. Chang C, Glover GH (2010) Time–frequency dynamics of resting-state brain connectivity measured with fmri. Neuroimage 50: 81–98.
14. Hutchison RM, Womelsdorf T, Gati JS, Everling S, Menon RS (2012) Resting-state networks show dynamic functional connectivity in awake humans and anesthetized macaques. Human brain mapping 34: 2154–2177.
15. Tagliazucchi E, Balenzuela P, Fraiman D, Chialvo DR (2012) Criticality in large-scale brain fmridynamics unveiled by a novel point process analysis. Frontiers in Physiology 3: 15–25.
16. Liu X, Duyn JH (2013) Time-varying functional network information extracted from brief instances of spontaneous brain activity. Proceedings of the National Academy of Sciences 110: 4392–4397.
17. MacLaren R, Plamondon JM, Ramsay KB, Rocker GM, Patrick WD, et al. (2000) A prospective evaluation of empiric versus protocol-based sedation and analgesia. Pharmacotherapy: The Journal of Human Pharmacology and Drug Therapy 20: 662–672.
18. Power JD, Barnes KA, Snyder AZ, Schlaggar BL, Petersen SE (2012) Spurious but systematic correlations in functional connectivity mri networks arise from subject motion. Neuroimage 59: 2142–2154.
19. Fransson P, Marrelec G (2008) The precuneus/posterior cingulate cortex plays a pivotal role in the default mode network: Evidence from a partial correlation network analysis. Neuroimage 42: 1178–1184.
20. Leech R, Kamourieh S, Beckmann CF, Sharp DJ (2011) Fractionating the default mode network: distinct contributions of the ventral and dorsal posterior cingulate cortex to cognitive control. The Journal of Neuroscience 31: 3217–3224.
21. Hastie T, Tibshirani R, Friedman J, Hastie T, Friedman J, et al. (2009) The elements of statistical learning, volume 2. Springer.
22. Genovese CR, Lazar NA, Nichols T (2002) Thresholding of statistical maps in functional neuroimaging using the false discovery rate. Neuroimage 15: 870–878.
23. Alkire MT, Hudetz AG, Tononi G (2008) Consciousness and anesthesia. Science 322: 876–880.
24. Fiset P, Paus T, Daloze T, Plourde G, Meuret P, et al. (1999) Brain mechanisms of propofolinduced loss of consciousness in humans: a positron emission tomographic study. The Journal of neuroscience 19: 5506–5513.
25. Boveroux P, Bonhomme V, Boly M, Vanhaudenhuyse A, Maquet P, et al. (2008) Brain function in physiologically, pharmacologically, and pathologically altered states of consciousness. International anesthesiology clinics 46: 131–146.
26. Sanders RD, Tononi G, Laureys S, Sleigh J (2012) Unresponsiveness≠unconsciousness. Anesthesiology 116: 946.
27. Wu GR, Liao W, Stramaglia S, Ding JR, Chen H, et al. (2013) A blind deconvolution approach to recover effective connectivity brain networks from resting state fmri data. Medical image analysis 17: 365–374.
28. Peigneux P, Orban P, Balteau E, Degueldre C, Luxen A, et al. (2006) Offline persistence of memoryrelated cerebral activity during active wakefulness. PLoS biology 4: e100.
29. Lee U, Mashour GA, Kim S, Noh GJ, Choi BM (2009) Propofol induction reduces the capacity for neural information integration: implications for the mechanism of consciousness and general anesthesia. Consciousness and cognition 18: 56–64.
30. John ER, Prichep LS (2005) The anesthetic cascade: a theory of how anesthesia suppresses consciousness. Anesthesiology 102: 447–471.
31. Ying SW, Goldstein PA (2005) Propofol-block of sk channels in reticular thalamic neurons enhances gabaergic inhibition in relay neurons. Journal of neurophysiology 93: 1935–1948.
32. Guldenmund P, Demertzi A, Boveroux P, Boly M, Vanhaudenhuyse A, et al. (2013) Thalamus, brainstem and salience network connectivity changes during propofol-induced sedation and unconsciousness. Brain connectivity 3: 273–285.
33. Vijayan S, Ching S, Purdon PL, Brown EN, Kopell NJ (2013) Thalamocortical mechanisms for the anteriorization of alpha rhythms during propofol-induced unconsciousness. The Journal of Neuroscience 33: 11070–11075.
34. Lamme VA, Zipser K, Spekreijse H (1998) Figure-ground activity in primary visual cortex is suppressed by anesthesia. Proceedings of the National Academy of Sciences 95: 3263–3268.
35. Tenenbein PK, Lam AM, Klein M, Lee L (2006) Effects of sevourane and propofol on ash visual evoked potentials. Journal of Neurosurgical Anesthesiology 18: 310.
36. Ziemann U, Lönnecker S, Steinhoff B, Paulus W (1996) Effects of antiepileptic drugs on motor cortex excitability in humans: a transcranial magnetic stimulation study. Annals of neurology 40: 367–378.
37. Kalkman CJ, Drummond JC, Ribberink AA, Patel PM, Sano T, et al. (1992) Effects of propofol, etomidate, midazolam, and fentanyl on motor evoked responses to transcranial electrical or magnetic stimulation in humans. Anesthesiology 76: 502–509.
38. Gaese BH, Ostwald J (2001) Anesthesia changes frequency tuning of neurons in the rat primary auditory cortex. Journal of neurophysiology 86: 1062–1066.
39. Plourde G, Belin P, Chartrand D, Fiset P, Backman SB, et al. (2006) Cortical processing of complex auditory stimuli during alterations of consciousness with the general anesthetic propofol. Anesthesiology 104: 448–457.
40. Dueck M, Petzke F, Gerbershagen H, Paul M, Hesselmann V, et al. (2005) Propofol attenuates responses of the auditory cortex to acoustic stimulation in a dose-dependent manner: A fmri study. Acta anaesthesiologica scandinavica 49: 784–791.
41. Untergehrer G, Jordan D, Kochs EF, Ilg R, Schneider G (2014) Fronto-parietal connectivity is a non-static phenomenon with characteristic changes during unconsciousness. PloS one 9: e87498.

SUPPORTING INFORMATION FIGURES

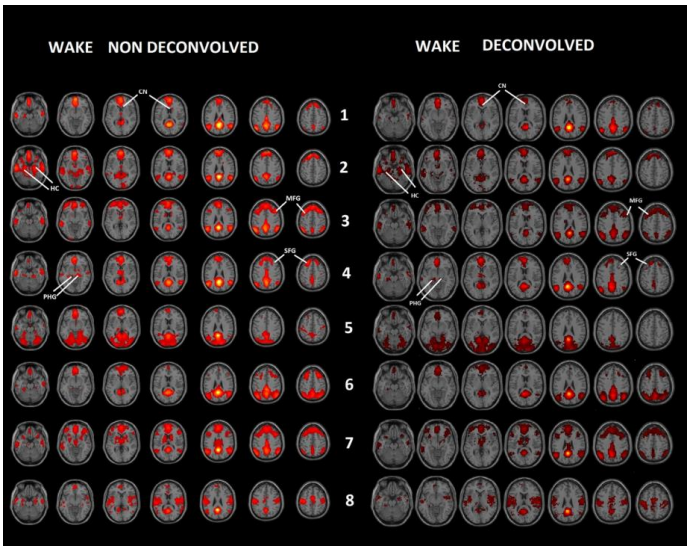

Fig. S1

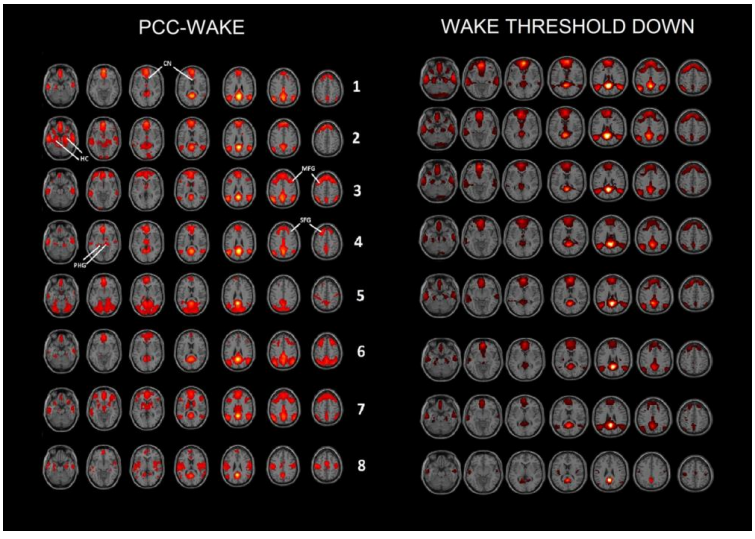

Fig. S2

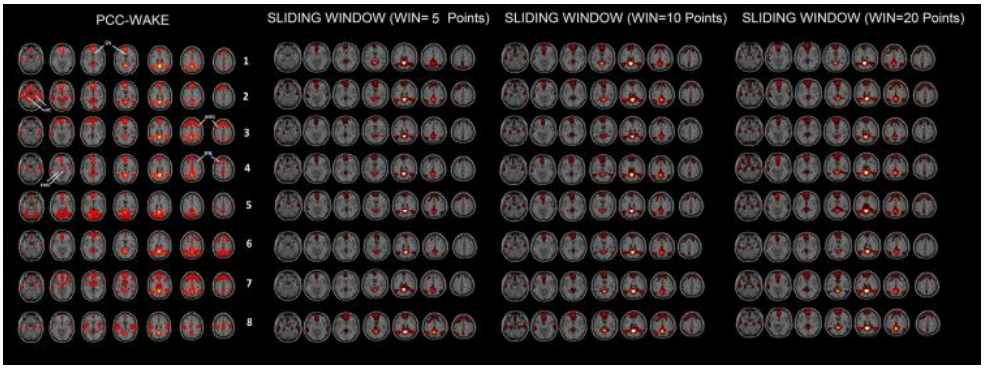
PCC-WAKE
SLIDING WINDOW (WIN= 5 Points)
SLIDING WINDOW (WIN=10 Points)
SLIDING WINDOW (WIN=20 Points)
1
2
3
4
5
6
7
8

Fig S3

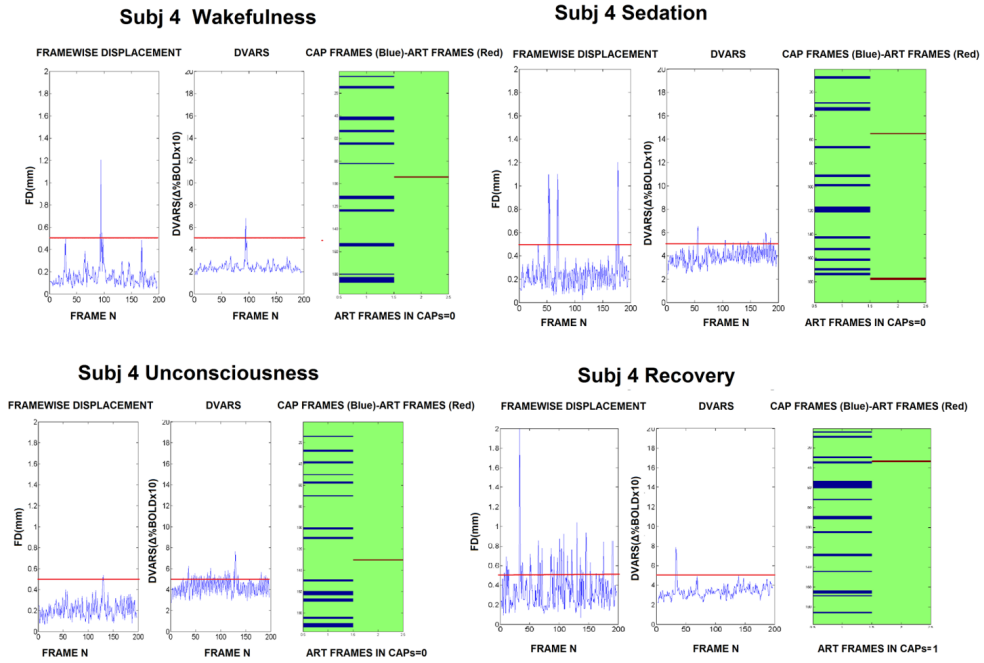
Subj 4 Wakefulness
FRAMEWISE DISPLACEMENT
DVARS
CAP FRAMES (Blue)-ART FRAMES (Red)
FD(mm)
DVARS(Δ%BOLDx10)
FRAME N
ART FRAMES IN CAPs=0
Subj 4 Sedation
FRAMEWISE DISPLACEMENT
DVARS
CAP FRAMES (Blue)-ART FRAMES (Red)
FD(mm)
DVARS(Δ%BOLDx10)
FRAME N
ART FRAMES IN CAPs=0
Subj 4 Unconsciousness
FRAMEWISE DISPLACEMENT
DVARS
CAP FRAMES (Blue)-ART FRAMES (Red)
FD(mm)
DVARS(Δ%BOLDx10)
FRAME N
ART FRAMES IN CAPs=0
Subj 4 Recovery
FRAMEWISE DISPLACEMENT
DVARS
CAP FRAMES (Blue)-ART FRAMES (Red)
FD(mm)
DVARS(Δ%BOLDx10)
FRAME N
ART FRAMES IN CAPs=1

Fig. S4

PAPER II

B

Structural constraints to information flow within cortical circuits: a TMS/EEG-dMRI study

Amico E., Bodart, O., Gosseries, O.,
Heine, L., Rosanova, M., Van Mierlo, P.,
Martial, C., Massimini, M., Marinazzo, D., Laureys, S.

Brain Stimulation, submitted.

Structural constraints to directed functional connectivity within cortical circuits: a TMS/EEG-DTI study.

Enrico Amico[1,2,†], Olivier Bodart[1], Olivia Gosseries[1,5], Lizette Heine[1], Mario Rosanova[3], Pieter Van Mierlo[4], Charlotte Martial[1], Marcello Massimini[3], Daniele Marinazzo[2*] and Steven Laureys[1*]

1 Coma Science Group, Cyclotron Research Center & GIGA Research Center, University and University Hospital of Liège, Liège, Belgium

2 Department of Data-analysis, University of Ghent, B9000 Ghent, Belgium

3 Department of Biomedical and Clinical Sciences "Luigi Sacco", University of Milan, Milan, Italy

4Medical Image and Signal Processing Group, Department of Electronics and Information Systems, Ghent University-IBBT, B9000 Ghent, Belgium

5Department of Psychiatry, University of Wisconsin, Madison, WI, USA

Abstract

Transcranial magnetic stimulation (TMS) in combination with neuroimaging techniques allows to measure the effects of a non invasive and direct perturbation of the brain. When coupled to high density electroencephalography (TMS/hd-EEG), TMS pulses revealed the electrophysiological signatures of different cortical modules in health and disease. However, the neural underpinnings of these signatures remain unclear. Here, by applying multimodal analyses of cortical response to TMS recordings and diffusion magnetic resonance imaging (dMRI) tractography, we investigated the relationship between functional and structural features of different cortical modules in a cohort of awake healthy volunteers. We observed that the relationship between directed functional connectivity and structural connections depend on the stimulation site and on the

*Marinazzo D. and Laureys S. contributed equally to this work.

†Corresponding author. E-mail: eamico@ulg.ac.be
Tel: +32 4 366 23 62 Fax: +32 4 366 29 46

frequency of the TMS-induced brain rhythms. These results shed further light on the link between structure and function of human cortical networks in health and pave the way for a novel and non-invasive approach to study neurological and psychiatric conditions.

Keywords: `TMS/EEG, DTI, directed functional connectivity, structural connectivity, structure-function, brain directed functional connectivity`

1. Introduction

Transcranial magnetic stimulation (TMS) has been used for more than 20 years to investigate connectivity and plasticity in the human cortex. By combining TMS with high-density electroencephalography (hd-EEG), one can stimulate any cortical area and measure the effects produced by this perturbation in the rest of the cerebral cortex [1, 2]. It has been shown that cortical potentials elicited by TMS stimulation (TMS-evoked potentials, i.e. TEPs) last for up to 600 ms in normal wakefulness, during their spread from the area of stimulation to remote interconnected brain areas [3, 4]. To date, TMS/EEG recordings have provided new and reliable insights [5] on the whole brain cortical excitability with reasonable spatial and excellent temporal resolution [6].

The amount of information contained in the hd-EEG response to TMS has appeared to contain inner signatures of the functional organization in a brain network. Two recent studies [7, 8] in healthy awake subjects showed that TMS can also induce EEG oscillations at different frequencies. The TMS pulse gives rise to different connected cortical regions in the brain, generating a complex EEG pattern composed of strong fluctuations at the "natural" frequency of the stimulated area. These oscillations are thought to reflect neurophysiological activity that is transiently elicited by the TMS pulse and possibly engaged through brain connections [7, 9, 10].

Recently, researchers have started to investigate how the TMS/hd-EEG perturbation might be constrained and shaped by brain structure, either by explor-

ing the correlation between TMS-induced interhemispheric signal propagation and neuroanatomy [11, 12], or by improving the modeling of the TMS-induced electric field using realistic neural geometry [13, 14]. Besides, it has lately been shown that cortical networks derived from source EEG connectivity partially reflects both direct and indirect underlying white matter connectivity in a broad range of frequencies [15].

In this respect, the development of diffusion magnetic resonance imaging (dMRI) [16] might add information on the structural architecture of the brain [17]. The application of deterministic and probabilistic tractography methods allows for the spatial topography of the white matter, which represents bundles coherently organized and myelinated axons [18]. The output of tractography algorithms permits anatomically plausible visualization of white matter pathways [19] and has led to reliable quantification [20] of structural connections between brain regions (i.e. the human connectome [21, 22]).

The purpose of this paper is to investigate EEG changes of directed functional connectivity in the brain induced by TMS from both a functional and structural perspective, using multimodal modeling of source reconstructed TMS/hd-EEG recordings and dMRI tractography. The study of functional connectivity changes after the perturbation can possibly help in understanding the structure-function modulation caused by TMS (i.e. the extent to which TMS-induced EEG dynamics is constrained by white matter pathways) and the specific frequency bands of the involved brain regions. Functional and structural connectivity in the brain are known to be closely correlated [22, 23, 15], but their interactions remain only poorly understood [24].

Taking the aforementioned recent findings as a starting point, we here aim to assess: 1) if the extent to which functional changes in a cortical region, as a consequence of the induced perturbation, is related to the number of fiber pathways passing through it [15]; 2) whether the temporal variability of the response to TMS has specific spectral EEG signatures [7]; 3) the role of these "natural frequencies" in the flow spread during TMS and in the structure-function interactions [25, 26, 7].

We will first present the processing pipelines for TMS-EEG and dMRI data. Second, the mathematical methodology for the evaluation of the directed functional connectivity between brain regions and its correlation with the structural connectome will be presented. Finally, results obtained in a cohort of healthy volunteers ($n = 14$) will be presented and discussed.

2. Materials and Methods

2.1. TMS/hd-EEG recordings

Acquisition and preprocessing. TMS/hd-EEG data were acquired in 14 healthy awake adults (6 males and 8 females, age range 23-37 years) as published elsewhere [26, 27]. In brief, subjects were lying with eyes open looking at a fixation point on a screen. All participants gave written informed consent and underwent clinical examinations to rule out any potential adverse effect of TMS. The TMS/hd-EEG experimental procedure, approved by the Local Ethical Committee of University of Liège, was performed using a figure-of-eight coil driven by a mobile unit (eXimia TMS Stimulator, Nexstim Ltd., Finland), targeting two cortical areas (left precuneus and left premotor) for at least 200 trials.

The left precuneus and left premotor targets were identified on the subjects 3D T1 brain scan and reached through the neuronavigation system (NBS, Nexstim Ltd, Finland) using stereoscopic infrared tracking camera and reflective sensors on the subject's head and the stimulating coil. Stability of the coil position was assured by using an aiming device allowing the stimulation only when the deviation from the target was less than 2 mm. The intensity was chosen in order to assure an induced electrical field at the cortical level between 100 and 140 V/m. Stimulation was delivered with an interstimulus interval jittering randomly between 2000 and 2300 ms (0.4–0.5Hz).

Trigeminal stimulation and muscle artefacts were minimized by placing the coil on a scalp area close to the midline [28], far away from facial or temporal muscles and nerve endings. To prevent contamination of TMS-evoked EEG potentials by the auditory response to the coil's click, subjects wore earphones

through which a noise masking was played throughout each TMS/hd-EEG session [29].

Out of the initial 14 subjects, we excluded 5 of them for the precuneus and 2 for premotor, because of a low signal-to-noise ratio of TMS/EEG-evoked responses. TMS trials containing noise, muscle activity, or eye movements were detected and rejected [27]. EEG data were average referenced, downsampled at half of the original sampling rate (from 725 Hz to 362 Hz), and bandpass filtered (2 to 80 Hz).

Source reconstruction was performed as in [26]. Conductive head volume was modeled according to the 3-spheres BERG method [30] and constrained to the cerebral cortex that was modeled as a three-dimensional grid of 3004 fixed dipoles oriented normally to cortical surface. This model was adapted to the anatomy of each subject using the Statistical Parametric Mapping software package (SPM8, freely available at: `http://www.fil.ion.bpmf.ac.uk/spm`) as follows: binary masks of skull and scalp obtained from individual MRIs were warped to the corresponding canonical meshes of the Montreal Neurological Institute (MNI) atlas. Then, the inverse transformation was applied to the MNI canonical mesh of the cortex for approximating to real anatomy. Finally, the single trial distribution of electrical sources in the brain was estimated by applying the empirical Bayesian approach as described in [31, 32].

In order to summarize significant functional measures over anatomically and/or functionally identifiable brain regions, the time courses of the 3004 reconstructed sources were then averaged into the specific 90 cortical and subcortical areas of the Automated Anatomical Labeling (AAL) [33] parcellation (Fig.1), according to their position on the cortical mesh.

2.2. dMRI data

Acquisition and preprocessing. A series of diffusion-weighted magnetic resonance images (dwi) of brain anatomy were acquired in each participant using a Siemens Trio Magnetom 3 Tesla system (Siemens Trio, University Hospital of Liege, Belgium). Diffusion-weighted images were acquired at a b-value of 1000

s/mm^2 using 64 encoding gradients that were uniformly distributed in space by an electrostatic repulsion approach [34]. Voxels had dimensions of 1.8 x 1.8 x 3.3 mm^3 and volumes were acquired in 45 transverse slices using a 128 x 128 voxel matrix. A single T1-weighted 3D magnetization-prepared rapid gradient echo sequence (MPRAGE) image, with isotropic resolution of 1 mm^3, was also acquired for each subject.

Diffusion volumes were analysed using typical preprocessing steps in dMRI [35, 36]. Eddy current correction for each participant was achieved using FDT, v2.0, the diffusion toolkit within FSL 5.0 (FMRIBs Software Library; `http://www.fmrib.ox.ac.uk/fsl`). Rotations applied to the diffusion-weighted volumes were also applied to the corresponding gradient directions [37]. A fractional anisotropy (FA) image was estimated using weighted linear least squares fitted to the log-transformed data for each subject.

Registration of the anatomical image and atlas parcellation. We segmented each subject's T1-weighted image into whole-brain white matter (WM), gray matter (GM), and cerebrospinal fluid (CSF) masks using FAST, part of FSL (FMRIB Software Library v 5.0). The corresponding white matter mask image was registered without resampling to the relevant dwi series [38]. Next, the AAL atlas was first registered to the T1 space using linear (FSL flirt) and non-linear warping (FSL FNIRT) in order to achieve the best registration into each subject's space. Then, the single subject AAL template was finally registered without resampling to the dwi space using the affine transform resulting from the WM registration. This transformation matrix was also applied to the T1-derived GM mask which was used as termination mask for the tractography analysis.

Tractography and connectome construction. The fiber response model was estimated for each subject from the high b-value (b = 1000 s/mm2) diffusion-weighted images. A mask of single fiber voxels was extracted from the thresholded and eroded FA images [39, 40]. Using non-negativity constrained spherical deconvolution, fiber orientation distribution (FOD) functions were obtained at each voxel using the MRTRIX3 package (J-D Tournier, Brain Research Insti-

tute, Melbourne, Australia, `https://github.com/jdtournier/mrtrix3`) [41]. For both the response estimation and spherical deconvolution steps we chose a maximum harmonic order l_{max} of 6.

Probabilistic tractography was performed using randomly placed seeds within subject-specific white matter masks, registered as mentioned in the latter. Fiber tracking settings were as follows: number of tracks = 10 million, FOD magnitude cutoff for terminating tracks = 0.1, minimum track length = 5 mm, maximum track length = 200 mm, minimum radius of curvature = 1 mm, tracking algorithm step size = 0.5 mm. Streamlines were terminated when they extended out of the WM-GM mask interface, or could not progress along a direction with an FOD magnitude or curvature radius higher than the minimum cutoffs.

The streamlines obtained were mapped to the relevant nodes defined by the AAL parcellation registered in the subject's dwi space, using MRTRIX3 [41]. Each streamline termination was assigned to the nearest gray matter parcel within a 2 mm search radius. The resulting connectome was finally examined by determining the connection density (number of fiber connections per unit surface) between any two regions of the AAL template, as in [36] (see also Fig.1). This correction was needed to account for the variable size of the cortical ROIs of the AAL template [42].

2.3. TMS/hd-EEG directed functional connectivity estimation

Spectrum-weighted adaptive directed transfer function. We evaluated directed functional connectivity using a multivariate model of spectral coefficients, i.e. the directed transfer function (DTF) [45, 46, 47]. In order to cope with the non-stationary nature of the signals under study, we used the adaptive directed transfer function (ADTF) [48, 49]. Specifically, we adopted the spectrum-weighted adaptive directed transfer function (swADTF)[44], which has been successfully used for connectivity modeling of epileptic intracranial EEG data [43, 44].

A time-variant multivariate autoregressive (TVAR) model is built from the TMS/hd-EEG sources by using the Kalman filtering algorithm [50, 51, 43]. The time-variant connectivity measure, the swADTF, is calculated from the

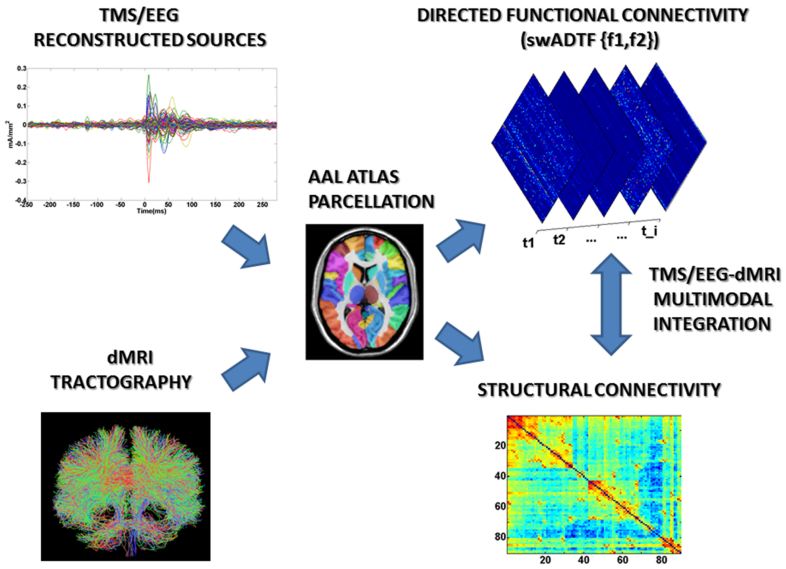

Figure 1: **Flow chart of TMS/EEG-dMRI modeling.** Up: the time courses of the 3004 reconstructed dipoles were averaged into the parcels of the Automated Anatomical Labeling (AAL) atlas [33], consisting of 90 unique brain regions (cerebellar regions were excluded from the analysis). The 90 time courses obtained were modeled using spectrum-weighted adaptive directed transfer function (swADTF)[43, 44]. swADTF returns the causal interactions between the cortical regions ($90x90$ time varying directed functional connectivity matrices) at a specific frequency interval (f1,f2). Bottom: for each dMRI dataset whole-brain probabilistic tractography was performed using a combination of FSL and MRTRIX (see **Materials and methods**). The AAL atlas was then used to segment the fiber bundles between each pair of ROIs. Next, we determined the percentage of tracts between each pair of regions of the AAL template, resulting in a $90x90$ structural connectivity matrix.

coefficients of the TVAR model as follows:

$$swADTF_{ij}(t) = \frac{\sum_{f=f_1}^{f_2} |H_{ij}(f,t)|^2 \sum_{k=1}^{K} |H_{jk}(f,t)|^2}{\sum_{l=1}^{K} \sum_{f'=f_1}^{f_2} |H_{il}(f',t)^2 \sum_{s=1}^{K} |H_{ls}(f',t)|^2} \quad (1)$$

where $H_{ij}(f,t)$ in eq. 1 is the time-variant transfer matrix of the system describing the directed functional connectivity from signal j to i at frequency f at time t, for each of the K signals. Each term $H_{ij}(f,t)$ is weighted by the autospectrum of the sending (in this case j) signal.

The swADTF allows us to investigate the causal relation between all the signals at a predefined frequency band over time. The measure weighs all outgoing directed functional connectivity present in the terms $H_{ij}(f,t)$ by the power spectrum of the sending signal j. Each swADTF value corresponds to the directed time-variant strength of the directed functional connectivity between two nodes. This dynamic interaction between nodes can also be represented as a series of time-varying directed matrices (see also Fig.1). The swADTF is normalized so that the sum of incoming directed functional connectivity into a channel at each time point is equal to 1:

$$\sum_{k=1}^{K} swADTF_{ik}(t) = 1 \quad (2)$$

2.4. TMS/EEG-dMRI multimodal integration

Outdegree computation and statistical assessment. We computed directed functional connectivity (swADTF) on the brain network defined by the anatomical atlas (AAL) reconstructed sources for each subject. A detailed discussion on the implementation and the setup of the parameters can be found in [43].

The swADTF was calculated in 3 frequency bands: α (8-12 Hz), β (13-20 Hz), $\beta 2/\gamma$ (21-50 Hz). This choice followed the evidence that TMS on healthy awake subjects consistently evoked dominant EEG oscillations in different cortical areas [7].

In order to track modulations of directed functional connectivity due to TMS, we considered 2 different non-overlapping windows of 300 ms: a "baseline", pre TMS stimulus, extended from 500 ms to 200 ms before the TMS pulse;

a "post stimulus", directly after TMS, which captures the dynamics from 20 to 320 ms after the pulse (the first 20 ms were discarded to minimize the effect of possible artifacts occurring at the time of stimulation, [52, 7]).

We obtained the mean global outgoing flow from a region j before and after the stimulation by averaging the swADTF time courses in each of the two time windows and by summing the average amount of directed connectivity transferred from j to each node of the network. In network terms, this quantity is called Outdegree. In our case, for each frequency band and window (i.e. baseline or post stimulus):

$$Outdegree_j = \sum_{k=1}^{K} C_{jk}, \quad \forall\, k,\, j = 1...K, \tag{3}$$

where $K = 90$ in our case (i.e. the number of AAL regions), and C is the connectivity matrix constructed by averaging the swADTF time courses within each window. All self-edges were set to 0. By using this procedure we aimed to obtain an illustrative snapshot of the total directed functional connectivity from a region j at a specific stage of the TMS process (i.e. baseline or post stimulus).

In order to detect significant group changes in the Outdegree before and after the stimulation, a two-sample t-test of the post stimulus Outdegree against the correspondent baseline Outdegree was performed in each region. Post stimulus Outdegree values were considered significant at $p \leq 0.05$, False Discovery Rate (FDR) corrected for multiple comparisons (i.e. for $K = 90$ independent tests).

For each subject, the structural degree of a node j (SCdegree) was simply calculated from the structural connectivity matrix S by summing over its columns.

$$SCdegree_j = \sum_{k=1}^{K} S_{jk}, \quad \forall\, j = 1...K, \tag{4}$$

Structure-function correlations and statistical assessment. The dynamic interaction between regions modeled by swADTF can be represented as a series of

time-varying directed connectivity matrices (see also Fig.1). In each frequency band, dynamic spatial correlation was defined as the mean row-by-row Pearson's correlation at each time point between each subject's directed functional connectivity matrix and the correspondent structural connectivity matrix. The 95% confidence intervals for the Pearson's correlation distribution at the baseline were calculated by using a non-parametric bootstrap procedure [53].

3. Results

The significant differences (Table 1) in directed functional connectivity across cortical regions after TMS perturbation are illustrated by projecting the Out-Degree onto the anatomical template (Fig.2). The two sites of stimulation have peaks in the Outdegree at different frequency bands. In particular, the precuneus area has a maximum of directed functional connectivity in the β band in proximity of the stimulation site, whereas the premotor has a maxima in the $\beta 2/\gamma$ band, more spread towards the controlateral hemisphere. These findings are in line with previous studies [7, 8], where the authors showed that TMS on healthy awake subjects consistently evokes EEG oscillations with dominant frequencies that depend on the site of stimulation. In particular, precuneus was shown to respond to TMS in the β band and premotor in $\beta 2/\gamma$. The peaks in directed functional connectivity at different frequencies in the areas depicted in Fig.2 confirm the hypothesis that different brain regions might be normally tuned to oscillate at a characteristic rate (i.e. natural frequency)[7, 8]. Furthermore, despite the fast and chaotic functional response generated by the TMS pulse in the brain network, the cortical regions significantly recruited by TMS seem to maintain peaks of functional activation at the specific natural frequency consistently over time (Fig.3, see also the movies in **Supplementary Material**).

The dynamic spatial correlation between the directed functional connectivity (swADTF) and the connectome, for the two different sites of stimulation (i.e. left precuneus and left premotor) and for each of the three chosen frequency

Figure 2: **Directed functional connectivity across cortical regions after TMS.** Snapshot of differences between baseline and post TMS stimulus directed functional connectivity (i.e. Outdegree) at $p < 0.05$, FDR corrected (see **Materials and Methods**) across cortical regions, for the three predefined frequency bands (α, β, $\beta 2/\gamma$ [7]), obtained by averaging the swADTF time courses from 20 to 320 ms after the pulse. The red circles represent the stimulation site. Note that the precuneus area has a maximum of directed functional connectivity in the β band in proximity of the stimulation site, whereas the premotor has a maxima in the $\beta 2/\gamma$ band, more spread towards the hemisphere controlateral to the stimulation site. These brain images were obtained using BrainNet Viewer [54].

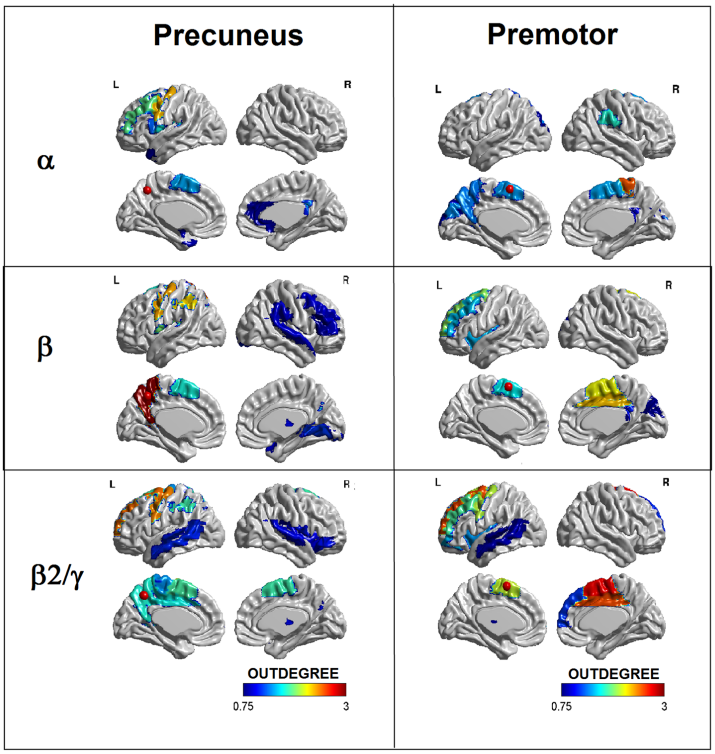

Figure 3: **Flow of directed functional connectivity over time.** Selected frames from the video in the **Supplementary Material**, of the functional connectivity across cortical regions, for both sites of stimulation (top two rows), after the TMS pulse. The temporal changes of the Outdegree for the natural frequency of the site of stimulation (i.e. β for precuneus, $\beta 2/\gamma$ for premotor [7], see also Fig.2) is illustrated in four different time points after the TMS pulse. The red circles represent the stimulation site. A grand average plot of the EEG reconstructed sources is also shown on the third row. The red marker denotes the time instant along the ERP time series for the associated frame (on top). A z–scored map of the group averaged SCdegree (fixed, does not change over time) is depicted on the right. These brain images were obtained using BrainNet Viewer [54].

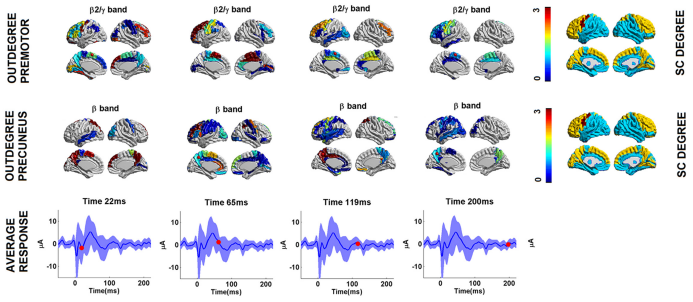

bands (i.e. α, β, $\beta 2/\gamma$) deviates from baseline directly after the TMS pulse (Fig.4). This global network behavior does not depend on the subject or the stimulation site. The stable baseline configuration is then recovered after 200-300 ms, depending on the frequency band. The evidence that different brain area can be normally tuned by TMS to oscillate at a characteristic rate (i.e. natural frequency) might also explain the drop in structure-function correlation depicted in Fig.4. In fact, assuming that each of the 90 AAL cortical regions respond to TMS by oscillating at its peculiar natural frequency, the emergence of this complex between-band interaction might generate a consequent deflection in the within-band structure-function correlation (Fig.4). Specifically, this TMS-induced modulation of EEG rhythms over the brain network is more pronounced (i.e. higher deviation from the baseline correlation) and faster in the $\beta 2/\gamma$ and β bands, while the return to baseline is slower and less pronounced in the α band. This effect might be due to the region-specific variability in the intensity and the duration of the cortical response to TMS at the different natural frequencies, but it might also depend on the degree to which each recruited region is structurally connected to the rest of the network.

To further investigate this hypothesis, we evaluated the local dynamic spatial correlation between the directed functional connectivity (swADTF) for the cortical regions near to the stimulation site and the connectome, for both sites of stimulation (Fig.5). Notably, the structure-function correlation significantly increases over time in the right premotor area after TMS, when its natural frequency band (i.e. $\beta 2/\gamma$) is taken into consideration. This effect is not reproduced in the precuneus area (Fig.5).

4. Discussion

In this work we studied the interplay between directed functional connectivity computed from TMS reconstructed EEG sources and the connectome extracted from whole-brain dMRI tractography.

It is known that stimulating peripheral receptors of different sensory systems

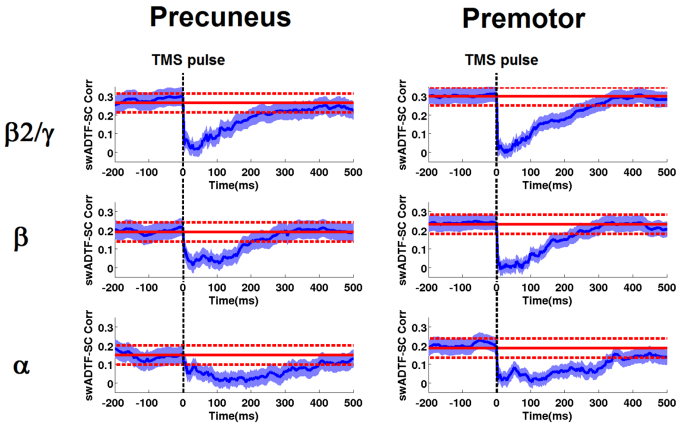

Figure 4: **Time-varying spatial correlation between directed functional connectivity and structural connectivity.** Each plot shows the average over subjects of the dynamic spatial correlation between the directed functional connectivity (swADTF) matrices and the structural connectivity (SC) in function of time (blue line, standard error in shaded blue), for the three different frequency bands (α, β, $\beta 2/\gamma$, [7]). The red line indicates the mean baseline value, the dashed lines represent 95% confidence interval of the empirical baseline distribution (see **Materials and Methods**). Note the TMS-induced decrease in the observed structure-function correlation, for both stimulation sites and in each frequency band.

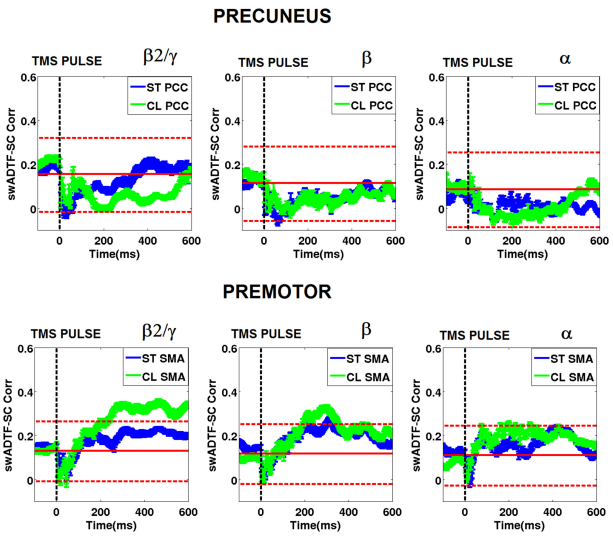

Figure 5: **Time-varying spatial correlation for the stimulated cortical regions.** Each row shows the average over subjects of the dynamic spatial correlation (blue and green line, standard error in shaded blue and green) between the directed functional connectivity (swADTF) and structural connectivity (SC) for the AAL ROIs comprising left and right premotor areas (stimulated and controlateral, i.e. ST SMA, CL SMA) and the left and right precuneus (stimulated and controlateral, i.e. ST PCC, CL PCC) respectively, for the three different frequency bands (i.e. α, β, $\beta 2/\gamma$ respectively [7]). The continuous red line indicates the mean baseline value, the dashed lines represent 95% confidence interval of the empirical baseline distribution (see **Materials and Methods**). Note the constant increase over time in the structure–function correlation for the controlateral SMA following the TMS pulse, when taking into account its natural frequency (i.e. $\beta 2/\gamma$, Fig.2).

results in evoked potentials with specific latencies, waveforms, and spectral components [55]. TMS is also known to evoke electrical activations not only at the stimulated site but also in distant cortical regions [1, 25]. A previous study by Rosanova and colleagues revealed that distant areas, when activated by TMS, responded with oscillations closer to their own "natural" frequency [7].

Our analysis on peaks of significant changes in directed functional connectivity and local structure-function interactions at different frequency bands corroborated the hypothesis that TMS evokes dominant oscillation in different cortical areas at a characteristic rate [7]. Each stimulated area appeared to mainly respond to the stimulation by being functionally elicited in specific "natural" frequency bands, i.e. β for precuneus and $\beta 2/\gamma$ for premotor (Fig. 2, Table 1). Furthermore, these peaks of functional changes at the natural frequency of the stimulation site after TMS seem to be quite stable over time (Fig.3, see also the movies in **Supplementary Material**).

We compared structural and directed functional connectivity at the whole network level for different EEG bands (α, β, $\beta 2/\gamma$). We observed a temporary decrease in the correlation between directed connectivity and structural connectivity after TMS. In particular, we showed that, after stimulation, precuneus responds mostly in the β band, whereas premotor has peaks of directed functional connectivity in the $\beta 2/\gamma$ band (Fig 2, Table 1). Assuming that the each region in the brain reacts to the perturbation at a characteristic operating frequency, then the decrease in function-structure correlation in each frequency (Fig.4) might be caused by the complex pattern of between-frequency interactions rising after TMS in the whole-brain network. The return to baseline might then depend on two things: one is the temporal duration of the functional activation of the elicited area; the second is the extent to which it is related to its structural connectivity pattern.

These considerations brought us to explore the link between the "natural" frequency response of the stimulated cortical areas and their structural architecture. Interestingly, for the premotor area controlateral to the stimulation site the correlation between directed functional connectivity at the natural fre-

Table 1: Percentage increase before/after stimulation for the AAL areas illustrated in Fig. 2 where directed functional connectivity after TMS was significantly higher than baseline ($p < 0.05$, FDR corrected, see **Materials and Methods**), for the two sites of stimulation (left precuneus and left premotor) and the three different frequency band (F.B., i.e. α, β, $\beta 2/\gamma$). Top increment for each site of stimulation is highlighted in bold.

TMS SITE: LEFT PRECUNEUS			TMS SITE: LEFT PREMOTOR		
AAL REGION	INCREASE (%)	F.B.	AAL REGION	INCREASE (%)	F.B.
Precentral_L	120	α	Supp_Motor_Area_L	210	α
Frontal_Mid_L	133	α	Supp_Motor_Area_R	190	α
$\text{Frontal\_Inf\_Oper}_L$	70	α	Cingulum_Post_R	60	α
Rolandic_Oper_L	60	α	Cuneus_L	120	α
Supp_Motor_Area_L	40	α	Occipital_Sup_L	90	α
Cingulum_Post_R	53	α	SupraMarginal_R	50	α
			Precuneus_L	80	α
			$\text{Paracentral\_Lobule}_R$	110	α
Precentral_L	150	β	Frontal_Sup_L	185	β
Frontal_Mid_R	70	β	Frontal_Mid_L	150	β
Rolandic_Oper_L	50	β	Supp_Motor_Area_L	220	β
Supp_Motor_Area_L	90	β	Supp_Motor_Area_R	260	β
Parietal_Inf_L	167	β	Insula_L	50	β
Precuneus_L	**280**	***β***	Cingulum_Mid_R	52	β
			Cingulum_Post_R	35	β
			Cuneus_R	30	β
			Cingulum_Mid_R	45	β
Precentral_L	233	$\beta 2/\gamma$	Precentral_L	118	$\beta 2/\gamma$
Frontal_Sup_L	152	$\beta 2/\gamma$	Frontal_Sup_L	363	$\beta 2/\gamma$
Supp_Motor_Area_L	126	$\beta 2/\gamma$	Frontal_Mid_L	203	$\beta 2/\gamma$
Supp_Motor_Area_R	130	$\beta 2/\gamma$	Frontal_Mid_Orb_L	153	$\beta 2/\gamma$
Cingulum_Mid_L	100	$\beta 2/\gamma$	Supp_Motor_Area_L	330	$\beta 2/\gamma$
Parietal_Inf_L	110	$\beta 2/\gamma$	**Supp_Motor_Area_R**	**432**	***β2/γ***
Precuneus_L	150	$\beta 2/\gamma$	$\text{Frontal\_Sup\_Medial}_R$	65	$\beta 2/\gamma$
			Insula_L	33	$\beta 2/\gamma$
			Cingulum_Mid_R	110	$\beta 2/\gamma$
			Thalamus_L	33	$\beta 2/\gamma$
			Temporal_Mid_L	53	$\beta 2/\gamma$

quency and structural connections increases after the stimulation and reveals a long-lasting effect over time (Fig.5). The fact that this effect is not reproduced for precuneus might be due to a number of reasons. First, the precuneal area is located deeper in the cortex then the premotor area, and thus more difficult to elicit. Secondly, it is possible that the different frequency responses in each cortical area might reflect different anatomical background. Indeed, recent studies have reported that there is a strong correlation between cytoarchitecture and anatomical and functional connectivity in cat, macaque and humans [56, 57], with precuneus showing both a different cytoarchitecture as well as a different connectivity architecture than supplementary motor regions [58]. This might explain why the functional activation at specific resonant frequencies is related to the structural coupling (i.e. the amount of tracts connecting them) differently depending on the anatomical architecture of the specific brain region.

These results lead to three main concluding remarks. First, this work confirms the hypothesis that different rhythms in the brain emerge after TMS, and that this modulation is influenced by the structural connectivity among regions. This dynamic interaction at different natural frequencies seems to reflect intrinsic properties of cortical regions, and the way those are interconnected [7, 9].

Secondly, our analysis permitted to evaluate the dynamic interactions between directed functional connectivity and anatomical connectivity, before and after TMS (Fig.4, Fig. 5). The interplay between directed functional connectivity and structural connectivity at baseline is in line with findings reported in recent fMRI-dMRI studies [59, 23], where the rich repertoire of brain states do not necessarily correlate with the structural pattern. Here, our directed connectivity approach also allowed the investigation of the causal effects of systematic TMS-induced perturbations of the system, extending the insight on the relationship between structure and function. We showed that the way directed functional connectivity changes due to TMS at the natural frequency might depend on the different structural architecture of the specific cortical region (Fig. 5).

Thirdly, our multimodal whole-brain approach gives new insight on how

TMS causally interferes with the brain network in healthy controls. More specifically, our study points out the importance of taking into account the major role played by different cortical oscillations when investigating the mechanisms for integration and segregation of information in the human brain [60, 26]. An interesting follow up of this study would indeed be to look at differences in structure-function interactions either when the cognitive function is pharmacologically modulated (i.e. anesthesia), or following pathology, damage or disruption in structural connections (i.e. coma and disorder of consciousness)[61].

5. Limitations

Given the intrinsic limitations of the EEG in terms of spatial resolution, it is important to stress that the patterns of connectivity detected by TMS/hd-EEG are necessarily coarse. Even though TEPs are characterized by a good test-retest reproducibility [4], the inter–individual reproducibility of the outgoing flow of information could be improved by a better computation of the electric field induced by TMS. More advanced models (boundary, or finite, element models) could improve the accuracy of the source localization [62].

Another limitation of our study concerns the relatively small sample size and the inter-subject variability at the tractography level. In addition, it has been shown that there are many brain regions with complex fiber architecture, also referred to as crossing fibers [63, 41]. In this context, tractography approaches based on more advanced diffusion models [63], or on more refined anatomical constraints [64] may provide more accurate anatomical connectivity patterns of brain networks. Therefore, our approach works best for studying large scale interactions than fine scale, local dynamics.

Finally, a b-value of 1000 s/mm^2 is lower than the optimal one for performing CSD, about 2500-3000 s/mm^2 [65]. However, despite of a low b-value, with a sufficient amount of directions crossing fibers can be reliably modeled with CSD and the result is still significantly better than with a simple DTI-based model, e.g. see [66] for a successful application.

6. Acknowledgements

We thank Timo Roine, Erik Ziegler, Gianluca Frasso, Andrea Piarulli and Georgos Antonopoulos for the insightful discussion and comments on the manuscript. We thank Marie-Aurelie Bruno, Athena Demertzi, Audrey Vanhaudenhuyse and Melanie Boly for help in acquiring the data. This research was supported by the Wallonia-Brussels Federation of Concerted Research Action (ARC), Fonds National de la Recherche Scientifique de Belgique (FNRS), Belgian Science Policy (CEREBNET, BELSPO), McDonnell Foundation, European Space Agency, Mind Science Foundation, University Hospital and University of Liège. OB is a research fellow, OG a post doctoral fellow and SL a research director at FNRS.

[1] R. J. Ilmoniemi, J. Virtanen, J. Ruohonen, J. Karhu, H. J. Aronen, T. Katila, et al., Neuronal responses to magnetic stimulation reveal cortical reactivity and connectivity, Neuroreport 8 (16) (1997) 3537–3540.

[2] S. Komssi, S. Kähkönen, The novelty value of the combined use of electroencephalography and transcranial magnetic stimulation for neuroscience research, Brain research reviews 52 (1) (2006) 183–192.

[3] C. Bonato, C. Miniussi, P. Rossini, Transcranial magnetic stimulation and cortical evoked potentials: a tms/eeg co-registration study, Clinical neurophysiology 117 (8) (2006) 1699–1707.

[4] P. Lioumis, D. Kičić, P. Savolainen, J. P. Mäkelä, S. Kähkönen, Reproducibility of tmsevoked eeg responses, Human brain mapping 30 (4) (2009) 1387–1396.

[5] O. Gosseries, S. Sarasso, S. Casarotto, M. Boly, C. Schnakers, M. Napolitani, M.-A. Bruno, D. Ledoux, J.-F. Tshibanda, M. Massimini, et al., On the cerebral origin of eeg responses to tms: Insights from severe cortical lesions, Brain stimulation 8 (1) (2015) 142–149.

[6] N. C. Rogasch, P. B. Fitzgerald, Assessing cortical network properties using tms–eeg, Human brain mapping 34 (7) (2013) 1652–1669.

[7] M. Rosanova, A. Casali, V. Bellina, F. Resta, M. Mariotti, M. Massimini, Natural frequencies of human corticothalamic circuits, The Journal of Neuroscience 29 (24) (2009) 7679–7685.

[8] F. Ferrarelli, S. Sarasso, Y. Guller, B. A. Riedner, M. J. Peterson, M. Bellesi, M. Massimini, B. R. Postle, G. Tononi, Reduced natural oscillatory frequency of frontal thalamocortical circuits in schizophrenia, Archives of general psychiatry 69 (8) (2012) 766–774.

[9] F. Cona, M. Zavaglia, M. Massimini, M. Rosanova, M. Ursino, A neural mass model of interconnected regions simulates rhythm propagation observed via tms-eeg, NeuroImage 57 (3) (2011) 1045–1058.

[10] F. Ferrarelli, S. Sarasso, Y. Guller, B. A. Riedner, M. J. Peterson, M. Bellesi, M. Massimini, B. R. Postle, G. Tononi, Reduced natural oscillatory frequency of frontal thalamocortical circuits in schizophrenia, Archives of general psychiatry 69 (8) (2012) 766–774.

[11] S. Groppa, M. Muthuraman, B. Otto, G. Deuschl, H. R. Siebner, J. Raethjen, Subcortical substrates of tms induced modulation of the cortico-cortical connectivity, Brain stimulation 6 (2) (2013) 138–146.

[12] A. N. Voineskos, F. Farzan, M. S. Barr, N. J. Lobaugh, B. H. Mulsant, R. Chen, P. B. Fitzgerald, Z. J. Daskalakis, The role of the corpus callosum in transcranial magnetic stimulation induced interhemispheric signal propagation, Biological psychiatry 68 (9) (2010) 825–831.

[13] N. De Geeter, G. Crevecoeur, A. Leemans, et al., Effective electric fields along realistic dti-based neural trajectories for modelling the stimulation mechanisms of tms, Physics in medicine and biology 60 (2) (2015) 453.

[14] M. Bortoletto, D. Veniero, G. Thut, C. Miniussi, The contribution of tms–eeg coregistration in the exploration of the human cortical connectome, Neuroscience & Biobehavioral Reviews 49 (2015) 114–124.

[15] C. Chu, N. Tanaka, J. Diaz, B. Edlow, O. Wu, M. Hämäläinen, S. Stufflebeam, S. Cash, M. Kramer, Eeg functional connectivity is partially predicted by underlying white matter connectivity, Neuroimage 108 (1) (2015) 23–33.

[16] P. J. Basser, Inferring microstructural features and the physiological state of tissues from diffusion-weighted images, NMR in Biomedicine 8 (7) (1995) 333–344.

[17] M. Catani, R. J. Howard, S. Pajevic, D. K. Jones, Virtual in vivo interactive dissection of white matter fasciculi in the human brain, Neuroimage 17 (1) (2002) 77–94.

[18] S.-K. Song, S.-W. Sun, M. J. Ramsbottom, C. Chang, J. Russell, A. H. Cross, Dysmyelination revealed through mri as increased radial (but unchanged axial) diffusion of water, Neuroimage 17 (3) (2002) 1429–1436.

[19] S. Hofer, J. Frahm, Topography of the human corpus callosum revisited-comprehensive fiber tractography using diffusion tensor magnetic resonance imaging, Neuroimage 32 (3) (2006) 989–994.

[20] A. N. Voineskos, L. J. O'Donnell, N. J. Lobaugh, D. Markant, S. H. Ameis, M. Niethammer, B. H. Mulsant, B. G. Pollock, J. L. Kennedy, C. F. Westin, et al., Quantitative examination of a novel clustering method using magnetic resonance diffusion tensor tractography, Neuroimage 45 (2) (2009) 370–376.

[21] O. Sporns, G. Tononi, R. Kötter, The human connectome: a structural description of the human brain, PLoS computational biology 1 (4) (2005) e42.

[22] E. Bullmore, O. Sporns, Complex brain networks: graph theoretical analysis of structural and functional systems, Nature Reviews Neuroscience 10 (3) (2009) 186–198.

[23] C. Honey, O. Sporns, L. Cammoun, X. Gigandet, J.-P. Thiran, R. Meuli, P. Hagmann, Predicting human resting-state functional connectivity from structural connectivity, Proceedings of the National Academy of Sciences 106 (6) (2009) 2035–2040.

[24] C. J. Honey, J.-P. Thivierge, O. Sporns, Can structure predict function in the human brain?, Neuroimage 52 (3) (2010) 766–776.

[25] M. Massimini, F. Ferrarelli, R. Huber, S. K. Esser, H. Singh, G. Tononi, Breakdown of cortical effective connectivity during sleep, Science 309 (5744) (2005) 2228–2232.

[26] A. G. Casali, O. Gosseries, M. Rosanova, M. Boly, S. Sarasso, K. R. Casali, S. Casarotto, M.-A. Bruno, S. Laureys, G. Tononi, et al., A theoretically based index of consciousness independent of sensory processing and behavior, Science translational medicine 5 (198) (2013) 198ra105–198ra105.

[27] M. Rosanova, O. Gosseries, S. Casarotto, M. Boly, A. G. Casali, M.-A. Bruno, M. Mariotti, P. Boveroux, G. Tononi, S. Laureys, et al., Recovery of cortical effective connectivity and recovery of consciousness in vegetative patients, Brain (2012) awr340.

[28] T. Mutanen, H. Mäki, R. J. Ilmoniemi, The effect of stimulus parameters on tms–eeg muscle artifacts, Brain stimulation 6 (3) (2013) 371–376.

[29] E. M. ter Braack, C. C. de Vos, M. J. van Putten, Masking the auditory evoked potential in tms–eeg: A comparison of various methods, Brain topography 28 (3) (2015) 520–528.

[30] P. Berg, M. Scherg, A multiple source approach to the correction of eye artifacts, Electroencephalography and clinical neurophysiology 90 (3) (1994) 229–241.

[31] C. Phillips, J. Mattout, M. D. Rugg, P. Maquet, K. J. Friston, An empirical bayesian solution to the source reconstruction problem in eeg, NeuroImage 24 (4) (2005) 997–1011.

[32] J. Mattout, C. Phillips, W. D. Penny, M. D. Rugg, K. J. Friston, Meg source localization under multiple constraints: an extended bayesian framework, NeuroImage 30 (3) (2006) 753–767.

[33] N. Tzourio-Mazoyer, B. Landeau, D. Papathanassiou, F. Crivello, O. Etard, N. Delcroix, B. Mazoyer, M. Joliot, Automated anatomical labeling of activations in spm using a macroscopic anatomical parcellation of the mni mri single-subject brain, Neuroimage 15 (1) (2002) 273–289.

[34] D. Jones, M. Horsfield, A. Simmons, Optimal strategies for measuring diffusion in anisotropic systems by magnetic resonance imaging, Magn Reson Med 42.

[35] A. Zalesky, H. Akhlaghi, L. A. Corben, J. L. Bradshaw, M. B. Delatycki, E. Storey, N. Georgiou-Karistianis, G. F. Egan, Cerebello-cerebral connectivity deficits in friedreich ataxia, Brain Structure and Function 219 (3) (2014) 969–981.

[36] K. Caeyenberghs, A. Leemans, C. De Decker, M. Heitger, D. Drijkoningen, C. V. Linden, S. Sunaert, S. Swinnen, Brain connectivity and postural control in young traumatic brain injury patients: A diffusion mri based network analysis, NeuroImage: clinical 1 (1) (2012) 106–115.

[37] A. Leemans, D. K. Jones, The b-matrix must be rotated when correcting for subject motion in dti data, Magnetic Resonance in Medicine 61 (6) (2009) 1336–1349.

[38] S. M. Smith, M. Jenkinson, M. W. Woolrich, C. F. Beckmann, T. E. Behrens, H. Johansen-Berg, P. R. Bannister, M. De Luca, I. Drobnjak, D. E. Flitney, et al., Advances in functional and structural mr image analysis and implementation as fsl, Neuroimage 23 (2004) S208–S219.

[39] J. Tournier, F. Calamante, D. G. Gadian, A. Connelly, et al., Direct estimation of the fiber orientation density function from diffusion-weighted mri data using spherical deconvolution, NeuroImage 23 (3) (2004) 1176–1185.

[40] J. Tournier, C.-H. Yeh, F. Calamante, K.-H. Cho, A. Connelly, C.-P. Lin, et al., Resolving crossing fibres using constrained spherical deconvolution: validation using diffusion-weighted imaging phantom data, Neuroimage 42 (2) (2008) 617–625.

[41] J. Tournier, F. Calamante, A. Connelly, et al., Mrtrix: diffusion tractography in crossing fiber regions, International Journal of Imaging Systems and Technology 22 (1) (2012) 53–66.

[42] P. Hagmann, L. Cammoun, X. Gigandet, R. Meuli, C. J. Honey, V. J. Wedeen, O. Sporns, Mapping the structural core of human cerebral cortex, PLoS biology 6 (7) (2008) e159.

[43] P. Van Mierlo, E. Carrette, H. Hallez, K. Vonck, D. Van Roost, P. Boon, S. Staelens, Accurate epileptogenic focus localization through time-variant functional connectivity analysis of intracranial electroencephalographic signals, Neuroimage 56 (3) (2011) 1122–1133.

[44] P. Van Mierlo, E. Carrette, H. Hallez, R. Raedt, A. Meurs, S. Vandenberghe, D. Roost, P. Boon, S. Staelens, K. Vonck, Ictal-onset localization through connectivity analysis of intracranial eeg signals in patients with refractory epilepsy, Epilepsia 54 (8) (2013) 1409–1418.

[45] M. Kaminski, K. Blinowska, A new method of the description of the information flow in the brain structures, Biological cybernetics 65 (3) (1991) 203–210.

[46] M. Kamiński, M. Ding, W. A. Truccolo, S. L. Bressler, Evaluating causal relations in neural systems: Granger causality, directed transfer function and statistical assessment of significance, Biological cybernetics 85 (2) (2001) 145–157.

[47] F. Babiloni, F. Cincotti, C. Babiloni, F. Carducci, D. Mattia, L. Astolfi, A. Basilisco, P. Rossini, L. Ding, Y. Ni, et al., Estimation of the cortical functional connectivity with the multimodal integration of high-resolution

eeg and fmri data by directed transfer function, Neuroimage 24 (1) (2005) 118–131.

[48] L. Astolfi, F. Cincotti, D. Mattia, F. de Vico Fallani, A. Tocci, A. Colosimo, S. Salinari, M. G. Marciani, W. Hesse, H. Witte, et al., Tracking the time-varying cortical connectivity patterns by adaptive multivariate estimators, Biomedical Engineering, IEEE Transactions on 55 (3) (2008) 902–913.

[49] C. Wilke, L. Ding, B. He, Estimation of time-varying connectivity patterns through the use of an adaptive directed transfer function, Biomedical Engineering, IEEE Transactions on 55 (11) (2008) 2557–2564.

[50] M. Arnold, X. Milner, H. Witte, R. Bauer, C. Braun, Adaptive ar modeling of nonstationary time series by means of kalman filtering, Biomedical Engineering, IEEE Transactions on 45 (5) (1998) 553–562.

[51] A. Schlögl, S. Roberts, G. Pfurtscheller, A criterion for adaptive autoregressive models, in: Proceedings of the 22 nd IEEE International Conference on Engineering in Medicine and Biology, 2000, pp. 1581–1582.

[52] N. C. Rogasch, R. H. Thomson, Z. J. Daskalakis, P. B. Fitzgerald, Short-latency artifacts associated with concurrent tms–eeg, Brain stimulation 6 (6) (2013) 868–876.

[53] B. Efron, R. Tibshirani, Bootstrap methods for standard errors, confidence intervals, and other measures of statistical accuracy, Statistical science (1986) 54–75.

[54] M. Xia, J. Wang, Y. He, et al., Brainnet viewer: a network visualization tool for human brain connectomics, PloS one 8 (7) (2013) e68910.

[55] E. Neidermeyer, The normal eeg of the waking adult, Electroencephalography: basic principles, clinical applications and related fields, 4th ed. Baltimore, MD: Williams and Wilkins (1999) 149–173.

[56] L. H. Scholtens, R. Schmidt, M. A. de Reus, M. P. van den Heuvel, Linking macroscale graph analytical organization to microscale neuroarchitectonics in the macaque connectome, The Journal of Neuroscience 34 (36) (2014) 12192–12205.

[57] S. F. Beul, S. Grant, C. C. Hilgetag, A predictive model of the cat cortical connectome based on cytoarchitecture and distance, Brain Structure and Function 220 (6) (2015) 3167–3184.

[58] M. P. van den Heuvel, L. H. Scholtens, L. F. Barrett, C. C. Hilgetag, M. A. de Reus, Bridging cytoarchitectonics and connectomics in human cerebral cortex, The Journal of Neuroscience 35 (41) (2015) 13943–13948.

[59] P. Barttfeld, L. Uhrig, J. D. Sitt, M. Sigman, B. Jarraya, S. Dehaene, Signature of consciousness in the dynamics of resting-state brain activity, Proceedings of the National Academy of Sciences 112 (3) (2015) 887–892.

[60] D. Balduzzi, G. Tononi, Integrated information in discrete dynamical systems: motivation and theoretical framework, PLoS computational biology 4 (6) (2008) e1000091.

[61] A. Fornito, A. Zalesky, M. Breakspear, The connectomics of brain disorders, Nature Reviews Neuroscience 16 (3) (2015) 159–172.

[62] T. Wagner, J. Rushmore, U. Eden, A. Valero-Cabre, Biophysical foundations underlying tms: setting the stage for an effective use of neurostimulation in the cognitive neurosciences, Cortex 45 (9) (2009) 1025–1034.

[63] B. Jeurissen, A. Leemans, D. K. Jones, J.-D. Tournier, J. Sijbers, Probabilistic fiber tracking using the residual bootstrap with constrained spherical deconvolution, Human brain mapping 32 (3) (2011) 461–479.

[64] R. E. Smith, J.-D. Tournier, F. Calamante, A. Connelly, Anatomically-constrained tractography: improved diffusion mri streamlines tractography through effective use of anatomical information, Neuroimage 62 (3) (2012) 1924–1938.

[65] J. Tournier, F. Calamante, A. Connelly, et al., Determination of the appropriate b value and number of gradient directions for high-angular-resolution diffusion-weighted imaging, NMR in Biomedicine 26 (12) (2013) 1775–1786.

[66] U. Roine, J. Salmi, T. Roine, T. Nieminen-von Wendt, S. Leppämäki, P. Rintahaka, P. Tani, A. Leemans, M. Sams, Constrained spherical deconvolution-based tractography and tract-based spatial statistics show abnormal microstructural organization in asperger syndrome, Molecular autism 6 (1) (2015) 1–12.

PAPER III

C

Mapping the functional connectome traits of levels of consciousness

Amico E., Marinazzo, D., Di Perri, C.,
Heine, L., Annen, J., Martial, C.,
Dzemidzic, M., Laureys, S., Goñi, J.,

eprint arXiv:1605.03031

Mapping the functional connectome traits of levels of consciousness.

Enrico Amico[a,b], Daniele Marinazzo[b], Carol DiPerri[a,c], Lizette Heine[a,c], Jitka Annen[a,c], Charlotte Martial[a,c], Mario Dzemidzic[d], Steven Laureys[a,c,*] and Joaquín Goñi[e,f,g,*]

[a]Coma Science Group, GIGA Research Center, University of Liège, Liège, Belgium

[b]Department of Data-analysis, University of Ghent, B9000 Ghent, Belgium

[c]University Hospital of Liège, Liège, Belgium

[d]Department of Neurology and Radiology and Imaging Sciences, Indiana University School of Medicine, Indianapolis, IN, USA

[e]School of Industrial Engineering, Purdue University, West-Lafayette, IN, USA

[f]Weldon School of Biomedical Engineering, Purdue University, West-Lafayette, IN, USA

[g]Purdue Institute for Integrative Neuroscience, Purdue University, West-Lafayette, IN, USA

*Authors contributed equally.

steven.laureys@ulg.ac.be

jgonicor@purdue.edu

Classification: NEUROSCIENCE

Keywords: fMRI, Brain Connectivity, Network Science, Consciousness

Short title: Mapping the functional traits of consciousness.

Abstract

Examining task-free functional connectivity (FC) in the human brain offers insights on how spontaneous integration and segregation of information relate to human cognition, and how this organization may be altered in different conditions, and neurological disorders. This is particularly relevant for patients in disorders of consciousness (DOC) following severe acquired brain damage and coma, one of the most devastating conditions in modern medical care.

We present a novel data-driven methodology, *connICA*, which implements Independent Component Analysis (ICA) for the extraction of robust independent FC patterns (FC-traits) from a set of individual functional connectomes, without imposing any a priori data stratification into groups.

We here apply *connICA* to investigate associations between network-traits derived from task-free FC and cognitive/clinical features that define levels of consciousness. Three main independent FC-traits were identified and linked to consciousness-related clinical features. The first one represents the functional configuration of an “awake resting” brain, and is associated to the level of arousal. The second FC-trait reflects the disconnection of the visual and sensory-motor connectivity patterns and relates to the ability of communicating with the external environment. The third FC-trait isolates the connectivity pattern encompassing the fronto-parietal and the default-mode network areas as well as the interaction between left and right hemisphere, which are also associated to the awareness of the self and its surroundings.

Each FC-trait represents a distinct functional process with a role in the degradation of conscious states in functional brain networks, shedding further light on the functional sub-circuits that get disrupted in severe brain-damage.

Significance Statement

In this study we propose a novel methodology for the analysis of functional brain connectomes, namely connICA, which consists of the extraction of robust independent patterns of functional connectivity between cortical areas in healthy and diseased human brains. We apply connICA to investigate associations between robust functional traits and

cognitive/clinical features that define levels of consciousness based on resting-state fMRI connectivity in patients at different levels of consciousness after severe brain damage.

The versatility and simplicity of the connICA framework presented here constitute a powerful approach to extract and disentangle underlying functional processes embedded within healthy and diseased human brains, which might pave the way for innovative and clinically highly relevant brain connectivity analyses.

\body

Introduction

Disorders of consciousness (DOC) remain among the most challenging and poorly understood conditions in modern medical care. The term spreads over several pathological states qualified by dissociation between awareness and arousal (1, 2). Among these, patients in coma show no signs of awareness nor arousal; patients with unresponsive wakefulness syndrome/vegetative state (UWS) show no signs of awareness but do have an altered sleep and wake cycle; patients in a minimally conscious state (MCS) retain minimal non-reflexive and highly fluctuating signs of awareness. When patients regain functional object use and/or reliable communication they are referred to as emerging from MCS (EMCS) (3, 4). A particular outcome is represented by patients with a locked-in syndrome (LIS), who have no means of producing speech, limb or facial movements (except mostly for eye movement and/or blinking) but are still awake and fully conscious (5, 6). To date, the most validated diagnosis of these patients is based on the behavioral presentation of the patient. The distinction between these pathological levels of consciousness can be very challenging, as the boundaries between these states are often uncertain and ambiguous (4).

In the last decade, advances in neuroimaging techniques have allowed the medical community to gain important insights into the pathophysiology of DOC and to observe that altered states of consciousness are related to complex disruptions in the functional and structural organization of the brain (7-11).

At the same time, quantitative analysis based on complex networks have become more commonly used to study the brain as a network (12), giving rise to the area of research so

called Brain Connectomics (13, 14). In brain network models, nodes correspond to grey-matter regions (based on functional or structural, atlas-based parcellations that constitute a partition).while links or edges correspond either to structural connections as modeled based on white matter fiber-tracts or to the functional coupling between brain regions while subjects are either at rest or performing a task (15). Recent advances in functional neuroimaging have provided new tools to measure and examine *in vivo* the whole-brain temporal dependence of the dynamics of anatomically separated brain regions, defined as functional connectivity (FC) (16-18).

In parallel to the development of methods and network features in Brain Connectomics, analyses of functional magnetic resonance imaging (fMRI) data based on independent component analysis (ICA) have become an increasingly popular voxel-level approach (19). ICA, by relying upon a general assumption of independence, is a powerful and versatile data-driven approach for studying the brain, at temporal and spatial scales (20).

Examining functional connectivity in the human brain can give insight on how integration and segregation of information relates to human behavior and how this organization may be altered in diseases (7, 21). In the case of disorders of consciousness, voxel-level ICA-based fMRI studies of levels of consciousness in DOC patients have mainly shown alterations in the functional connectivity of the default mode network area (DMN) (22-24). Recent studies have also shown disrupted functional connectivity in resting state networks other than DMN (25) and possibility to correctly classify patients based on the level of connectivity of the “auditory” network (26).Furthermore, analyses of the functional networks of comatose brains have also evidenced a radical reorganization of high degree “hub” regions (27) and that most of the affected regions in patients belonged to highly interconnected central nodes (11, 28).

The potential of functional connectivity (FC) in particular and Brain Connectomics in general in exploring the diseased human brain as a network going through systemic changes is undisputed. However, there is still no clear way to accomplish two critical steps. of great clinical importance. First, separate underlying FC patterns representing different functional mechanisms and, second, relate those FC patterns or subsequent network features to individual cognitive performance or clinical evaluations. This is specially the case when studying a continuum of states, where the stratification of the cohort-subjects into categories

or groups is inappropriate and/or poorly defined. Furthermore, standard FC techniques are not able to model and disentangle common underlying forces or competing processes arising from different functional patterns of healthy and diseased human brains in a data-driven fashion, as for instance ICA does in the case of fMRI voxel time series (19, 20). This was indeed our motivation for the approach presented here.

In this study we bridge this gap by presenting a novel data-driven methodology, *connICA*, which consists of the extraction of robust independent patterns (traits) from a set of individual functional connectomes (see scheme in Figure 1). In this sense, *connICA* is a multiplex network framework both in the input (i.e., layers are individual FC connectomes) and in the output (i.e., layers are independent patterns or FC-traits). Here we apply *connICA* to investigate the link between cognitive/clinical features that define states of consciousness and resting-state functional connectivity (FC) data. The method allows the assessment of individual FC patterns (or FC layers) in a joint data-driven fashion providing as outputs multivariate independent FC-traits, which model independent sources or phenomena present in the input (i.e. the aforementioned individual FC patterns). In a final step, we assess the predictability of the weights (fingerprints) of each FC-trait on each subject from demographic and consciousness related variables, allowing for a continuous mapping of levels of consciousness within functional connectomes.

Results

Following individual subject BOLD fMRI data processing (see Figure S1 for examples of four individual sessions) and subsequent modeling of the individual task-free functional connectomes, connICA (see scheme at Figure 1) was run on the cohort of 88 subjects (32 conscious controls and 56 severely brain-damaged patients at different levels of consciousness; see Methods for details) without imposing any *a priori* information or stratification into groups. The procedure included 100 runs of *connICA* and allowed us to identify a total of 5 robust FC-traits (see Figure S2). In other words, they were present with high frequency and reproducibility across runs (see connICA section in Methods for details). Each FC-trait consists of two elements: an FC map of the same dimensions as an individual FC matrix with connectivity units being unitless and represented by weights, and a vector indicating the *amount* of the FC-trait present on each individual functional connectome (i.e.

the weight of the trait on each subject). Importantly, this latter *connICA* outcome allows us to associate individual cognitive and clinical features to each trait. Each of these 5 components (FC-traits) was then evaluated in terms of explained FC variance and Newman's modularity quality function Q (29) generalized for signed networks (30) with respect to the partition into RSNs proposed by Yeo and colleagues (31). The highest explained variance components were 1, 2 and 4, with a dominant FC-trait 1 explaining 18% of variance on average. It is important to note that the FC explained variance does not quantify the meaningfulness of the FC-trait with respect to the variables of interest (i.e. those related to levels of consciousness in this case), but only the average prominence of the trait in the set of the FC connectivity matrices extracted from the population of subjects.

Of the 5 extracted traits, both FC-traits 1 and 2 had a high modularity ratio Q score (see Figure 2A), which denotes that both FC traits have a strong fingerprint on the underlying RSNs organization (see insert in Figure 2B) in functional communities. We focused our subsequent analysis on FC traits 1, 2 and 4, which were the ones with highest R^2 and at the same time captured different aspects of the RSNs modular architecture.

The dominant FC-trait extracted using *connICA* (i.e. the one with the highest explained FC variance in the cohort) is shown in Figure 3D. Interestingly, it conforms to all the connectivity blocks or modules of the resting-state functional networks (RSNs, see insert Figure 2B) as introduced by Yeo and colleagues (31). For this reason, this FC-trait was denominated the *RSNs* trait. An incremental multi-linear model predicting the weight or *quantity* of the *RSNs* trait on each subject (see Figure 3A) was used, based on up to 7 predictors (see Figure 3G). A significant association with arousal, a subscore of the Coma Recovery Scale-Revised (CRS-R) (32-34), was found, after controlling for age, gender, traumatic brain injury (TBI), sedation, onset and CRS-R total score (with none of them being significant terms). In other words, the more aroused the subject (Figure 3G), the higher the subject-weight associated to the *RSNs* trait and hence the higher the presence of such trait. This might be due to the fact that this trait is reflecting a functional configuration of an *awake resting* brain. Therefore, this configuration might give a significant fingerprint for discriminating the “baseline wakefulness activity” of a human brain.

The other two FC-traits linked to cognitive features associated with levels of consciousness (i.e. the CRS-R total score and the communication subscore (32, 33)) are shown in Figure 3E and 3F.

In particular, the FC-trait depicted in Figure 3E mainly captures changes of intra-hemispheric functional connectivity in the visual and sensory motor networks across subjects in different levels of consciousness. We will refer to it as the *VIS-SM* trait. A significant link with the CRS-R communication subscore (32, 33) was found, as well as with three other variables previously added to the multilinear model (precisely with TBI, sedation and onset, see Figure 3H).

The positive sign of the beta coefficient associated to the communication subscore indicates that the trend of the linear fit follows the correspondent individual weights of the FC trait. In other words, the higher the communication subscore of a subject, the higher the contribution or presence of the *VIS-SM* trait in his/her functional connectome (Figure 3B). Interestingly, when adding etiology, sedation and time since onset (quantified here as the inverse of the days since the insult, see Methods), the explained variance of the model significantly increased. The negative sign of the associated beta coefficients for the three nuisance variables indicates a negative slope in the fit with the FC individual weights. That is, in the case of etiology, TBI patients have a lower amount of the *VIS-SM* trait in their functional connectomes; in the case of sedation, sedated patients have a lower contribution of the trait on their individual FC patterns; in the case of time since onset, the more recent the insult, the lower the prominence of the *VIS-SM* trait on the individual FC of the patient.

The trait shown in Figure 3F mainly captures modifications in the connectivity between DMN and fronto-parietal networks (hence denominated *FP-DMN* trait). Interestingly, the *FP-DMN* trait is linked to the CRS-R sum of scores, but also to the CRS-R communication subscore, even when the sum of scores is already added to the multilinear model (Figure 3I). The positive sign of the beta coefficient associated to these two predictors indicates that the higher the CRS-R sum of scores (communication subscore) for a subject, the higher the presence of the *FP-DMN* trait on his functional connectome. Notably, as one goes lower in the levels of consciousness, the contribution of the *FP-DMN* trait on the FC of a subject flips sign from negative to positive –(see the sorted individual weights associated to *FP-DMN* trait,

Figure 3C, 3F). There is an analogous effect in a few subjects for the *VIS-SM* trait (Figure 3B, 3E).

The *RSNs* trait was mostly characterized by the underlying RSNs. We further characterized *VIS-SM* and *FP-DMN* traits by identifying the regions with a higher functional strength. The strength of participation of each brain region to the two FC-traits was measured as its absolute weighted degree (i.e. computed as the sum over columns of the absolute value of the FC-trait). The higher the strength, the more influential is the role of the brain region to the FC-trait, and hence to the disruption of the level of consciousness. *VIS-SM* trait mainly involves the occipital and visual areas, whereas fronto-parietal areas are the most involved in the *FP-DMN* trait (Figure 4).

Further analyses were performed on *VIS-SM* and *FP-DMN* traits to assess the presence of communities (Figure 5) by using consensus clustering (35) over 100 modularity solutions computed using the Louvain algorithm (36) with quality function Q extended to signed networks (30) (see Methods). Note that the obtained modular configuration gives insights on the data-driven organization of the functional cores common to the whole cohort. When going back to the individual space, the multiplication by the subject's weight may preserve or change this core modular organization depending on the sign (i.e. it changes the FC-trait signed network, see Figure 3). Hence, performing consensus clustering on the FC-traits allowed us to track the "normal conscious" (positive weights) configuration that gets disrupted towards "lower altered" (negative weights) levels of consciousness (Fig. 3A, 3B, 3C).

We looked at the prominence of each community by averaging the correspondent connectivity values within each module. Interactions between every two communities in the FC-traits were then evaluated by averaging the connectivity values connecting them, hence providing a representation of the "coupling" between communities.

For both traits, the highest modularity was associated to partitions of three modules. In line with results of Figure 4, the most influential module (the highest within-module average) for the *VIS-SM* trait appears to be the one comprising the occipital cortex and higher order visual areas. Notably, the latter is strongly decoupled from the DMN module (highest between-modules negative connectivity, Figure 5B), suggesting that in a healthy brain these two

modules are negatively correlated. This modular configuration is then altered after modifications of levels of consciousness.

The modular organization of *FP-DMN* trait revealed a substantial division of the brain in two hemispheres. The between-modules average weight shows that the most "antagonistic" communities encompass the two different hemispheres (Figure 5D), indicating that in normal consciousness the hemispheres are also anti-correlated. This "decoupling" or negative inter-module connectivity might change (i.e. it turns to positive, Figure 3C, 3F) following loss of consciousness.

Discussion

In this work we applied a novel data-based methodology, *connICA*, to the field of Brain Connectomics. Our approach is based on extracting independent connectivity traits from a set of individual functional connectomes to extract and map robust independent mechanisms or processes that explain the FC patterns of an entire cohort of subjects, without setting any *a priori* stratification into groups. We used the *connICA* framework to assess rsfMRI in 88 subjects with different levels of consciousness: 32 conscious controls and 56 severely damaged patients (2 coma, 17 UWS, 20 MCS, 13 EMCS, 4 LIS) of different etiology and duration, 31 of whom were acquired while receiving sedative drugs to control for movement artifacts. We investigated the functional connectivity traits underlining specific sensorimotor/cognitive capacities related to consciousness.

We showed how these traits separate the FC data into network subsystems with significant associations to levels of consciousness. Notably, this methodology allowed us to map and match the most meaningful functional traits to consciousness-related predictors taken at the patient's bedside. This approach established the link between the alteration of levels of consciousness and the connectivity core associated to it.

The *connICA* framework provides a multiplex data-driven way to extract and compact (dimensionality reduction) the most meaningful multivariate information contained in the functional connectomes in a relatively small set of connectivity traits. In this work we showed how the modification of levels of consciousness is associated to specific connectivity disruptions using as reference seven widely accepted RSNs (i.e., visual, somatomotor, dorsal attention, ventral attention, limbic system, fronto-parietal, default mode network (31), and for

completeness, also subcortical regions (SUBC) and cerebellum (CER), see insert in Figure 2B).

One additional advantage of this approach is that the dimensionality of the output is significantly reduced, both in the number of the robust components extracted with respect to the initial population size (in the study analyzed here, 5 FC-traits starting from 88 FC matrices) and in the number of variables to be encoded in the multi-linear models, hence notably decreasing number of multiple comparisons. As opposed to univariate approaches mapping up to *N(N-1)/2* functional connections and their subsequent multi-linear models (*N* being the number of brain regions), the multi-layered output of *connICA* allows to focus on a small subset of robust FC-traits (by definition, a subset smaller or equal to the number of components set). This dimensionality reduction does not compromise but rather considerably facilitates the interpretability of the results, by compressing the individual variability into the most meaningful independent functional cores. It is noteworthy that most if not all the traits would have been missed with a standard group-average analysis of the functional connectomes.

By using connICA, we extracted three independent functional connectivity traits linked to cognitive features of levels of consciousness. Below is a characterization of each FC-trait and its association to different aspects of consciousness.

The *RSNs* trait (Figure 3D) is also the one which explains the most of the FC variance (Figure 2A) and is the closest to the Yeo's RSNs organization (31). It seems mainly associated to a global drop in the functional connectivity within each of the networks, and correlates with the CRS-R arousal subscore. We might think of this trait as the one of an *awake resting brain*. It reflects the connectivity organization of a functioning brain, which might be at least partially driven by its underlying structural connectivity (37-39).

The *VIS-SM* trait seems more associated to the effect of the pathology (i.e. etiology, time since onset) and the sedation level (Figure 3H). It shows a more prominent disruption in the occipital and sensorimotor areas as the level of consciousness decreases (Figure 3E), and it also correlates with functional communication (Figure 3H). Interestingly, the modularity analysis suggests that visual areas and DMN are anti-correlated in normal wakefulness (Figure 4A, 4B), stressing the importance of the interaction between the so called sensory

"slave" regions (40) and higher order cognitive regions as the DMN, for consciousness and functional communication (11). This corroborates the hypothesis that loss of consciousness might correlate with the disruption of primary sensory areas and higher-order associative cortices, which are thought to be required for conscious perception (i.e. global workspace, (26, 41)).

However, the recovery of this connectivity pattern seems not a sufficient condition for the restoration of levels of consciousness. Another independent functional trait appears to be linked to behavioral assessment of levels of consciousness, particularly to both the CRS-R total score and the communication subscore (*FP-DMN* trait, Figure 3F).

The *FP-DMN* trait captures changes in the anti-correlation between the FP-DMN networks. Notably, as one goes towards the deepest unconsciousness, the FP-DMN anti-correlation decreases, until the point where it "flips" to positive correlation, (see Figure 3C, 3F). This is in line with previous studies showing decreasing anti-correlation in anesthesia (42, 43), sleep (44) and UWS patients (45). Particularly, a recent study (46) showed that negative connectivity between DMN and FP networks was significantly different between patients and healthy controls. Indeed, UWS and MCS patients showed a pathological positive connectivity between these two networks, whereas patients who emerged from MCS and recovered a level of consciousness sufficient for functional communication and/or object use, exhibited partial preserved between-network negative connectivity (46). In this respect, the fact that the *FP-DMN* trait is strongly correlated to the communication subscore corroborates the idea that recovery of the FP-DMN between-network negative connectivity is prerequisite in order to regain functional communication.

Notably, the modularity analysis on *FP-DMN* trait reveals that the *decoupling* between the two hemispheres (Figure 5C) represents a "healthy" way of communication between left and right brain areas. The anti-correlation between hemispheres tends to disappear (i.e. goes towards zero or even positive correlation, see the individual weights of *FP-DMN* trait in Figure 3C) as levels of consciousness decrease.

Indeed, there is evidence suggesting that communication and coordination between the two hemispheres is essential for consciousness and conscious perception (47). It has been reported that transection of corpus callosum in refractory epileptic patients (i.e. split brain

patients) caused each hemisphere to have its own separate perception, concepts, and impulses to act (48). The conscious abilities of the two hemispheres are strongly differentiated in specialized cognitive modules (49), modulated by the thalamo-cortical system (subcortical regions are also split in left and right modules in *FP-DMN* trait, see Figure 5C). In this study we show that the interaction between specialized modules, as the VIS-SM interaction with DMN or the FP-DMN between-networks negative connectivity, is crucial for the emergence of consciousness. Perhaps this laterality enhances the complexity of ongoing brain processes and facilitates demanding cognitive processes such as consciousness of the self and the surrounding.

Taken together, these findings suggest that the connectivity core which differentiates across levels of consciousness is a combination of positive and negative interactions between functional sub-networks. This evidence stresses the importance of a whole-brain network modulation between coherent and non-coherent functional states. The disruption of the equilibrium between these two might lead to changes in levels of consciousness and, ultimately, to reduced levels of consciousness.

In fact, the *connICA* results presented in this paper depict a very challenging reality. Within the set of individual functional connectomes analyzed here, there is not just one but at least three independent mechanisms, namely FC-traits, whose predictability by consciousness related features is present but different on each one, and hence is most likely capturing different phenomena or mechanisms. A first *RSNs* trait only predicted by arousal, a very *sensitive* FC-trait, which isolates the functional connectivity blocks of typical RSNs present in an *alive and awake* brain (Figure 3D); a second *VIS-SM* trait, with predominant influence of visual and sensory regions, which links disruption of sensory networks to the CRS-R functional communication subscore (Figure 3E); a third *FP-DMN* trait, significantly associated to CRS-R sum of scores and communication, which stresses the key role of the negative connectivity between FP and DMN networks (Figure 3F) and inter-hemispheric communication (Figure 5 C,D) in the alteration of levels of consciousness.

The study presented here adds to recent studies from Iraji et al. (50), where ICA components of voxel-based functional connectivity were assessed, and from Misic et al. (51), where levels of integration of joint structural-functional connectivity patterns are assessed from sets of

individual connectomes by means of a single-value decomposition approach (47). Together with the methodology presented here, these recent efforts suggest that the area of Brain Connectomics is evolving into new data-driven ways of analyzing connectivity data at different spatial scales without stratifying subjects into *a priori* groups and hence, also without performing group-averages of individual connectivity matrices.

Our study has several limitations. The optimal size of the cohort for the extraction of the *connICA* components needs to be further investigated. Similarly, the best choice of the starting number of ICA components (here fixed to 15) and the threshold for the final selection of the most frequent components over multiple ICA runs (here fixed to 75%) need to be characterized in more detail. In this work we used the Shen parcellation (52) because of the uniformity of the size of brain regions and its functional data-driven approach. We also used the well-assessed RSNs decomposition provided by Yeo as obtained in a large cohort (n=1000) of healthy volunteers (31). However, other parcellations (53, 54) or finer decompositions (25, 26) might be beneficial in the *connICA* framework, depending on the research problem at hand and the desired level of spatial resolution.

Future work can be extended to the use of *connICA* for structural connectivity patterns, hence identifying SC-traits within a population of subjects. This approach is not limited to assessing consciousness, but has the potential of studying other progressive diseases and disorders, drug-induced effects (i.e. anesthesia), and also differences based on aging or gender. When associating traits with cognitive/clinical features, multi-linear models employed here can be expanded by allowing for non-linear terms and interactions, which could capture more complex associations between connectivity patterns and cognition.

In conclusion, we here proposed a novel data-driven approach, *connICA*, to extract the most influential connectivity patterns in the alteration of levels of consciousness. Our results shed light on isolating key functional core changes involved in the degradation of conscious states and establish links between isolated clinical/cognitive features and specific FC-traits.

Materials and methods

Subjects

The cohort studied here consists of 88 subjects with different levels of consciousness. From those, 32 were healthy controls (mean age 44 years ± 15 years, 21 males, 11 females). We selected 56 patients from an initial cohort of 216 patients in different levels of consciousness. Exclusion criteria were: i) neuroimaging examination in an acute state, i.e. <28 days from brain insult, ii) large focal brain damage, i.e. >2/3 of one hemisphere, as stated by a certified neuroradiologist, iii) suboptimal segmentation, normalization and/or parcellation of the brain volumes after visual inspection. Out of the selected 56, 39 were patients with disorders of consciousness (2 coma, 17 UWS, 20 MCS), 13 EMCS and 4 LIS. 28 out of 56 patients had traumatic brain injury (TBI), and 31 were sedated during the fMRI acquisition.

Healthy volunteers were free of psychiatric or neurological history. The study was approved by the Ethics Committee of the Medical School of the University of Liège. Written informed consent to participate in the study was obtained from the healthy subjects and from the legal surrogates of the patients.

Demographics

Nuisance variables included age, gender, etiology (1 for TBI, 0 otherwise), sedation (1 for sedated subjects, 0 otherwise) and the inverse of the time since the insult (in days), as we assumed healthy subjects' time since onset to be infinite and hence corresponds to zero in our codification.

To assess the level of consciousness, we used the scores obtained from the JFK Coma Recovery Scale-Revised (CRS-R) (32-34) assessment for each DOC patient. The CRS-R is the most sensitive and validated (55) scale to fully characterize and monitor DOC patients and provide a global quantification of their levels of consciousness. In particular, CRS-R integrates 25 arranged items that comprise 6 sub-scales addressing auditory, visual, motor, oromotor, communication, and arousal processes. Each item assesses the presence or absence of a specific physical sign that represents the integrity of brain function at one of four levels: generalized, localized, emergent, or cognitively mediated responsiveness. Scoring is based on the presence or absence of specific behavioral responses to sensory stimuli administered in a standardized manner. The reader can refer to (33, 34, 56) for a detailed description of the scale.

Image acquisition

Each subject underwent structural MRI and a 10 minute fMRI resting-state (task-free) session. Whole-brain structural MRI T1 data (T1-weighted 3D MP-RAGE, 120 transversal slices, repetition time = 2300 ms, voxel size = 1.0 x 1.0 x 1.2 mm^3, flip angle = 9°, field of view = 256 x 256 mm^2) and resting state BOLD fMRI data (Echo Planar Imaging sequence, gradient echo, volumes = 300, repetition time = 2000 ms, echo time = 30ms, flip angle = 78°, voxel size = 3 x 3 x 3 mm^3, field of view = 192×192 mm^2, 32 transversal slices) were acquired on a Siemens 3T scanner. Healthy subjects were instructed to keep eyes open during the fMRI acquisition.

Data processing and Functional Connectivity modeling

Data processing was performed by combining functions from FSL (57) and in-house developed Matlab (MATLAB 6.1, The MathWorks Inc., Natick, MA, 2000) code. The individual functional connectomes were modeled in the native BOLD fMRI space of each subject.

Processing steps were based on state of the art fMRI processing guidelines (58, 59). Structural images were first denoised to improve the signal-to-noise ratio (60), bias-field corrected, and then segmented (FSL FAST) to extract white matter, grey matter and cerebrospinal fluid (CSF) tissue masks. These masks were warped in each individual subject's functional space by means of subsequent linear and non-linear registrations (FSL flirt 6dof, FSL flirt 12dof and fnirt).

BOLD fMRI functional volumes were processed according to the steps recommended by (59). These steps included: slice timing correction, motion correction, normalization to mode 1000, demeaning and linear detrending, inclusion of 18 regressors consisting of 3 translations [x,y,z], 3 rotations [pitch, yaw, roll], and 3 tissue regressors (mean signal of whole-brain, WM and CSF), and the 9 corresponding derivatives (backwards difference, see Figure S1). A scrubbing procedure censoring high motion volumes was based on Frame Displacement (FD), DVARS and SD. FD measures the movement of the head from one volume to the next, and is calculated as the sum of the absolute values of the differentiated realignment estimates (by backwards differences) at every time-point (59); DVARS measures the change in signal intensity from one volume to the next, and is calculated as the root mean square value of the differentiated BOLD time-series (by backwards differences) within a spatial mask at every time-point (61); SD is the standard deviation of the BOLD signal within brain voxels at every

time-point (outlier volumes higher than 75 percentile +1.5 of the interquartile range were discarded, see Fig. S1).

A bandpass first-order Butterworth filter in forward and reverse directions [0.001 Hz, 0.08 Hz] was then applied. After that, the 3 principal components of the BOLD signal in the WM and CSF tissue were regressed out of the GM signal.

A whole-brain data-driven functional parcellation based on 278 regions, as obtained by Shen and colleagues (52), was first warped into each subject's T1 space (FSL flirt 6dof, FSL flirt 12dof and finally fnirt) and then into each subject's fMRI space. To improve the registration of the structural masks and the parcellation to the functional volumes FSL boundary-base-registration was also applied. Individual functional connectivity matrices (FC) were then estimated by means of pairwise Pearson correlations between the averaged signals of the regions of the parcellation, excluding the censored volumes as determined by the above-mentioned scrubbing procedure. Finally, the resulting FC matrices were ordered according to 7 resting-state sub-networks (RSNs) as proposed by Yeo and colleagues ((31), see insert of Fig 2B). For completeness, we added two more sub-networks: an 8th sub-network representing the subcortical regions and a 9th sub-network representing the cerebellum.

ConnICA: Independent component analyses of sets of individual functional connectomes

The input of ConnICA consists of all the individual FC profiles embedded into a dataset matrix where each row contains all the entries of the upper triangular part of the FC matrix for each subject (given the symmetry of FC) and hence provides an individual FC pattern. Note that this includes all FC matrices from all subjects, without any *a priori* information or any stratification of the data into groups (see scheme at Fig. 1). With this input, ICA decomposition of the FC patterns was applied by running fastICA algorithm (62) and setting the number of independent components to 15.

The output of connICA consists of two vectors per component. The first output vector will be referred to as *FC-trait*, which represents an independent pattern of functional connectivity. Interestingly, this vector can be represented back to its *spatial* form, i.e. a square symmetric matrix with brain regions in rows and columns. While the values here express connectivity units, they are not Pearson correlation coefficients and hence not restricted tothe [-1,1] range.

The second output vector is the weight of the FC-trait on each subject, which quantifies the prominence or presence of the trait in each individual FC matrix (note that this value can be positive or negative). In that sense, connICA is maximizing the individual variance explained by the multilinear regression of the obtained collection of FC-traits and subsequent subject weights.

Given the non-deterministic nature of ICA decomposition into components, we selected only the most robust ones (from now on simply denominated FC-traits), i.e. only those independent patterns that are frequently observed during the ICA decomposition of the FC data. To do so, instead of analyzing the connICA components from a single run, we evaluated the similarity of the *connICA* components over 100 runs. For an FC-trait to be robust, it has to appear (correlation of 0.75 or higher across runs) in at least 75% of the runs. This criterion resulted in 5 robust FC-traits. Each of these traits is obtained by averaging the correspondent "representations" found along the runs (see Fig. S2).

Each FC-trait was characterized by the mean and standard deviation of explained variance with respect to the individual FC matrices. The subject weights associated to each assessed FC-traits was then used as response in an incremental multi-linear regression model with up to 7 predictors. Predictors included the Coma Recovery Scale Revised (30) clinical subscores of each patient (Arousal, Auditory, Communication, Motor, Oromotor, Visual), and the sum of these scores. The control population was assumed to have the highest scores for each of the subscales. As aforementioned, the following variables were also included: age, gender, etiology (traumatic/non traumatic), sedation level and the inverse of the time since onset.

We then identified the FC-traits whose presence (weights) in individual FCs was significantly explained by a cognitive predictor (statistical significance set at p-value ≤ 0.05, Fig. 3G, 3H, 3I). The aim was to extract the connectivity patterns or traits associated to clinical features that go from wakefulness to the deepest level of unawareness.

Modularity analyses

Modularity is a measure of the strength of division of a network into modules or communities. Networks with high modularity have dense connections between the nodes within modules but sparse connections between nodes in different modules. The Newman-Girvan quality function Q is a way of quantifying network modularity. It is defined as the fraction of edges

that fall within modules minus the expected number of edges for a random graph with the same node degree distribution as the given network (29). Particularly, we here used the extension of Q for signed undirected networks proposed by Mucha et al. (30), and inspired by (63, 64).

To investigate the functional organization properties of the FC-traits extracted with connICA, we first assessed the similarity of each trait with Yeo's partitions using Newman-Girvan modularity function Q for signed undirected networks (30). In other words, we wanted to evaluate to what extent each FC-trait can be well-separated into communities based on a partition based on RSNs.

We then assessed the community structure of each FC-trait by using the Louvain method for identifying communities in large networks (36). In order to improve the stability of the community detection procedure, we performed consensus clustering (35) out of a set of 100 partitions obtained by the Louvain method. Consensus clustering is a technique that seeks for a median (or consensus) partition, i.e. the partition that is most similar, on average, to all the input partitions. The similarity can be measured in several ways, for instance co-occurrence of the nodes in the clusters of the input partitions (35). This "consensus" partition was finally selected as the most robust one.

Acknowledgements

We thank Marie-Aurelie Bruno, Athena Demertzi and Audrey Vanhaudenhuyse for help in acquiring the data. This research was supported by the This research was supported by the Belgian Funds for Scientific Research (FRS), European Commission, James McDonnell Foundation, European Space Agency, Belgian Science Policy (CEREBNET, BELSPO), Wallonia-Brussels Federation Concerted Research Action, Mind Science Foundation, Public Utility Foundation "Université Européenne du Travail" and "Fondazione Europea di Ricerca Biomedica", University and University Hospital of Liège. LH is a research fellow and SL a research director at FNRS.

References

1. Laureys S (2005) The neural correlate of (un)awareness: lessons from the vegetative state. *Trends Cogn Sci* 9(12):556-559.
2. Bernat JL (2009) Chronic consciousness disorders. *Annu Rev Med* 60:381-392.
3. Laureys S, Owen AM, & Schiff ND (2004) Brain function in coma, vegetative state, and related disorders. *Lancet Neurol* 3(9):537-546.
4. Giacino JT, Fins JJ, Laureys S, & Schiff ND (2014) Disorders of consciousness after acquired brain injury: the state of the science. *Nat Rev Neurol* 10(2):99-114.
5. Laureys S*, et al.* (2005) The locked-in syndrome: what is it like to be conscious but paralyzed and voiceless? *Progress in brain research* 150:495-611.
6. Giacino JT*, et al.* (1995) Recommendations for use of uniform nomenclature pertinent to patients with severe alterations in consciousness. *Archives of Physical Medicine and Rehabilitation* 76(2):205-209.
7. Boly M*, et al.* (2012) Brain connectivity in disorders of consciousness. *Brain Connect* 2(1):1-10.
8. Di Perri C, Stender J, Laureys S, & Gosseries O (2014) Functional neuroanatomy of disorders of consciousness. *Epilepsy Behav* 30:28-32.
9. Fernández-Espejo D*, et al.* (2012) A role for the default mode network in the bases of disorders of consciousness. *Annals of neurology* 72(3):335-343.
10. Owen AM, Schiff ND, & Laureys S (2009) A new era of coma and consciousness science. *Progress in brain research* 177:399-411.
11. Koch C, Massimini M, Boly M, & Tononi G (2016) Neural correlates of consciousness: progress and problems. *Nature Reviews Neuroscience* 17(5):307-321.
12. Bullmore E & Sporns O (2009) Complex brain networks: graph theoretical analysis of structural and functional systems. *Nat Rev Neurosci* 10(3):186-198.
13. Sporns O (2011) *Networks of the Brain* (MIT press).
14. Fornito A, Zalesky A, & Bullmore ET (2016) Fundamentals of Brain Network Analysis. (Academic Press).
15. van den Heuvel MP & Hulshoff Pol HE (2010) Exploring the brain network: a review on resting-state fMRI functional connectivity. *Eur Neuropsychopharmacol* 20(8):519-534.
16. Friston KJ, Frith CD, Liddle PF, & Frackowiak RS (1993) Functional connectivity: the principal-component analysis of large (PET) data sets. *J Cereb Blood Flow Metab* 13(1):5-14.
17. Fox MD*, et al.* (2005) The human brain is intrinsically organized into dynamic, anticorrelated functional networks. *Proc Natl Acad Sci U S A* 102(27):9673-9678.
18. Fox MD & Raichle ME (2007) Spontaneous fluctuations in brain activity observed with functional magnetic resonance imaging. *Nature Reviews Neuroscience* 8(9):700-711.
19. Calhoun VD, Liu J, & Adali T (2009) A review of group ICA for fMRI data and ICA for joint inference of imaging, genetic, and ERP data. *Neuroimage* 45(1 Suppl):S163-172.
20. Erhardt EB*, et al.* (2011) Comparison of multi-subject ICA methods for analysis of fMRI data. *Hum Brain Mapp* 32(12):2075-2095.
21. Greicius M (2008) Resting-state functional connectivity in neuropsychiatric disorders. *Curr Opin Neurol* 21(4):424-430.
22. Heine L*, et al.* (2012) Resting state networks and consciousness: alterations of multiple resting state network connectivity in physiological, pharmacological, and pathological consciousness States. *Front Psychol* 3:295.

23. Soddu A*, et al.* (2012) Identifying the default-mode component in spatial IC analyses of patients with disorders of consciousness. *Hum Brain Mapp* 33(4):778-796.
24. Vanhaudenhuyse A*, et al.* (2010) Default network connectivity reflects the level of consciousness in non-communicative brain-damaged patients. *Brain* 133(Pt 1):161-171.
25. Demertzi A*, et al.* (2014) Multiple fMRI system-level baseline connectivity is disrupted in patients with consciousness alterations. *Cortex* 52:35-46.
26. Demertzi A*, et al.* (2015) Intrinsic functional connectivity differentiates minimally conscious from unresponsive patients. *Brain* 138(Pt 9):2619-2631.
27. Achard S*, et al.* (2012) Hubs of brain functional networks are radically reorganized in comatose patients. *Proc Natl Acad Sci U S A* 109(50):20608-20613.
28. Crone JS*, et al.* (2014) Altered network properties of the fronto-parietal network and the thalamus in impaired consciousness. *Neuroimage Clin* 4:240-248.
29. Newman MEJ & Girvan M (2004) Finding and evaluating community structure in networks. *Physical review E* 69(2):026113.
30. Mucha PJ, Richardson T, Macon K, Porter MA, & Onnela J-P (2010) Community structure in time-dependent, multiscale, and multiplex networks. *science* 328(5980):876-878.
31. Yeo BT*, et al.* (2011) The organization of the human cerebral cortex estimated by intrinsic functional connectivity. *J Neurophysiol* 106(3):1125-1165.
32. Kalmar K & Giacino JT (2005) The JFK Coma Recovery Scale--Revised. *Neuropsychol Rehabil* 15(3-4):454-460.
33. Giacino J & Kalmar K (2006) Coma recovery scale-revised. *The Center for Outcome Measurement in Brain Injury*:36-51.
34. Schnakers C*, et al.* (2008) A french validation study of the Coma Recovery Scale-Revised (CRS-R). *Brain Injury* 22(10):786-792.
35. Lancichinetti A & Fortunato S (2012) Consensus clustering in complex networks. *Scientific reports* 2.
36. Blondel VD, Guillaume J-L, Lambiotte R, & Lefebvre E (2008) Fast unfolding of communities in large networks. *Journal of statistical mechanics: theory and experiment* 2008(10):P10008.
37. Honey CJ*, et al.* (2009) Predicting human resting-state functional connectivity from structural connectivity. *Proc Natl Acad Sci U S A* 106(6):2035-2040.
38. Vincent JL*, et al.* (2007) Intrinsic functional architecture in the anaesthetized monkey brain. *Nature* 447(7140):83-86.
39. Lutkenhoff ES*, et al.* (2015) Thalamic and extrathalamic mechanisms of consciousness after severe brain injury. *Annals of neurology* 78(1):68-76.
40. Crick F & Koch C (1995) Are we aware of neural activity in primary visual cortex? *Nature* 375(6527):121-123.
41. Dehaene S & Changeux JP (2011) Experimental and theoretical approaches to conscious processing. *Neuron* 70(2):200-227.
42. Boveroux P*, et al.* (2010) Breakdown of within- and between-network resting state functional magnetic resonance imaging connectivity during propofol-induced loss of consciousness. *Anesthesiology* 113(5):1038-1053.
43. Amico E*, et al.* (2014) Posterior cingulate cortex-related co-activation patterns: a resting state FMRI study in propofol-induced loss of consciousness. *PLoS One* 9(6):e100012.

44. Sämann PG*, et al.* (2011) Development of the brain's default mode network from wakefulness to slow wave sleep. *Cerebral cortex*:bhq295.
45. Boly M*, et al.* (2009) Functional connectivity in the default network during resting state is preserved in a vegetative but not in a brain dead patient. *Hum Brain Mapp* 30(8):2393-2400.
46. Di Perri C*, et al.* (2016) Neural correlates of consciousness in patients who have emerged from a minimally conscious state: a cross-sectional multimodal imaging study. *Lancet Neurol*.
47. Gazzaniga MS (2005) Forty-five years of split-brain research and still going strong. *Nature Reviews Neuroscience* 6(8):653-659.
48. Gazzaniga MS (2014) The split-brain: rooting consciousness in biology. *Proc Natl Acad Sci U S A* 111(51):18093-18094.
49. Marinsek N, Turner BO, Gazzaniga M, & Miller MB (2014) Divergent hemispheric reasoning strategies: reducing uncertainty versus resolving inconsistency. *Front Hum Neurosci*, Switzerland), Vol 8, p 839.
50. Iraji A*, et al.* (2016) The connectivity domain: Analyzing resting state fMRI data using feature-based data-driven and model-based methods. *Neuroimage*.
51. Misic B*, et al.* (2016) Network-Level Structure-Function Relationships in Human Neocortex. *Cereb Cortex*.
52. Shen X, Tokoglu F, Papademetris X, & Constable RT (2013) Groupwise whole-brain parcellation from resting-state fMRI data for network node identification. *Neuroimage* 82:403-415.
53. Desikan RS*, et al.* (2006) An automated labeling system for subdividing the human cerebral cortex on MRI scans into gyral based regions of interest. *Neuroimage* 31(3):968-980.
54. Gordon EM*, et al.* (2016) Generation and evaluation of a cortical area parcellation from resting-state correlations. *Cerebral cortex* 26(1):288-303.
55. Seel RT*, et al.* (2010) Assessment scales for disorders of consciousness: evidence-based recommendations for clinical practice and research. *Archives of physical medicine and rehabilitation* 91(12):1795-1813.
56. Giacino JT, Kezmarsky MA, DeLuca J, & Cicerone KD (1991) Monitoring rate of recovery to predict outcome in minimally responsive patients. *Archives of Physical Medicine and Rehabilitation* 72(11):897-901.
57. Jenkinson M, Beckmann CF, Behrens TEJ, Woolrich MW, & Smith SM (2012) Fsl. *Neuroimage* 62(2):782-790.
58. Power JD, Barnes KA, Snyder AZ, Schlaggar BL, & Petersen SE (2012) Spurious but systematic correlations in functional connectivity MRI networks arise from subject motion. *Neuroimage* 59(3):2142-2154.
59. Power JD*, et al.* (2014) Methods to detect, characterize, and remove motion artifact in resting state fMRI. *Neuroimage* 84:320-341.
60. Coupé P, Manjón JV, Robles M, & Collins DL (2012) Adaptive multiresolution non-local means filter for three-dimensional magnetic resonance image denoising. *Image Processing, IET* 6(5):558-568.
61. Smyser CD, Snyder AZ, & Neil JJ (2011) Functional connectivity MRI in infants: exploration of the functional organization of the developing brain. *Neuroimage* 56(3):1437-1452.
62. Hyvarinen A (1999) Fast and robust fixed-point algorithms for independent component analysis. *IEEE Trans Neural Netw* 10(3):626-634.

63. Gómez S, Jensen P, & Arenas A (2009) Analysis of community structure in networks of correlated data. *Physical Review E* 80(1):016114.
64. Traag VA & Bruggeman J (2009) Community detection in networks with positive and negative links. *Physical Review E* 80(3):036115.

Figure Legends

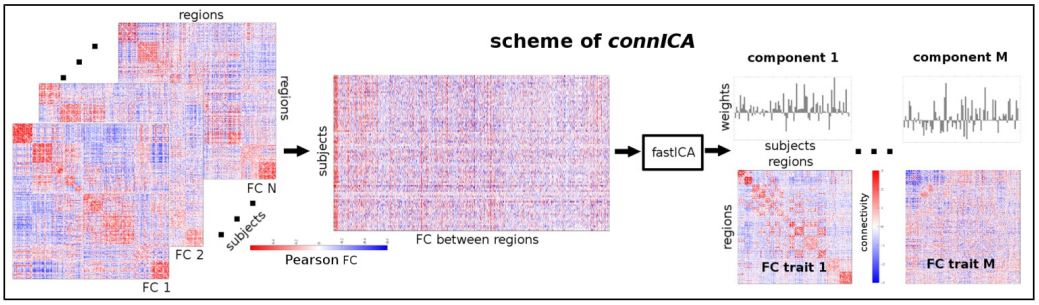

Figure 1. Workflow scheme of the proposed Connectivity Independent Component Analysis (*ConnICA*). The *N* individual functional connectivity (FC) matrices (left) are concatenated into a matrix where rows are the subjects and columns are the functional connectivity entries in the FC matrix). The ICA algorithm extracts the M independent components (i.e. functional traits) associated to the whole population and their relative weights across subjects. Colorbars indicate positive (red) and negative (blue) connectivity values, being Pearson's correlation coefficient values in the case of individual FC matrices (left side of scheme), and unitless connectivity weights in the case of FC-traits (right side of the scheme).

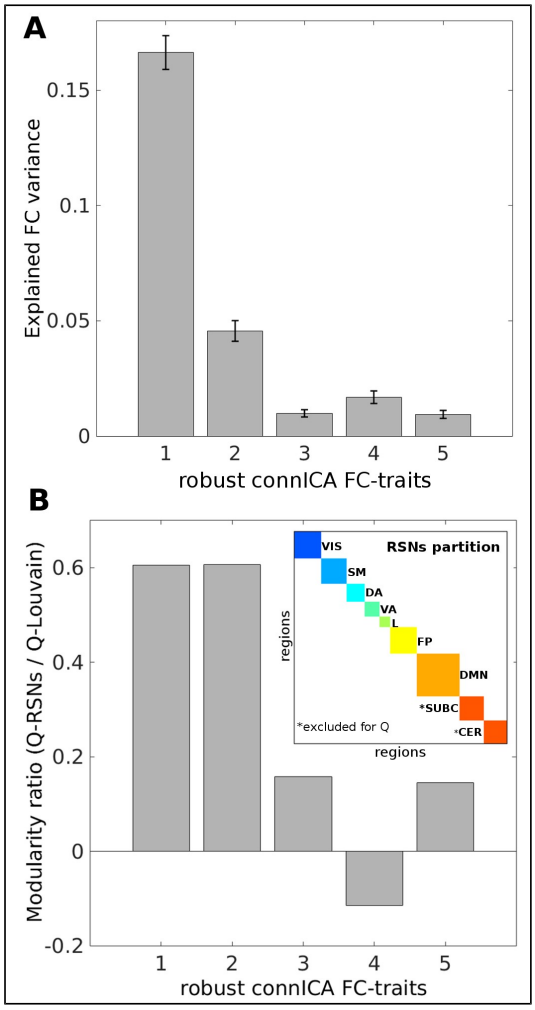

Figure 2. *connICA*-extracted robust FC traits A) Bar plot of the explained FC variance for the 5 most robust traits extracted with *connICA*. Error bars show the standard error across subjects. **B)** Bar plot of the modularity ratio for the 5 robust FC-traits extracted with connICA. This ratio is defined as the quality function Q ((30), see Materials and Methods) for the imposed a priori Resting State Networks' (RSNs) partition (encompassing 7 networks: visual (VIS), sensorimotor (SM), dorsal attention (DA), ventral attention (VA), limbic (L), fronto-parietal (FP), default mode network (DMN), see top right insert in panel B), divided by the quality function Q (30) for the data-driven partition obtained from consensus clustering (35) and Louvain's algorithm (36).

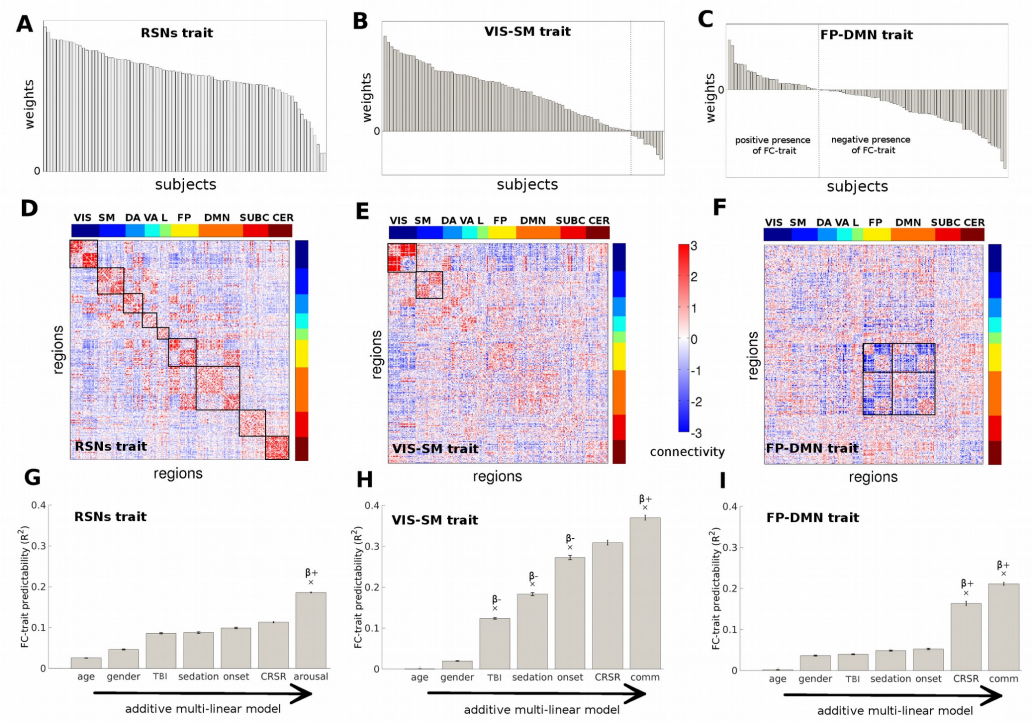

Figure 3 Mapping of the three main functional traits and their predictability by consciousness features. **A-C)** Quantified presence of each FC-trait on each individual functional connectome. Subject weights are sorted from greater to smaller on each FC-trait. **D-F)** Visualization of the three FC-traits associated to consciousness features. The brain regions are ordered according to Yeo's (31) functional RSNs as indicated : Visual (V), Somato-Motor (SM), Dorsal Attention (DA), Ventral Attention (VA), Limbic system (L), Fronto-Parietal (FP), Default Mode Network (DMN), and for completeness, also subcortical regions (SUBC) and cerebellum (CER). **G-I)** Bar-plot of the FC-traits predictability based on additive multi-linear regression models when predictors are sequentially introduced in the following order: age, gender, trauma, sedation, inverse of the time since onset, Coma Recovery Scale – Revised (CRS-R) total scores and the CRS-R communication subscore. Error bars show the standard error across the 100 ICA runs. Crosses on the top of a bar indicate that the inclusion of the correspondent predictor significantly increased the predictability of the model. The sign of the beta coefficient associated to each significant variable is shown below each asterisk, indicating whether there is a negative or positive trend with respect to the weights of the FC traits.

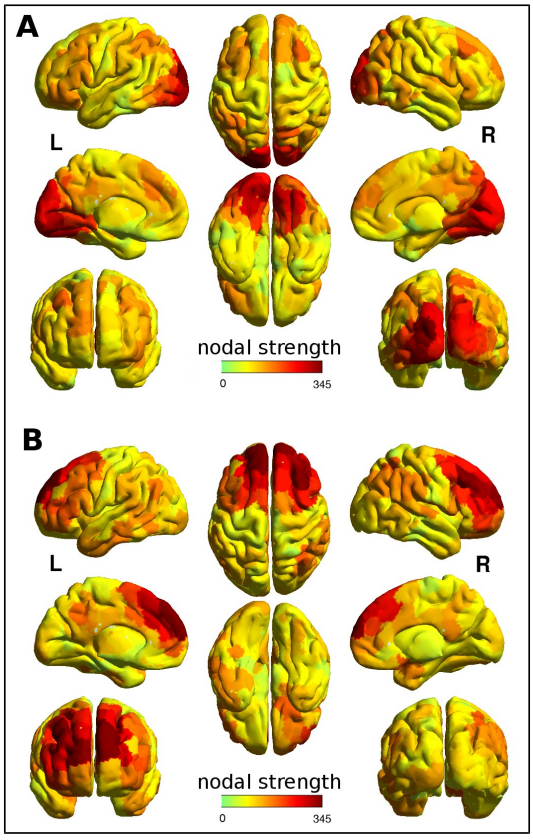

Figure 4. The strength per region computed as absolute sum of component weights allows an assessment of the overall centrality of each region for **A)** VIS-SM trait and **B)** FP-DMN trait.

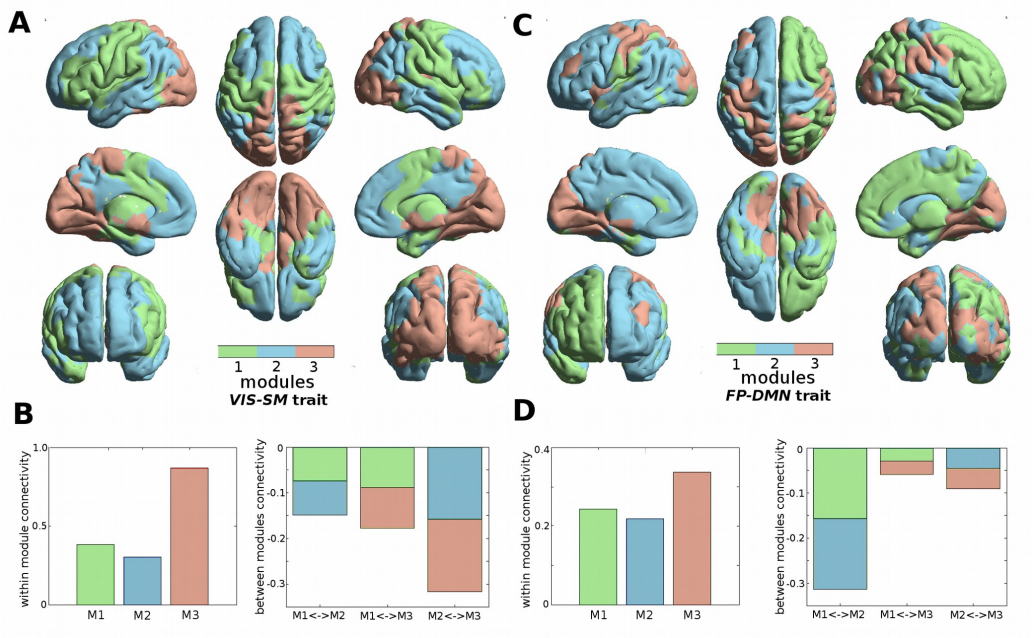

Fig. 5 A) Brain render of the modules obtained on *VIS-SM* trait (see Materials and Methods). Each color represents region's membership in a module. **B)** Left: bar plot of the average weight within each module in *VIS-SM* trait. Right: bar plot of the average between-module weight in *VIS-SM* trait. **C)** Brain render of the modules obtained on *FP-DMN* trait. **D)** Left: bar plot of the average weight within each module in *FP-DMN* trait. Right: bar plot of the average between-module weight in *FP-DMN* trait.

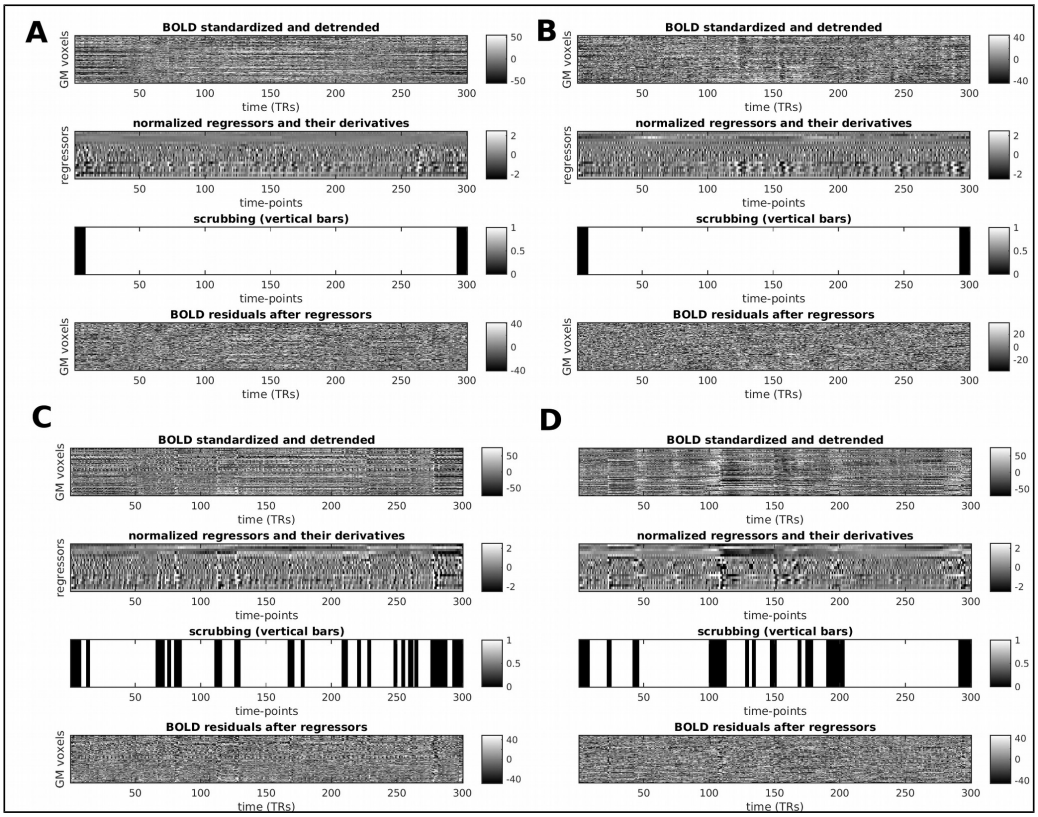

Figure. S1: Illustration of the fMRI preprocessing steps described in the Materials and Methods section on four subjects. Task-free session for four single subjects (A-D). For each subject, the 4 plots from top to bottom: 1) The fMRI time courses in GM voxels after slice timing and motion correction, normalization to mode 1000, demeaning and detrending; 2) The 18 motion and physiological noise regressors; [x, y , z, pitch, yaw, roll], the tissue mean signal of whole-brain, WM and CSF and their corresponding nine derivatives (backwards difference); 3) Visual representation of the scrubbing procedure based on Frame Displacement (FD), DVARS and SD to drop or censor volumes with motion (indicated by the dark vertical bars) from the computation of the pairwise correlations; 4) Residuals of the BOLD time courses of GM voxels after regressing out the 18 regressors. Subjects A and B had no censored volumes, with C and D having 14% and 11% censored volumes, respectively. Note that first and last 7 volumes in each session were always excluded.

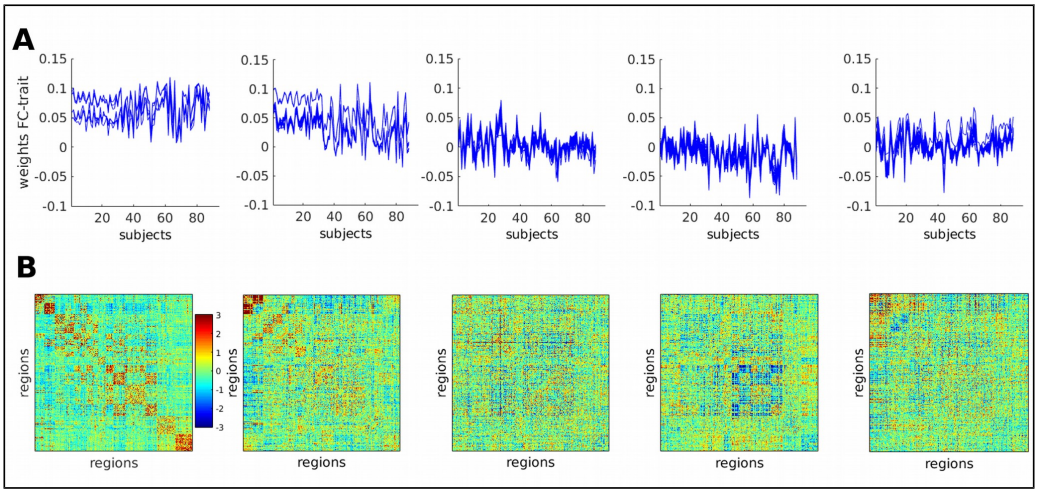

Figure S2: **A)** Plot of the correspondent weights per subjects for each single connICA run. **B)** Plot of the five robust connectivity traits extracted using connICA based on 100 runs. Only three of the FC traits were associated with cognitive scores linked to levels of consciousness.

BIBLIOGRAPHY

[1] N. K. Logothetis and B. A. Wandell, "Interpreting the bold signal," *Annu. Rev. Physiol.*, vol. 66, pp. 735–769, 2004.

[2] R. A. Brooks, J. H. Battocletti, A. Sances, S. J. Larson, R. L. Bowman, and V. Kudravcev, "Nuclear magnetic relaxation in blood," *Biomedical Engineering, IEEE Transactions on*, no. 1, pp. 12–18, 1975.

[3] S. Ogawa, T.-M. Lee, A. R. Kay, and D. W. Tank, "Brain magnetic resonance imaging with contrast dependent on blood oxygenation," *Proceedings of the National Academy of Sciences*, vol. 87, no. 24, pp. 9868–9872, 1990.

[4] D. J. Heeger and D. Ress, "What does fmri tell us about neuronal activity?," *Nature Reviews Neuroscience*, vol. 3, no. 2, pp. 142–151, 2002.

[5] N. K. Logothetis, J. Pauls, M. Augath, T. Trinath, and A. Oeltermann, "Neurophysiological investigation of the basis of the fmri signal," *Nature*, vol. 412, no. 6843, pp. 150–157, 2001.

[6] N. K. Logothetis, "What we can do and what we cannot do with fmri," *Nature*, vol. 453, no. 7197, pp. 869–878, 2008.

[7] R. B. Buxton, "Dynamic models of bold contrast," *Neuroimage*, vol. 62, no. 2, pp. 953–961, 2012.

[8] B. B. Biswal, J. V. Kylen, and J. S. Hyde, "Simultaneous assessment of flow and bold signals in resting-state functional connectivity maps," *NMR in Biomedicine*, vol. 10, no. 45, pp. 165–170, 1997.

[9] M. D. Greicius, B. Krasnow, A. L. Reiss, and V. Menon, "Functional connectivity in the resting brain: a network analysis of the default mode

hypothesis," *Proceedings of the National Academy of Sciences*, vol. 100, no. 1, pp. 253–258, 2003.

[10] B. Biswal, F. Zerrin Yetkin, V. M. Haughton, and J. S. Hyde, "Functional connectivity in the motor cortex of resting human brain using echo-planar mri," *Magnetic resonance in medicine*, vol. 34, no. 4, pp. 537–541, 1995.

[11] R. L. Buckner and J. L. Vincent, "Unrest at rest: default activity and spontaneous network correlations," *Neuroimage*, vol. 37, no. 4, pp. 1091–1096, 2007.

[12] M. N. Moussa, M. R. Steen, P. J. Laurienti, and S. Hayasaka, "Consistency of network modules in resting-state fmri connectome data," *PLoS One*, vol. 7, no. 8, p. e44428, 2012.

[13] M. J. Lowe, M. Dzemidzic, J. T. Lurito, V. P. Mathews, and M. D. Phillips, "Correlations in low-frequency bold fluctuations reflect cortico-cortical connections," *Neuroimage*, vol. 12, no. 5, pp. 582–587, 2000.

[14] Y. Nir, I. Dinstein, R. Malach, and D. J. Heeger, "Bold and spiking activity," *Nature neuroscience*, vol. 11, no. 5, pp. 523–524, 2008.

[15] A. Fick, "V. on liquid diffusion," *The London, Edinburgh, and Dublin Philosophical Magazine and Journal of Science*, vol. 10, no. 63, pp. 30–39, 1855.

[16] A. Einstein, "The theory of the brownian movement," *Ann. der Physik*, vol. 17, p. 549, 1905.

[17] M. Rosenbloom, E. V. Sullivan, and A. Pfefferbaum, "Using magnetic resonance imaging and diffusion tensor imaging to assess brain damage in alcoholics," *Alcohol Research and Health*, vol. 27, no. 2, pp. 146–152, 2003.

[18] D. Le Bihan, E. Breton, D. Lallemand, P. Grenier, E. Cabanis, and M. Laval-Jeantet, "Mr imaging of intravoxel incoherent motions: application to diffusion and perfusion in neurologic disorders.," *Radiology*, vol. 161, no. 2, pp. 401–407, 1986.

[19] E. O. Stejskal and J. E. Tanner, "Spin diffusion measurements: spin echoes in the presence of a time-dependent field gradient," *The journal of chemical physics*, vol. 42, no. 1, pp. 288–292, 1965.

[20] J.-D. Tournier, S. Mori, and A. Leemans, "Diffusion tensor imaging and beyond," *Magnetic Resonance in Medicine*, vol. 65, no. 6, pp. 1532–1556, 2011.

[21] C. G. Koay, J. D. Carew, A. L. Alexander, P. J. Basser, and M. E. Meyerand, "Investigation of anomalous estimates of tensor-derived quantities in diffusion tensor imaging," *Magnetic Resonance in Medicine*, vol. 55, no. 4, pp. 930–936, 2006.

[22] S. Pajevic, C. Pierpaoli, *et al.*, "Color schemes to represent the orientation of anisotropic tissues from diffusion tensor data: application to white matter fiber tract mapping in the human brain," *Magnetic resonance in medicine*, vol. 42, no. 3, pp. 526–540, 1999.

[23] P. Mukherjee, J. Berman, S. Chung, C. Hess, and R. Henry, "Diffusion tensor mr imaging and fiber tractography: theoretic underpinnings," *American journal of neuroradiology*, vol. 29, no. 4, pp. 632–641, 2008.

[24] B. Jeurissen, A. Leemans, J.-D. Tournier, D. K. Jones, and J. Sijbers, "Investigating the prevalence of complex fiber configurations in white matter tissue with diffusion magnetic resonance imaging," *Human brain mapping*, vol. 34, no. 11, pp. 2747–2766, 2013.

[25] J.-D. Tournier, F. Calamante, D. G. Gadian, and A. Connelly, "Direct estimation of the fiber orientation density function from diffusion-weighted mri data using spherical deconvolution," *NeuroImage*, vol. 23, no. 3, pp. 1176–1185, 2004.

[26] P. Fillard, M. Descoteaux, A. Goh, S. Gouttard, B. Jeurissen, J. Malcolm, A. Ramirez-Manzanares, M. Reisert, K. Sakaie, F. Tensaouti, *et al.*, "Quantitative evaluation of 10 tractography algorithms on a realistic diffusion mr phantom," *Neuroimage*, vol. 56, no. 1, pp. 220–234, 2011.

[27] D. K. Jones, T. R. Knösche, and R. Turner, "White matter integrity, fiber count, and other fallacies: the do's and don'ts of diffusion mri," *Neuroimage*, vol. 73, pp. 239–254, 2013.

[28] R. E. Smith, J.-D. Tournier, F. Calamante, and A. Connelly, "Anatomically-constrained tractography: improved diffusion mri streamlines tractography through effective use of anatomical information," *NeuroImage*, vol. 62, no. 3, pp. 1924–1938, 2012.

[29] L. Haas, "Hans berger (1873–1941), richard caton (1842–1926), and electroencephalography," *Journal of Neurology, Neurosurgery & Psychiatry*, vol. 74, no. 1, pp. 9–9, 2003.

[30] F. L. da Silva, "Eeg and meg: relevance to neuroscience," *Neuron*, vol. 80, no. 5, pp. 1112–1128, 2013.

[31] E. Niedermeyer and F. L. da Silva, *Electroencephalography: basic principles, clinical applications, and related fields*. Lippincott Williams & Wilkins, 2005.

[32] J. C. De Munck, B. W. Van Dijk, and H. Spekreijse, "Mathematical dipoles are adequate to describe realistic generators of human brain activity," *Biomedical Engineering, IEEE Transactions on*, vol. 35, no. 11, pp. 960–966, 1988.

[33] R. Grech, T. Cassar, J. Muscat, K. P. Camilleri, S. G. Fabri, M. Zervakis, P. Xanthopoulos, V. Sakkalis, and B. Vanrumste, "Review on solving the inverse problem in eeg source analysis," *Journal of neuroengineering and rehabilitation*, vol. 5, no. 1, p. 1, 2008.

[34] R. J. Ilmoniemi and D. Kičić, "Methodology for combined tms and eeg," *Brain topography*, vol. 22, no. 4, pp. 233–248, 2010.

[35] A. Barker, I. Freeston, R. Jalinous, and J. Jarratt, "Magnetic stimulation of the human brain and peripheral nervous system: an introduction and the results of an initial clinical evaluation," *Neurosurgery*, vol. 20, no. 1, pp. 100–109, 1987.

[36] L. Heller and D. B. van Hulsteyn, "Brain stimulation using electromagnetic sources: theoretical aspects.," *Biophysical journal*, vol. 63, no. 1, p. 129, 1992.

[37] O. Gosseries, O. Bodart, and M. Massimini, "Transcranial magnetic stimulation and electroencephalography," in *Clinical Neurophysiology in Disorders of Consciousness*, pp. 125–132, Springer, 2015.

[38] T. Krings, B. R. Buchbinder, W. E. Butler, K. H. Chiappa, H. J. Jiang, B. R. Rosen, and G. R. Cosgrove, "Stereotactic transcranial magnetic stimulation: correlation with direct electrical cortical stimulation," *Neurosurgery*, vol. 41, no. 6, pp. 1319–1326, 1997.

[39] S. Neggers, T. Langerak, D. Schutter, R. Mandl, N. Ramsey, P. Lemmens, and A. Postma, "A stereotactic method for image-guided transcranial magnetic stimulation validated with fmri and motor-evoked potentials," *Neuroimage*, vol. 21, no. 4, pp. 1805–1817, 2004.

[40] R. J. Ilmoniemi, J. Virtanen, J. Ruohonen, J. Karhu, H. J. Aronen, T. Katila, *et al.*, "Neuronal responses to magnetic stimulation reveal cortical reactivity and connectivity," *Neuroreport*, vol. 8, no. 16, pp. 3537–3540, 1997.

[41] S. Komssi, S. Kähkönen, and R. J. Ilmoniemi, "The effect of stimulus intensity on brain responses evoked by transcranial magnetic stimulation," *Human brain mapping*, vol. 21, no. 3, pp. 154–164, 2004.

[42] S. Komssi and S. Kähkönen, "The novelty value of the combined use of electroencephalography and transcranial magnetic stimulation for neuroscience research," *Brain research reviews*, vol. 52, no. 1, pp. 183–192, 2006.

[43] A. Pascual-Leone, V. Walsh, and J. Rothwell, "Transcranial magnetic stimulation in cognitive neuroscience–virtual lesion, chronometry, and functional connectivity," *Current opinion in neurobiology*, vol. 10, no. 2, pp. 232–237, 2000.

[44] M. Massimini, F. Ferrarelli, R. Huber, S. K. Esser, H. Singh, and G. Tononi, "Breakdown of cortical effective connectivity during sleep," *Science*, vol. 309, no. 5744, pp. 2228–2232, 2005.

[45] M. S. Hämäläinen and R. J. Ilmoniemi, "Interpreting magnetic fields of the brain: minimum norm estimates," *Medical & biological engineering & computing*, vol. 32, no. 1, pp. 35–42, 1994.

[46] S. Komssi, H. J. Aronen, J. Huttunen, M. Kesäniemi, L. Soinne, V. V. Nikouline, M. Ollikainen, R. O. Roine, J. Karhu, S. Savolainen, *et al.*, "Ipsi-and contralateral eeg reactions to transcranial magnetic stimulation," *Clinical Neurophysiology*, vol. 113, no. 2, pp. 175–184, 2002.

[47] M. Guye, G. J. Parker, M. Symms, P. Boulby, C. A. Wheeler-Kingshott, A. Salek-Haddadi, G. J. Barker, and J. S. Duncan, "Combined functional mri and tractography to demonstrate the connectivity of the human primary motor cortex in vivo," *Neuroimage*, vol. 19, no. 4, pp. 1349–1360, 2003.

[48] E. R. Kandel, J. H. Schwartz, T. M. Jessell, *et al.*, *Principles of neural science*, vol. 4. McGraw-hill New York, 2000.

[49] E. Bullmore and O. Sporns, "Complex brain networks: graph theoretical analysis of structural and functional systems," *Nature Reviews Neuroscience*, vol. 10, no. 3, pp. 186–198, 2009.

[50] L. Euler, "Solutio problematis ad geometriam situs pertinentis," *Commentarii academiae scientiarum Petropolitanae*, vol. 8, pp. 128–140, 1741.

[51] D. J. Watts and S. H. Strogatz, "Collective dynamics of small-worldnetworks," *nature*, vol. 393, no. 6684, pp. 440–442, 1998.

[52] A.-L. Barabási and R. Albert, "Emergence of scaling in random networks," *science*, vol. 286, no. 5439, pp. 509–512, 1999.

[53] K. Börner, S. Sanyal, and A. Vespignani, "Network science," *Annual review of information science and technology*, vol. 41, no. 1, pp. 537–607, 2007.

[54] O. Sporns, D. R. Chialvo, M. Kaiser, and C. C. Hilgetag, "Organization, development and function of complex brain networks," *Trends in cognitive sciences*, vol. 8, no. 9, pp. 418–425, 2004.

[55] D. S. Bassett and E. Bullmore, "Small-world brain networks," *The neuroscientist*, vol. 12, no. 6, pp. 512–523, 2006.

[56] M. P. Van Den Heuvel and H. E. H. Pol, "Exploring the brain network: a review on resting-state fmri functional connectivity," *European Neuropsychopharmacology*, vol. 20, no. 8, pp. 519–534, 2010.

[57] C.-C. Hilgetag, G. A. Burns, M. A. O'Neill, J. W. Scannell, and M. P. Young, "Anatomical connectivity defines the organization of clusters of cortical areas in the macaque and the cat," *Philosophical Transactions of the Royal Society of London B: Biological Sciences*, vol. 355, no. 1393, pp. 91–110, 2000.

[58] S. Achard, R. Salvador, B. Whitcher, J. Suckling, and E. Bullmore, "A resilient, low-frequency, small-world human brain functional network with highly connected association cortical hubs," *The Journal of neuroscience*, vol. 26, no. 1, pp. 63–72, 2006.

[59] R. S. Desikan, F. Ségonne, B. Fischl, B. T. Quinn, B. C. Dickerson, D. Blacker, R. L. Buckner, A. M. Dale, R. P. Maguire, B. T. Hyman, *et al.*, "An automated labeling system for subdividing the human cerebral cortex on mri scans into gyral based regions of interest," *Neuroimage*, vol. 31, no. 3, pp. 968–980, 2006.

[60] C. Destrieux, B. Fischl, A. Dale, and E. Halgren, "Automatic parcellation of human cortical gyri and sulci using standard anatomical nomenclature," *Neuroimage*, vol. 53, no. 1, pp. 1–15, 2010.

[61] C. Echtermeyer, C. E. Han, A. Rotarska-Jagiela, H. Mohr, P. J. Uhlhaas, and M. Kaiser, "Integrating temporal and spatial scales: Human structural network motifs across age and region-of-interest size," *arXiv preprint arXiv:1107.3911*, 2011.

[62] R. Salvador, A. Martinez, E. Pomarol-Clotet, J. Gomar, F. Vila, S. Sarro, A. Capdevila, and E. Bullmore, "A simple view of the brain through

a frequency-specific functional connectivity measure," *Neuroimage*, vol. 39, no. 1, pp. 279–289, 2008.

[63] J. Tournier, F. Calamante, A. Connelly, *et al.*, "Mrtrix: diffusion tractography in crossing fiber regions," *International Journal of Imaging Systems and Technology*, vol. 22, no. 1, pp. 53–66, 2012.

[64] O. Sporns, G. Tononi, and R. Kötter, "The human connectome: a structural description of the human brain," *PLoS Comput Biol*, vol. 1, no. 4, p. e42, 2005.

[65] P. Hagmann, L. Cammoun, X. Gigandet, R. Meuli, C. J. Honey, V. J. Wedeen, and O. Sporns, "Mapping the structural core of human cerebral cortex," *PLoS Biol*, vol. 6, no. 7, p. e159, 2008.

[66] Y. Iturria-Medina, E. Canales-Rodriguez, L. Melie-Garcia, P. Valdes-Hernandez, E. Martinez-Montes, Y. Alemán-Gómez, and J. Sánchez-Bornot, "Characterizing brain anatomical connections using diffusion weighted mri and graph theory," *Neuroimage*, vol. 36, no. 3, pp. 645–660, 2007.

[67] Y. Iturria-Medina, R. C. Sotero, E. J. Canales-Rodríguez, Y. Alemán-Gómez, and L. Melie-García, "Studying the human brain anatomical network via diffusion-weighted mri and graph theory," *Neuroimage*, vol. 40, no. 3, pp. 1064–1076, 2008.

[68] J. Bottger, A. Schafer, G. Lohmann, A. Villringer, and D. S. Margulies, "Three-dimensional mean-shift edge bundling for the visualization of functional connectivity in the brain," *Visualization and Computer Graphics, IEEE Transactions on*, vol. 20, no. 3, pp. 471–480, 2014.

[69] K. Friston, C. Frith, P. Liddle, and R. Frackowiak, "Functional connectivity: the principal-component analysis of large (pet) data sets," *Journal of Cerebral Blood Flow & Metabolism*, vol. 13, no. 1, pp. 5–14, 1993.

[70] D. S. Bassett, E. T. Bullmore, A. Meyer-Lindenberg, J. A. Apud, D. R. Weinberger, and R. Coppola, "Cognitive fitness of cost-efficient brain functional networks," *Proceedings of the National Academy of Sciences*, vol. 106, no. 28, pp. 11747–11752, 2009.

[71] C. J. Stam, "Functional connectivity patterns of human magnetoencephalographic recordings: a small-worldnetwork?," *Neuroscience letters*, vol. 355, no. 1, pp. 25–28, 2004.

[72] M. Breakspear, M. J. Brammer, E. T. Bullmore, P. Das, and L. M. Williams, "Spatiotemporal wavelet resampling for functional neuroimaging data," *Human brain mapping*, vol. 23, no. 1, pp. 1–25, 2004.

[73] R. Salvador, J. Suckling, C. Schwarzbauer, and E. Bullmore, "Undirected graphs of frequency-dependent functional connectivity in whole brain networks," *Philosophical Transactions of the Royal Society of London B: Biological Sciences*, vol. 360, no. 1457, pp. 937–946, 2005.

[74] G. Marrelec, A. Krainik, H. Duffau, M. Pélégrini-Issac, S. Lehéricy, J. Doyon, and H. Benali, "Partial correlation for functional brain interactivity investigation in functional mri," *Neuroimage*, vol. 32, no. 1, pp. 228–237, 2006.

[75] M. E. Raichle, A. M. MacLeod, A. Z. Snyder, W. J. Powers, D. A. Gusnard, and G. L. Shulman, "A default mode of brain function," *Proceedings of the National Academy of Sciences*, vol. 98, no. 2, pp. 676–682, 2001.

[76] M. D. Fox and M. E. Raichle, "Spontaneous fluctuations in brain activity observed with functional magnetic resonance imaging," *Nature Reviews Neuroscience*, vol. 8, no. 9, pp. 700–711, 2007.

[77] B. T. Yeo, F. M. Krienen, J. Sepulcre, M. R. Sabuncu, D. Lashkari, M. Hollinshead, J. L. Roffman, J. W. Smoller, L. Zöllei, J. R. Polimeni, *et al.*, "The organization of the human cerebral cortex estimated by intrinsic functional connectivity," *Journal of neurophysiology*, vol. 106, no. 3, pp. 1125–1165, 2011.

[78] K. J. Friston, P. Fletcher, O. Josephs, A. Holmes, M. Rugg, and R. Turner, "Event-related fmri: characterizing differential responses," *Neuroimage*, vol. 7, no. 1, pp. 30–40, 1998.

[79] V. D. Calhoun, J. Liu, and T. Adalı, "A review of group ica for fmri data and ica for joint inference of imaging, genetic, and erp data," *Neuroimage*, vol. 45, no. 1, pp. S163–S172, 2009.

[80] B. Thirion, S. Dodel, and J.-B. Poline, "Detection of signal synchronizations in resting-state fmri datasets," *Neuroimage*, vol. 29, no. 1, pp. 321–327, 2006.

[81] M. Van Den Heuvel, R. Mandl, and H. H. Pol, "Normalized cut group clustering of resting-state fmri data," *PloS one*, vol. 3, no. 4, p. e2001, 2008.

[82] C. F. Beckmann, M. DeLuca, J. T. Devlin, and S. M. Smith, "Investigations into resting-state connectivity using independent component analysis," *Philosophical Transactions of the Royal Society of London B: Biological Sciences*, vol. 360, no. 1457, pp. 1001–1013, 2005.

[83] M. De Luca, C. Beckmann, N. De Stefano, P. Matthews, and S. M. Smith, "fmri resting state networks define distinct modes of long-distance interactions in the human brain," *Neuroimage*, vol. 29, no. 4, pp. 1359–1367, 2006.

[84] J. Damoiseaux, S. Rombouts, F. Barkhof, P. Scheltens, C. Stam, S. M. Smith, and C. Beckmann, "Consistent resting-state networks across healthy subjects," *Proceedings of the national academy of sciences*, vol. 103, no. 37, pp. 13848–13853, 2006.

[85] R. M. Hutchison, T. Womelsdorf, E. A. Allen, P. A. Bandettini, V. D. Calhoun, M. Corbetta, S. Della Penna, J. H. Duyn, G. H. Glover, J. Gonzalez-Castillo, *et al.*, "Dynamic functional connectivity: promise, issues, and interpretations," *Neuroimage*, vol. 80, pp. 360–378, 2013.

[86] K. J. Friston, L. Harrison, and W. Penny, "Dynamic causal modelling," *Neuroimage*, vol. 19, no. 4, pp. 1273–1302, 2003.

[87] K. Friston, R. Moran, and A. K. Seth, "Analysing connectivity with granger causality and dynamic causal modelling," *Current opinion in neurobiology*, vol. 23, no. 2, pp. 172–178, 2013.

[88] R. E. Passingham, K. E. Stephan, and R. Kötter, "The anatomical basis of functional localization in the cortex," *Nature Reviews Neuroscience*, vol. 3, no. 8, pp. 606–616, 2002.

[89] C. Honey, O. Sporns, L. Cammoun, X. Gigandet, J.-P. Thiran, R. Meuli, and P. Hagmann, "Predicting human resting-state functional connectivity from structural connectivity," *Proceedings of the National Academy of Sciences*, vol. 106, no. 6, pp. 2035–2040, 2009.

[90] C.-h. Park, S. Y. Kim, Y.-H. Kim, and K. Kim, "Comparison of the small-world topology between anatomical and functional connectivity in the human brain," *Physica A: statistical mechanics and its applications*, vol. 387, no. 23, pp. 5958–5962, 2008.

[91] C. J. Honey, R. Kötter, M. Breakspear, and O. Sporns, "Network structure of cerebral cortex shapes functional connectivity on multiple time scales," *Proceedings of the National Academy of Sciences*, vol. 104, no. 24, pp. 10240–10245, 2007.

[92] A. Ghosh, Y. Rho, A. McIntosh, R. Kötter, and V. Jirsa, "Cortical network dynamics with time delays reveals functional connectivity in the resting brain," *Cognitive neurodynamics*, vol. 2, no. 2, pp. 115–120, 2008.

[93] H.-J. Park and K. Friston, "Structural and functional brain networks: from connections to cognition," *Science*, vol. 342, no. 6158, p. 1238411, 2013.

[94] C. Stam, B. Jones, G. Nolte, M. Breakspear, and P. Scheltens, "Small-world networks and functional connectivity in alzheimer's disease," *Cerebral cortex*, vol. 17, no. 1, pp. 92–99, 2007.

[95] M. Rubinov, S. A. Knock, C. J. Stam, S. Micheloyannis, A. W. Harris, L. M. Williams, and M. Breakspear, "Small-world properties of nonlinear brain activity in schizophrenia," *Human brain mapping*, vol. 30, no. 2, pp. 403–416, 2009.

[96] K. Supekar, V. Menon, D. Rubin, M. Musen, and M. D. Greicius, "Network analysis of intrinsic functional brain connectivity in alzheimer's disease," *PLoS Comput Biol*, vol. 4, no. 6, p. e1000100, 2008.

[97] Y. Liu, M. Liang, Y. Zhou, Y. He, Y. Hao, M. Song, C. Yu, H. Liu, Z. Liu, and T. Jiang, "Disrupted small-world networks in schizophrenia," *Brain*, vol. 131, no. 4, pp. 945–961, 2008.

[98] D. S. Bassett, E. Bullmore, B. A. Verchinski, V. S. Mattay, D. R. Weinberger, and A. Meyer-Lindenberg, "Hierarchical organization of human cortical networks in health and schizophrenia," *The Journal of Neuroscience*, vol. 28, no. 37, pp. 9239–9248, 2008.

[99] S. Ponten, F. Bartolomei, and C. Stam, "Small-world networks and epilepsy: graph theoretical analysis of intracerebrally recorded mesial temporal lobe seizures," *Clinical neurophysiology*, vol. 118, no. 4, pp. 918–927, 2007.

[100] L. Wang, C. Zhu, Y. He, Y. Zang, Q. Cao, H. Zhang, Q. Zhong, and Y. Wang, "Altered small-world brain functional networks in children with attention-deficit/hyperactivity disorder," *Human brain mapping*, vol. 30, no. 2, pp. 638–649, 2009.

[101] F. D. V. Fallani, L. Astolfi, F. Cincotti, D. Mattia, M. G. Marciani, S. Salinari, J. Kurths, S. Gao, A. Cichocki, A. Colosimo, *et al.*, "Cortical functional connectivity networks in normal and spinal cord injured patients: evaluation by graph analysis," *Human brain mapping*, vol. 28, no. 12, pp. 1334–1346, 2007.

[102] A. Zeman, "What do we mean by conscious and aware?," *Neuropsychological rehabilitation*, vol. 16, no. 4, pp. 356–376, 2006.

[103] S. Dehaene and J.-P. Changeux, "Experimental and theoretical approaches to conscious processing," *Neuron*, vol. 70, no. 2, pp. 200–227, 2011.

[104] G. Tononi, "Consciousness as integrated information: a provisional manifesto," *The Biological Bulletin*, vol. 215, no. 3, pp. 216–242, 2008.

[105] C. D. Frith, "What brain plasticity reveals about the nature of consciousness: commentary," *Frontiers in psychology*, vol. 2, 2011.

[106] M. Boly, M. Massimini, M. I. Garrido, O. Gosseries, Q. Noirhomme, S. Laureys, and A. Soddu, "Brain connectivity in disorders of consciousness," *Brain connectivity*, vol. 2, no. 1, pp. 1–10, 2012.

[107] L. Heine, A. Soddu, F. A. Gomez Jaramillo, A. Vanhaudenhuyse, L. Tshibanda, M. Thonnard, V. Charland-Verville, M. Kirsch, S. Laureys, and A. Demertzi, "Resting state networks and consciousness alterations of multiple resting state network connectivity in physiological, pharmacological and pathological consciousness states," *Frontiers in psychology*, vol. 3, p. 295, 2012.

[108] C. Di Perri, J. Stender, S. Laureys, and O. Gosseries, "Functional neuroanatomy of disorders of consciousness," *Epilepsy & Behavior*, vol. 30, pp. 28–32, 2014.

[109] T. Nagel, "What is it like to be a bat?," *The philosophical review*, vol. 83, no. 4, pp. 435–450, 1974.

[110] S. Laureys, "The neural correlate of (un) awareness: lessons from the vegetative state," *Trends in cognitive sciences*, vol. 9, no. 12, pp. 556–559, 2005.

[111] J. L. Bernat, "Chronic consciousness disorders," *Annual review of medicine*, vol. 60, pp. 381–392, 2009.

[112] J. T. Giacino, J. J. Fins, S. Laureys, and N. D. Schiff, "Disorders of consciousness after acquired brain injury: the state of the science," *Nature Reviews Neurology*, vol. 10, no. 2, pp. 99–114, 2014.

[113] S. Laureys, F. Pellas, P. Van Eeckhout, S. Ghorbel, C. Schnakers, F. Perrin, J. Berre, M.-E. Faymonville, K.-H. Pantke, F. Damas, *et al.*, "The locked-in syndrome: what is it like to be conscious but paralyzed and voiceless?," *Progress in brain research*, vol. 150, pp. 495–611, 2005.

[114] D. Fernández-Espejo, T. Bekinschtein, M. M. Monti, J. D. Pickard, C. Junque, M. R. Coleman, and A. M. Owen, "Diffusion weighted imaging distinguishes the vegetative state from the minimally conscious state," *Neuroimage*, vol. 54, no. 1, pp. 103–112, 2011.

[115] Q. Noirhomme, A. Soddu, R. Lehembre, A. Vanhaudenhuyse, P. Boveroux, M. Boly, and S. Laureys, "Brain connectivity in pathological and pharmacological coma," *Frontiers in systems neuroscience*, vol. 4, p. 160, 2010.

[116] A. Soddu, M. Boly, Y. Nir, Q. Noirhomme, A. Vanhaudenhuyse, A. Demertzi, A. Arzi, S. Ovadia, M. Stanziano, M. Papa, *et al.*, "Reaching across the abyss: recent advances in functional magnetic resonance imaging and their potential relevance to disorders of consciousness," *Progress in brain research*, vol. 177, pp. 261–274, 2009.

[117] L. Tshibanda, A. Vanhaudenhuyse, D. Galanaud, M. Boly, S. Laureys, and L. Puybasset, "Magnetic resonance spectroscopy and diffusion tensor imaging in coma survivors: promises and pitfalls," *Progress in brain research*, vol. 177, pp. 215–229, 2009.

[118] D. Graham, J. Adams, L. Murray, and B. Jennett, "Neuropathology of the vegetative state after head injury," *Neuropsychological rehabilitation*, vol. 15, no. 3-4, pp. 198–213, 2005.

[119] A. Vanhaudenhuyse, A. Demertzi, M. Schabus, Q. Noirhomme, S. Bredart, M. Boly, C. Phillips, A. Soddu, A. Luxen, G. Moonen, *et al.*, "Two distinct neuronal networks mediate the awareness of environment and of self," *Journal of cognitive neuroscience*, vol. 23, no. 3, pp. 570–578, 2011.

[120] A. Vanhaudenhuyse, Q. Noirhomme, L. J.-F. Tshibanda, M.-A. Bruno, P. Boveroux, C. Schnakers, A. Soddu, V. Perlbarg, D. Ledoux, J.-F. Brichant, *et al.*, "Default network connectivity reflects the level of consciousness in non-communicative brain-damaged patients," *Brain*, vol. 133, no. 1, pp. 161–171, 2010.

[121] A. E. Cavanna, "The precuneus and consciousness," *CNS spectrums*, vol. 12, no. 07, pp. 545–552, 2007.

[122] M. Boly, L. Tshibanda, A. Vanhaudenhuyse, Q. Noirhomme, C. Schnakers, D. Ledoux, P. Boveroux, C. Garweg, B. Lambermont, C. Phillips, *et al.*, "Functional connectivity in the default network during resting state is preserved in a vegetative but not in a brain dead patient," *Human brain mapping*, vol. 30, no. 8, pp. 2393–2400, 2009.

[123] C. Di Perri, S. Bastianello, A. J. Bartsch, C. Pistarini, G. Maggioni, L. Magrassi, R. Imberti, A. Pichiecchio, P. Vitali, S. Laureys, *et al.*, "Lim-

bic hyperconnectivity in the vegetative state," *Neurology*, vol. 81, no. 16, pp. 1417–1424, 2013.

[124] A. Demertzi, G. Antonopoulos, L. Heine, H. U. Voss, J. S. Crone, C. de Los Angeles, M. A. Bahri, C. Di Perri, A. Vanhaudenhuyse, V. Charland-Verville, *et al.*, "Intrinsic functional connectivity differentiates minimally conscious from unresponsive patients," *Brain*, vol. 138, no. 9, pp. 2619–2631, 2015.

[125] M. A. Eckert, N. V. Kamdar, C. E. Chang, C. F. Beckmann, M. D. Greicius, and V. Menon, "A cross-modal system linking primary auditory and visual cortices: Evidence from intrinsic fmri connectivity analysis," *Human brain mapping*, vol. 29, no. 7, pp. 848–857, 2008.

[126] S. Clavagnier, A. Falchier, and H. Kennedy, "Long-distance feedback projections to area v1: implications for multisensory integration, spatial awareness, and visual consciousness," *Cognitive, Affective, & Behavioral Neuroscience*, vol. 4, no. 2, pp. 117–126, 2004.

[127] S. Laureys, A. M. Owen, and N. D. Schiff, "Brain function in coma, vegetative state, and related disorders," *The Lancet Neurology*, vol. 3, no. 9, pp. 537–546, 2004.

[128] C. Di Perri, M. A. Bahri, E. Amico, A. Thibaut, L. Heine, G. Antonopoulos, V. Charland-Verville, S. Wannez, F. Gomez, R. Hustinx, *et al.*, "Neural correlates of consciousness in patients who have emerged from a minimally conscious state: a cross-sectional multimodal imaging study," *The Lancet Neurology*, 2016.

[129] M. Massimini, M. Boly, A. Casali, M. Rosanova, and G. Tononi, "A perturbational approach for evaluating the brain's capacity for consciousness," *Progress in brain research*, vol. 177, pp. 201–214, 2009.

[130] O. Gosseries, S. Sarasso, S. Casarotto, M. Boly, C. Schnakers, M. Napolitani, M.-A. Bruno, D. Ledoux, J.-F. Tshibanda, M. Massimini, *et al.*, "On the cerebral origin of eeg responses to tms: insights from severe cortical lesions," *Brain stimulation*, vol. 8, no. 1, pp. 142–149, 2015.

[131] M. Rosanova, O. Gosseries, S. Casarotto, M. Boly, A. G. Casali, M.-A. Bruno, M. Mariotti, P. Boveroux, G. Tononi, S. Laureys, *et al.*, "Recovery of cortical effective connectivity and recovery of consciousness in vegetative patients," *Brain*, p. awr340, 2012.

[132] M. Massimini, F. Ferrarelli, M. Murphy, R. Huber, B. Riedner, S. Casarotto, and G. Tononi, "Cortical reactivity and effective connectivity during rem sleep in humans," *Cognitive neuroscience*, vol. 1, no. 3, pp. 176–183, 2010.

[133] A. G. Casali, O. Gosseries, M. Rosanova, M. Boly, S. Sarasso, K. R. Casali, S. Casarotto, M.-A. Bruno, S. Laureys, G. Tononi, *et al.*, "A theoretically based index of consciousness independent of sensory processing and behavior," *Science translational medicine*, vol. 5, no. 198, pp. 198ra105–198ra105, 2013.

[134] R. S. Schwartz, E. N. Brown, R. Lydic, and N. D. Schiff, "General anesthesia, sleep, and coma," *New England Journal of Medicine*, vol. 363, no. 27, pp. 2638–2650, 2010.

[135] V. Bonhomme, P. Boveroux, J. F. Brichant, S. Laureys, and M. Boly, "Neural correlates of consciousness during general anesthesia using functional magnetic resonance imaging (fmri)," *Arch Ital Biol*, vol. 150, no. 2-3, pp. 155–163, 2012.

[136] A. J. Wood, J. A. Campagna, K. W. Miller, and S. A. Forman, "Mechanisms of actions of inhaled anesthetics," *New England Journal of Medicine*, vol. 348, no. 21, pp. 2110–2124, 2003.

[137] C. Grasshoff, U. Rudolph, and B. Antkowiak, "Molecular and systemic mechanisms of general anaesthesia: the multi-site and multiple mechanisms concept," *Current Opinion in Anesthesiology*, vol. 18, no. 4, pp. 386–391, 2005.

[138] K. Solt and S. A. Forman, "Correlating the clinical actions and molecular mechanisms of general anesthetics," *Current Opinion in Anesthesiology*, vol. 20, no. 4, pp. 300–306, 2007.

[139] P. Boveroux, A. Vanhaudenhuyse, M.-A. Bruno, Q. Noirhomme, S. Lauwick, A. Luxen, C. Degueldre, A. Plenevaux, C. Schnakers, C. Phillips, *et al.*, "Breakdown of within-and between-network resting state functional magnetic resonance imaging connectivity during propofol-induced loss of consciousness," *The Journal of the American Society of Anesthesiologists*, vol. 113, no. 5, pp. 1038–1053, 2010.

[140] J. P. Guldenmund, A. Vanhaudenhuyse, M. Boly, S. Laureys, and A. Soddu, "A default mode of brain function in altered states of consciousness.," *Archives italiennes de biologie*, vol. 150, no. 2-3, pp. 107–21, 2012.

[141] L. J. Velly, M. F. Rey, N. J. Bruder, F. A. Gouvitsos, T. Witjas, J. M. Regis, J. C. Peragut, and F. M. Gouin, "Differential dynamic of action on cortical and subcortical structures of anesthetic agents during induction of anesthesia," *The Journal of the American Society of Anesthesiologists*, vol. 107, no. 2, pp. 202–212, 2007.

[142] J. Schrouff, V. Perlbarg, M. Boly, G. Marrelec, P. Boveroux, A. Vanhaudenhuyse, M.-A. Bruno, S. Laureys, C. Phillips, M. Pélégrini-Issac, *et al.*, "Brain functional integration decreases during propofol-induced loss of consciousness," *Neuroimage*, vol. 57, no. 1, pp. 198–205, 2011.

[143] R. Martuzzi, R. Ramani, M. Qiu, X. Shen, X. Papademetris, and R. T. Constable, "A whole-brain voxel based measure of intrinsic connectivity contrast reveals local changes in tissue connectivity with anesthetic without a priori assumptions on thresholds or regions of interest," *Neuroimage*, vol. 58, no. 4, pp. 1044–1050, 2011.

[144] G. Deshpande, C. Kerssens, P. S. Sebel, and X. Hu, "Altered local coherence in the default mode network due to sevoflurane anesthesia," *Brain research*, vol. 1318, pp. 110–121, 2010.

[145] E. A. Allen, E. Damaraju, S. M. Plis, E. B. Erhardt, T. Eichele, and V. D. Calhoun, "Tracking whole-brain connectivity dynamics in the resting state," *Cerebral cortex*, p. bhs352, 2012.

[146] C. Chang and G. H. Glover, "Time–frequency dynamics of resting-state brain connectivity measured with fmri," *Neuroimage*, vol. 50, no. 1, pp. 81–98, 2010.

[147] R. M. Hutchison, L. S. Leung, S. M. Mirsattari, J. S. Gati, R. S. Menon, and S. Everling, "Resting-state networks in the macaque at 7t," *Neuroimage*, vol. 56, no. 3, pp. 1546–1555, 2011.

[148] E. Tagliazucchi, F. Von Wegner, A. Morzelewski, V. Brodbeck, and H. Laufs, "Dynamic bold functional connectivity in humans and its electrophysiological correlates," *Front Hum Neurosci*, vol. 6, no. 339.10, p. 3389, 2012.

[149] X. Liu and J. H. Duyn, "Time-varying functional network information extracted from brief instances of spontaneous brain activity," *Proceedings of the National Academy of Sciences*, vol. 110, no. 11, pp. 4392–4397, 2013.

[150] J. D. Power, K. A. Barnes, A. Z. Snyder, B. L. Schlaggar, and S. E. Petersen, "Spurious but systematic correlations in functional connectivity mri networks arise from subject motion," *Neuroimage*, vol. 59, no. 3, pp. 2142–2154, 2012.

[151] T. Hastie, R. Tibshirani, and J. Friedman, *Unsupervised learning*. Springer, 2009.

[152] M. T. Alkire, A. G. Hudetz, and G. Tononi, "Consciousness and anesthesia," *Science*, vol. 322, no. 5903, pp. 876–880, 2008.

[153] P. Fiset, T. Paus, T. Daloze, G. Plourde, P. Meuret, V. Bonhomme, N. Hajj-Ali, S. B. Backman, and A. C. Evans, "Brain mechanisms of propofol-induced loss of consciousness in humans: a positron emission tomographic study," *The Journal of neuroscience*, vol. 19, no. 13, pp. 5506–5513, 1999.

[154] S.-W. Ying and P. A. Goldstein, "Propofol-block of sk channels in reticular thalamic neurons enhances gabaergic inhibition in relay neurons," *Journal of neurophysiology*, vol. 93, no. 4, pp. 1935–1948, 2005.

[155] P. Guldenmund, A. Demertzi, P. Boveroux, M. Boly, A. Vanhaudenhuyse, M.-A. Bruno, O. Gosseries, Q. Noirhomme, J.-F. Brichant, V. Bonhomme, *et al.*, "Thalamus, brainstem and salience network connectivity changes during propofol-induced sedation and unconsciousness," *Brain connectivity*, vol. 3, no. 3, pp. 273–285, 2013.

[156] S. Vijayan, S. Ching, P. L. Purdon, E. N. Brown, and N. J. Kopell, "Thalamocortical mechanisms for the anteriorization of alpha rhythms during propofol-induced unconsciousness," *The Journal of Neuroscience*, vol. 33, no. 27, pp. 11070–11075, 2013.

[157] V. A. Lamme, K. Zipser, and H. Spekreijse, "Figure-ground activity in primary visual cortex is suppressed by anesthesia," *Proceedings of the National Academy of Sciences*, vol. 95, no. 6, pp. 3263–3268, 1998.

[158] P. K. Tenenbein, A. M. Lam, M. Klein, and L. Lee, "Effects of sevoflurane and propofol on flash visual evoked potentials," *Journal of Neurosurgical Anesthesiology*, vol. 18, no. 4, p. 310, 2006.

[159] U. Ziemann, S. Lönnecker, B. Steinhoff, and W. Paulus, "Effects of antiepileptic drugs on motor cortex excitability in humans: a transcranial magnetic stimulation study," *Annals of neurology*, vol. 40, no. 3, pp. 367–378, 1996.

[160] C. J. Kalkman, J. C. Drummond, A. A. Ribberink, P. M. Patel, T. Sano, and R. G. Bickford, "Effects of propofol, etomidate, midazolam, and fentanyl on motor evoked responses to transcranial electrical or magnetic stimulation in humans.," *Anesthesiology*, vol. 76, no. 4, pp. 502–509, 1992.

[161] B. H. Gaese and J. Ostwald, "Anesthesia changes frequency tuning of neurons in the rat primary auditory cortex," *Journal of neurophysiology*, vol. 86, no. 2, pp. 1062–1066, 2001.

[162] G. Plourde, P. Belin, D. Chartrand, P. Fiset, S. B. Backman, G. Xie, and R. J. Zatorre, "Cortical processing of complex auditory stimuli during alterations of consciousness with the general anesthetic propofol," *The Journal of the American Society of Anesthesiologists*, vol. 104, no. 3, pp. 448–457, 2006.

[163] M. Dueck, F. Petzke, H. Gerbershagen, M. Paul, V. Hesselmann, R. Girnus, B. Krug, B. Sorger, R. Goebel, R. Lehrke, *et al.*, "Propofol attenuates responses of the auditory cortex to acoustic stimulation in a dose-dependent manner: A fmri study," *Acta anaesthesiologica scandinavica*, vol. 49, no. 6, pp. 784–791, 2005.

[164] G. Untergehrer, D. Jordan, E. F. Kochs, R. Ilg, and G. Schneider, "Fronto-parietal connectivity is a non-static phenomenon with characteristic changes during unconsciousness," *PloS one*, vol. 9, no. 1, p. e87498, 2014.

[165] N. C. Rogasch and P. B. Fitzgerald, "Assessing cortical network properties using tms–eeg," *Human brain mapping*, vol. 34, no. 7, pp. 1652–1669, 2013.

[166] M. Rosanova, A. Casali, V. Bellina, F. Resta, M. Mariotti, and M. Massimini, "Natural frequencies of human corticothalamic circuits," *The Journal of Neuroscience*, vol. 29, no. 24, pp. 7679–7685, 2009.

[167] F. Ferrarelli, S. Sarasso, Y. Guller, B. A. Riedner, M. J. Peterson, M. Bellesi, M. Massimini, B. R. Postle, and G. Tononi, "Reduced natural oscillatory frequency of frontal thalamocortical circuits in schizophrenia," *Archives of general psychiatry*, vol. 69, no. 8, pp. 766–774, 2012.

[168] F. Cona, M. Zavaglia, M. Massimini, M. Rosanova, and M. Ursino, "A neural mass model of interconnected regions simulates rhythm propagation observed via tms-eeg," *NeuroImage*, vol. 57, no. 3, pp. 1045–1058, 2011.

[169] F. Ferrarelli, S. Sarasso, Y. Guller, B. A. Riedner, M. J. Peterson, M. Bellesi, M. Massimini, B. R. Postle, and G. Tononi, "Reduced natural oscillatory frequency of frontal thalamocortical circuits in schizophrenia," *Archives of general psychiatry*, vol. 69, no. 8, pp. 766–774, 2012.

[170] C. Chu, N. Tanaka, J. Diaz, B. Edlow, O. Wu, M. Hämäläinen, S. Stufflebeam, S. Cash, and M. Kramer, "Eeg functional connectivity is partially predicted by underlying white matter connectivity," *Neuroimage*, vol. 108, no. 1, pp. 23–33, 2015.

[171] C. J. Honey, J.-P. Thivierge, and O. Sporns, "Can structure predict function in the human brain?," *Neuroimage*, vol. 52, no. 3, pp. 766–776, 2010.

[172] P. Berg and M. Scherg, "A multiple source approach to the correction of eye artifacts," *Electroencephalography and clinical neurophysiology*, vol. 90, no. 3, pp. 229–241, 1994.

[173] C. Phillips, J. Mattout, M. D. Rugg, P. Maquet, and K. J. Friston, "An empirical bayesian solution to the source reconstruction problem in eeg," *NeuroImage*, vol. 24, no. 4, pp. 997–1011, 2005.

[174] J. Mattout, C. Phillips, W. D. Penny, M. D. Rugg, and K. J. Friston, "Meg source localization under multiple constraints: an extended bayesian framework," *NeuroImage*, vol. 30, no. 3, pp. 753–767, 2006.

[175] N. Tzourio-Mazoyer, B. Landeau, D. Papathanassiou, F. Crivello, O. Etard, N. Delcroix, B. Mazoyer, and M. Joliot, "Automated anatomical labeling of activations in spm using a macroscopic anatomical parcellation of the mni mri single-subject brain," *Neuroimage*, vol. 15, no. 1, pp. 273–289, 2002.

[176] P. Van Mierlo, E. Carrette, H. Hallez, K. Vonck, D. Van Roost, P. Boon, and S. Staelens, "Accurate epileptogenic focus localization through time-variant functional connectivity analysis of intracranial electroencephalographic signals," *Neuroimage*, vol. 56, no. 3, pp. 1122–1133, 2011.

[177] P. Van Mierlo, E. Carrette, H. Hallez, R. Raedt, A. Meurs, S. Vandenberghe, D. Roost, P. Boon, S. Staelens, and K. Vonck, "Ictal-onset localization through connectivity analysis of intracranial eeg signals in patients with refractory epilepsy," *Epilepsia*, vol. 54, no. 8, pp. 1409–1418, 2013.

[178] K. Caeyenberghs, A. Leemans, C. De Decker, M. Heitger, D. Drijkoningen, C. V. Linden, S. Sunaert, and S. Swinnen, "Brain connectivity and postural control in young traumatic brain injury patients: A diffusion mri based network analysis," *NeuroImage: clinical*, vol. 1, no. 1, pp. 106–115, 2012.

[179] A. Leemans and D. K. Jones, "The b-matrix must be rotated when correcting for subject motion in dti data," *Magnetic Resonance in Medicine*, vol. 61, no. 6, pp. 1336–1349, 2009.

[180] S. M. Smith, M. Jenkinson, M. W. Woolrich, C. F. Beckmann, T. E. Behrens, H. Johansen-Berg, P. R. Bannister, M. De Luca, I. Drobnjak, D. E. Flitney, *et al.*, "Advances in functional and structural mr image analysis and implementation as fsl," *Neuroimage*, vol. 23, pp. S208–S219, 2004.

[181] M. Kaminski and K. Blinowska, "A new method of the description of the information flow in the brain structures," *Biological cybernetics*, vol. 65, no. 3, pp. 203–210, 1991.

[182] M. Kamiński, M. Ding, W. A. Truccolo, and S. L. Bressler, "Evaluating causal relations in neural systems: Granger causality, directed transfer function and statistical assessment of significance," *Biological cybernetics*, vol. 85, no. 2, pp. 145–157, 2001.

[183] F. Babiloni, F. Cincotti, C. Babiloni, F. Carducci, D. Mattia, L. Astolfi, A. Basilisco, P. Rossini, L. Ding, Y. Ni, *et al.*, "Estimation of the cortical functional connectivity with the multimodal integration of high-resolution eeg and fmri data by directed transfer function," *Neuroimage*, vol. 24, no. 1, pp. 118–131, 2005.

[184] L. Astolfi, F. Cincotti, D. Mattia, F. de Vico Fallani, A. Tocci, A. Colosimo, S. Salinari, M. G. Marciani, W. Hesse, H. Witte, *et al.*, "Tracking the time-varying cortical connectivity patterns by adaptive multivariate estimators," *Biomedical Engineering, IEEE Transactions on*, vol. 55, no. 3, pp. 902–913, 2008.

[185] C. Wilke, L. Ding, and B. He, "Estimation of time-varying connectivity patterns through the use of an adaptive directed transfer function," *Biomedical Engineering, IEEE Transactions on*, vol. 55, no. 11, pp. 2557–2564, 2008.

[186] M. Arnold, X. Milner, H. Witte, R. Bauer, and C. Braun, "Adaptive ar modeling of nonstationary time series by means of kalman filtering,"

Biomedical Engineering, IEEE Transactions on, vol. 45, no. 5, pp. 553–562, 1998.

[187] A. Schlögl, S. Roberts, and G. Pfurtscheller, "A criterion for adaptive autoregressive models," in *Proceedings of the 22 nd IEEE International Conference on Engineering in Medicine and Biology*, pp. 1581–1582, 2000.

[188] N. C. Rogasch, R. H. Thomson, Z. J. Daskalakis, and P. B. Fitzgerald, "Short-latency artifacts associated with concurrent tms–eeg," *Brain stimulation*, vol. 6, no. 6, pp. 868–876, 2013.

[189] B. Efron and R. Tibshirani, "Bootstrap methods for standard errors, confidence intervals, and other measures of statistical accuracy," *Statistical science*, pp. 54–75, 1986.

[190] M. Xia, J. Wang, Y. He, *et al.*, "Brainnet viewer: a network visualization tool for human brain connectomics," *PloS one*, vol. 8, no. 7, p. e68910, 2013.

[191] L. H. Scholtens, R. Schmidt, M. A. de Reus, and M. P. van den Heuvel, "Linking macroscale graph analytical organization to microscale neuroarchitectonics in the macaque connectome," *The Journal of Neuroscience*, vol. 34, no. 36, pp. 12192–12205, 2014.

[192] S. F. Beul, S. Grant, and C. C. Hilgetag, "A predictive model of the cat cortical connectome based on cytoarchitecture and distance," *Brain Structure and Function*, vol. 220, no. 6, pp. 3167–3184, 2015.

[193] M. P. van den Heuvel, L. H. Scholtens, L. F. Barrett, C. C. Hilgetag, and M. A. de Reus, "Bridging cytoarchitectonics and connectomics in human cerebral cortex," *The Journal of Neuroscience*, vol. 35, no. 41, pp. 13943–13948, 2015.

[194] P. Barttfeld, L. Uhrig, J. D. Sitt, M. Sigman, B. Jarraya, and S. Dehaene, "Signature of consciousness in the dynamics of resting-state brain activity," *Proceedings of the National Academy of Sciences*, vol. 112, no. 3, pp. 887–892, 2015.

[195] D. Balduzzi and G. Tononi, "Integrated information in discrete dynamical systems: motivation and theoretical framework," *PLoS computational biology*, vol. 4, no. 6, p. e1000091, 2008.

[196] A. Fornito, A. Zalesky, and M. Breakspear, "The connectomics of brain disorders," *Nature Reviews Neuroscience*, vol. 16, no. 3, pp. 159–172, 2015.

[197] P. Lioumis, D. Kičić, P. Savolainen, J. P. Mäkelä, and S. Kähkönen, "Reproducibility of tmsevoked eeg responses," *Human brain mapping*, vol. 30, no. 4, pp. 1387–1396, 2009.

[198] T. Wagner, J. Rushmore, U. Eden, and A. Valero-Cabre, "Biophysical foundations underlying tms: setting the stage for an effective use of neurostimulation in the cognitive neurosciences," *Cortex*, vol. 45, no. 9, pp. 1025–1034, 2009.

[199] B. Jeurissen, A. Leemans, D. K. Jones, J.-D. Tournier, and J. Sijbers, "Probabilistic fiber tracking using the residual bootstrap with constrained spherical deconvolution," *Human brain mapping*, vol. 32, no. 3, pp. 461–479, 2011.

[200] J. Tournier, F. Calamante, A. Connelly, *et al.*, "Determination of the appropriate b value and number of gradient directions for high-angular-resolution diffusion-weighted imaging," *NMR in Biomedicine*, vol. 26, no. 12, pp. 1775–1786, 2013.

[201] U. Roine, J. Salmi, T. Roine, T. Nieminen-von Wendt, S. Leppämäki, P. Rintahaka, P. Tani, A. Leemans, and M. Sams, "Constrained spherical deconvolution-based tractography and tract-based spatial statistics show abnormal microstructural organization in asperger syndrome," *Molecular autism*, vol. 6, no. 1, pp. 1–12, 2015.

[202] J. Giacino and K. Kalmar, "Coma recovery scale-revised," *The Center for Outcome Measurement in Brain Injury*, pp. 36–51, 2006.

[203] C. Schnakers, S. Majerus, J. Giacino, A. Vanhaudenhuyse, M.-A. Bruno, M. Boly, G. Moonen, P. Damas, B. Lambermont, M. Lamy, *et al.*, "A

french validation study of the coma recovery scale-revised (crs-r)," *Brain Injury*, vol. 22, no. 10, pp. 786–792, 2008.

[204] R. T. Seel, M. Sherer, J. Whyte, D. I. Katz, J. T. Giacino, A. M. Rosenbaum, F. M. Hammond, K. Kalmar, T. L.-B. Pape, R. Zafonte, *et al.*, "Assessment scales for disorders of consciousness: evidence-based recommendations for clinical practice and research," *Archives of physical medicine and rehabilitation*, vol. 91, no. 12, pp. 1795–1813, 2010.

[205] M. Jenkinson, C. F. Beckmann, T. E. Behrens, M. W. Woolrich, and S. M. Smith, "Fsl," *Neuroimage*, vol. 62, no. 2, pp. 782–790, 2012.

[206] J. V. Manjón, P. Coupé, A. Buades, D. L. Collins, and M. Robles, "New methods for mri denoising based on sparseness and self-similarity," *Medical image analysis*, vol. 16, no. 1, pp. 18–27, 2012.

[207] J. D. Power, A. Mitra, T. O. Laumann, A. Z. Snyder, B. L. Schlaggar, and S. E. Petersen, "Methods to detect, characterize, and remove motion artifact in resting state fmri," *Neuroimage*, vol. 84, pp. 320–341, 2014.

[208] X. Shen, F. Tokoglu, X. Papademetris, and R. T. Constable, "Groupwise whole-brain parcellation from resting-state fmri data for network node identification," *Neuroimage*, vol. 82, pp. 403–415, 2013.

[209] A. Hyvärinen, "Fast and robust fixed-point algorithms for independent component analysis," *Neural Networks, IEEE Transactions on*, vol. 10, no. 3, pp. 626–634, 1999.

[210] M. E. Newman and M. Girvan, "Finding and evaluating community structure in networks," *Physical review E*, vol. 69, no. 2, p. 026113, 2004.

[211] P. J. Mucha, T. Richardson, K. Macon, M. A. Porter, and J.-P. Onnela, "Community structure in time-dependent, multiscale, and multiplex networks," *science*, vol. 328, no. 5980, pp. 876–878, 2010.

[212] S. Gómez, P. Jensen, and A. Arenas, "Analysis of community structure in networks of correlated data," *Physical Review E*, vol. 80, no. 1, p. 016114, 2009.

[213] V. Traag and J. Bruggeman, "Community detection in networks with positive and negative links," *Physical Review E*, vol. 80, no. 3, p. 036115, 2009.

[214] V. D. Blondel, J.-L. Guillaume, R. Lambiotte, and E. Lefebvre, "Fast unfolding of communities in large networks," *Journal of statistical mechanics: theory and experiment*, vol. 2008, no. 10, p. P10008, 2008.

[215] A. Lancichinetti and S. Fortunato, "Consensus clustering in complex networks," *Scientific reports*, vol. 2, 2012.

[216] J. Vincent, G. Patel, M. Fox, A. Snyder, J. Baker, D. Van Essen, J. Zempel, L. Snyder, M. Corbetta, and M. Raichle, "Intrinsic functional architecture in the anaesthetized monkey brain," *Nature*, vol. 447, no. 7140, pp. 83–86, 2007.

[217] F. Crick, C. Koch, *et al.*, "Are we aware of neural activity in primary visual cortex?," *Nature*, vol. 375, no. 6527, pp. 121–123, 1995.

[218] C. Koch, M. Massimini, M. Boly, and G. Tononi, "Neural correlates of consciousness: progress and problems," *Nature Reviews Neuroscience*, vol. 17, no. 5, pp. 307–321, 2016.

ACKNOWLEDGEMENTS

There is a long list of people I need to thank that help in so many different ways during my four years of PhD.

First and foremost, I would like to thank my family, for the unconditional support and everlasting care over all these years.

Special thanks to all my fantastic friends and colleagues in Liège, past and present. I feel very lucky to have been surrounded by them. I will try the impossible task of naming them all (in random order): Vincenzo, Gianluca, Cristiano, Giorgos (my "Neapolitan" brothers), Carol, Simona, "mbare" Emanuela, Erik, Lizette, Jitka, Sophie, Raph, Jochem, Susanna, Florian, Pacho, Andrea Soddu (it all started thanks to him!), Guillaume (my official translator!) and Sophie, Mohammed, Charlotte, Emma, Doro, Giulia, Kata, Audrey, Mariette, Athena, Quentin, Damien, Mathieu, Alessandra, Marina, Velia, Andrea Piarulli, Pot au Lait, Leonardo, Vanessa, Geraldine, Sarah, Olivier, Dina, Pieter, Stephen, Olivia, Camille, Aurore and Gauthier, Charlene, Kiril, Gaia, Felipe.

Thanks to the (almost) Dr. Marco Arzeo, as usual; thanks to Fiammetta, Gianpaolo, Enrica, Paoletta and all my friends in Angri, Italy.

All my colleagues in Montefiore, at the Cyclotron research Center, at GIGA.

My amazing friends and colleagues in Ghent! Alessandro, Roma, Guarong, Margarita, Hannelore, Frederik, Caroline, Elena, Hannes, Sanne.

Thanks, Manu, for your patience. We met in a very stressful time, but somehow you managed to get me through it, and I am grateful for that.

I would also like to express my sincere acknowledgements to all the members of the Jury for their interest and for the time devoted to reading and evaluating this thesis.

Many thanks to Professor Rodolphe Sepulchre, who offered me the opportunity to join his group during my first year. Despite the short period, I have learned a lot from him as a young student and researcher.

I would like to warmly thank my supervisor, Prof. Steven Laureys, who gave me the possibility to start this thesis, 4 years ago. I hope I partly repaid his trust with my work. I am particularly grateful to Steven for his constant support and for giving me so much freedom in my research.

I will never thank enough Prof. Daniele Marinazzo. It was all a PhD student can wish of: careful, supportive, present. And thanks to his wife Pilar for the Spanish lessons (and to Diego, Pablo, Sarita as well).

Finally, my heartfelt thanks to Prof. Joaquín Goñi and his wife Nieves, for "adopting" me during my visiting period in Indiana. It was a great pleasure to collaborate with him, I am sure it will be exciting to be Postdoc in his lab.